

# **Abstract Book & Schedule**



# PCSI-47 General Information

---

## Conference Hotel:

Millennium Harvest House, 1345 28th Street, Boulder, CO 80302, USA

**Conference Website:** [www.psicconference.org](http://www.psicconference.org)

---

## Chair:

Kirstin Alberi,  
National Renewable Energy Laboratory  
E-mail: [Kirstin.Alberi@nrel.gov](mailto:Kirstin.Alberi@nrel.gov)

## General Chair:

Chris Palmstrøm  
Univ. of California, Santa Barbara  
E-mail: [cpalmstrom@ece.ucsb.edu](mailto:cpalmstrom@ece.ucsb.edu)

## JVST Special Issue Editor:

Rudy Ludeke  
E-mail: [rudy\\_ludeke@msn.com](mailto:rudy_ludeke@msn.com)

## Registration:

Della Miller/Heather Korff  
AVS, 110 Yellowstone Dr., Suite 120  
Chico, CA 95973  
E-mail: [della@avs.org](mailto:della@avs.org) / [heather@avs.org](mailto:heather@avs.org)  
Phone: 530-896-0477

---

## Program Committee:

K. Arima, Osaka University  
A. Bhattacharya, Argonne National Lab  
L. Brillson, The Ohio State University  
H. Cohen, Weizmann Institute of Science  
S. Crooker, Los Alamos National Lab  
A. Demkov, University of Texas, Austin  
C. Eddy, Naval Research Lab  
H. Eisele, Technische Universität Berlin  
M. Flatté, University of Iowa  
A. Fontcuberta I Morral, École Polytechnique  
Fédérale de Lausanne (EPFL)  
J. Hilton, SPECS-TII Inc.  
T. Honda, Kogakuin University  
H. Hwang, Stanford University  
E. Johnston-Halperin, The Ohio State University  
K. Kavanagh, Simon Fraser University  
R. Kawakami, The Ohio State University

P. Koenraad, Eindhoven Univ. of Technology  
L. Lauhon, Northwestern University  
J. Lee, Ajou University  
R. Ludeke, IBM  
C. McConville, RMIT University  
A. Mikkelsen, Lund University  
J. Millunchick, University of Michigan  
R. Myers, The Ohio State University  
H. Riechert, Paul Drude Institute  
N. Samarth, Penn State University  
Y. Suzuki, Stanford University  
A. Talin, Sandia National Lab  
P. (Chakrapani) Varanasi, Army Research  
Office  
R. Wallace, University of Texas, Dallas  
E. Yu, University of Texas, Austin  
J. Zhu, Penn State University

---

## Presentation Formats:

**Invited Talks**—32-minute oral presentation, 8-minute discussion (40 minutes total), plus poster  
**Upgraded Talks**—16-minute oral presentation, 4-minute discussion (20 minutes total), plus poster  
**Contributed Talks**—4-minute oral presentation, 1-minute discussion (5 minutes total), plus poster  
**Posters**—Displayed all week (46 inches high x 46 inches wide)

# PCSI-47 Sponsors

## Gold Corporate Sponsors



## Silver Corporate and Media Sponsors



## Technical Sponsors



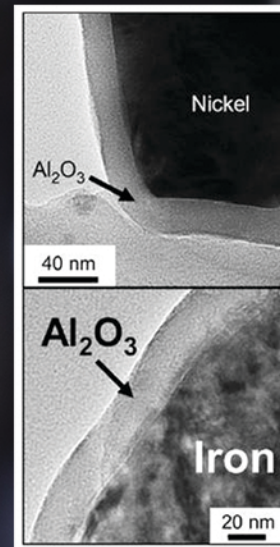
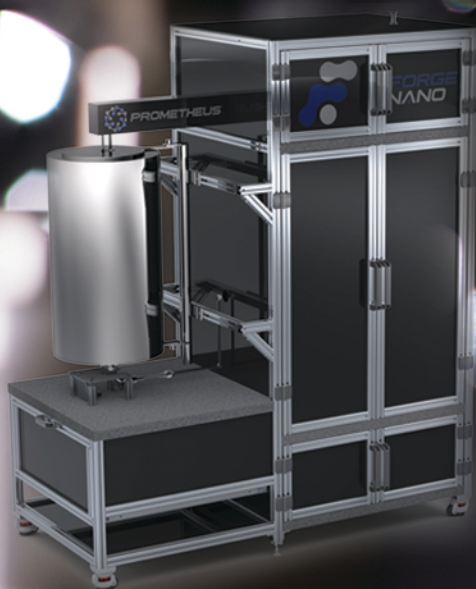


# FORGE NANO

## INNOVATION AT SCALE

### ADVANCED MATERIALS BY SURFACE ENGINEERING

Forge Nano is a global expert in particle ALD (Atomic Layer Deposition). Our proprietary, high throughput process enables coatings to be applied one atomic layer at a time. From our Lab-Scale tools designed for research, to our manufacturing ready Commercial solutions, Forge Nano makes ALD affordable, and Scaleable.



#### Surface-Properties improved with ALD

- Functionality • Resistivity • Processability • Volatility • Flowability • Solubility • Reflectivity • Opacity • Activity • Formability • Longevity • Wettability • Sustainability • Absorptivity • Phobicity • Philicity • Corrosivity • Viscosity • Reactivity • Selevctivity • Sinterability • Conformality • Permissivity • Porostiy • Reusability • Longevity • Dispersability • Homogeniety • Diffusivity • Compressibility • Cohesivity • Complexity • Density • Hardenability • Processability • Flamability • Conductivity • Stability • Phobicity • Emissivity • Lubricity • and many many more!

GLOBAL HEADQUARTERS  
1172 W. CENTURY DR.  
LOUISVILLE, CO 80027  
+1.720.531.8996  
WWW.FORGENANO.COM



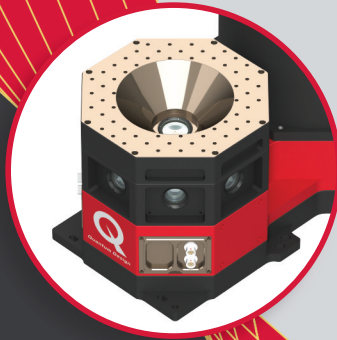
**FORGE NANO**  
Pioneering scalable nano coating technologies

# Instrumentation for Nextgen Quantum Technologies



## Materials Characterization

- PPMS® DynaCool & and MPMS® 3 SQUID Systems
- Magnetometry & Transport Options down to mK
- CryMOKE for 2D Materials
- Corelative Insitu Microscopy (AFM in SEM)
- Raman Spectroscopy for PPMS
- FMR Spectroscopy



## Optics & Cryogenics

- 7T Low Vibration Magneto-Optical Cryostat
- Multi-channel Single Photon (SNSPD) Detection System
- Time-Tagger & Time-to-Digital Converter
- Quantum Entanglement Demonstrator
- Education Kit for Quantum Sensing Using NV Centers
- Helium Liquefier & Recovery Systems

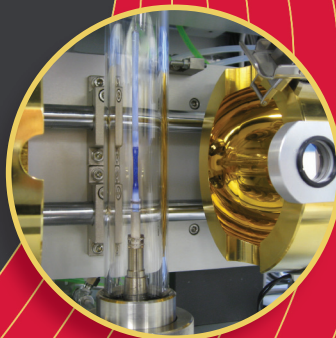


## Lithography

- Direct-Write Lithography
- Thermal Probe 3D Nanolithography
- E-Beam Lithography for SEM

## Sample Synthesis

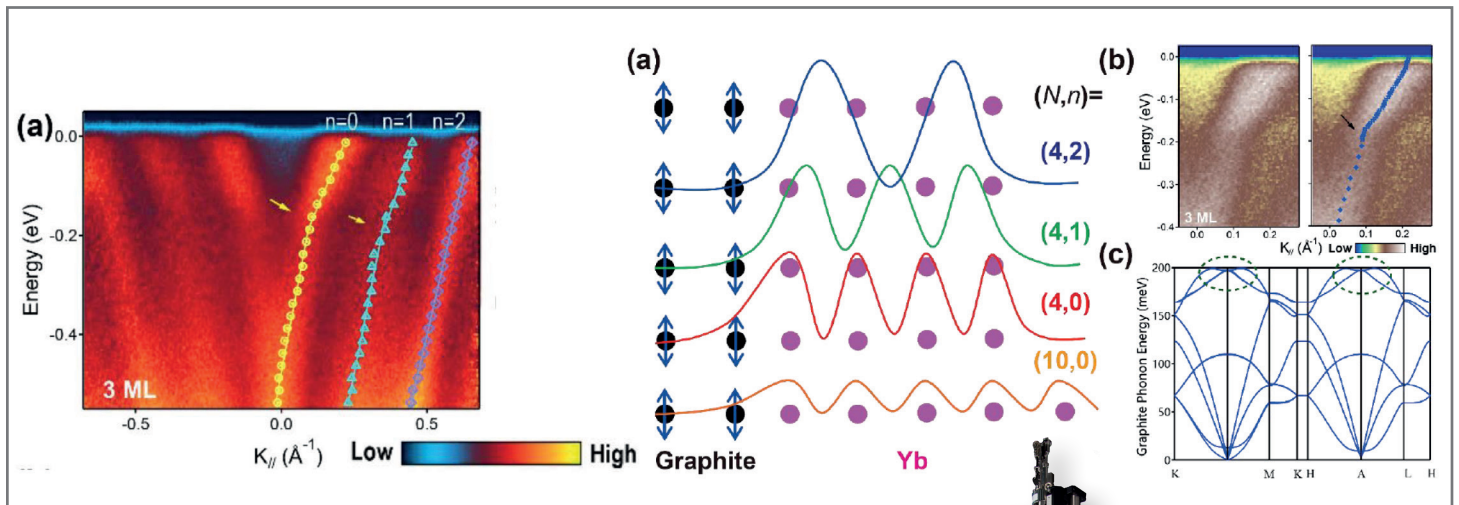
- Floating Zone IR Image furnace (3000° C)
- Tetra Arc Czochralski Furnace



10307 Pacific Center Court  
San Diego, CA 92121-4340  
info@qdusa.com  
[www.qdusa.com](http://www.qdusa.com)

## ARPES Lab

# Interfacial electron-phonon coupling in Yb thin films



In many thin films the electronic structure varies significantly with the exact amount of monolayers of the film. In this example, Yb films were grown with an exact film-thickness by MBE and then measured in ARPES.

An interfacial electron-phonon coupling between the Yb electrons and phonons of the underlying graphite lead to significant kinks in the bandstructure, which are most pronounced at a 4 monolayer film-thickness. The example shows, how nice MBE and ARPES can be used as platform to investigate innovative materials.

Please contact us for more information:

North America Headquarters

Scienta Omicron, Inc.

[sales-NA@scientaomicron.com](mailto:sales-NA@scientaomicron.com)

Equipment: ARPES-Lab, DA30-L analyser, VUV 5k, LHe cooled manipulator at 20 K, Lab10 MBE  
Yi Wu et al., arXiv:1906.08564 (2019)

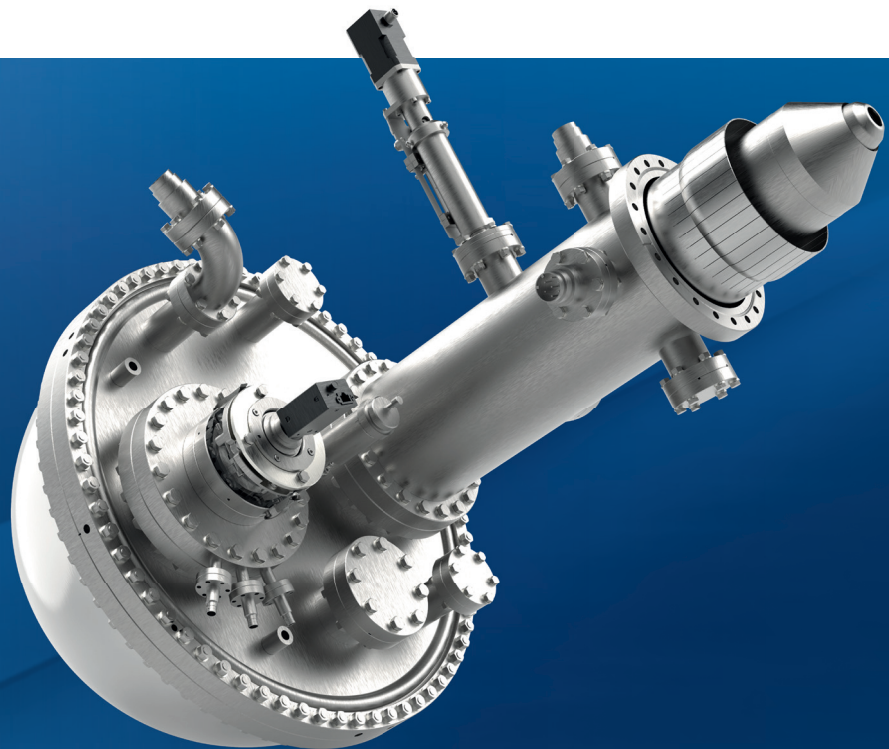


# ASTRAIOS 190

2D MOMENTUM MAPPING ELECTRON ANALYZER  
FOR UNRIVALED ARPES PERFORMANCE

## KEY FEATURES

- Single spot parallel shifting lens (patent applied)
- $\pm 30^\circ$  acceptance angle  
( $\pm 1 \text{ \AA}^{-1}$  (He I) |  $\pm 2.5 \text{ \AA}^{-1}$  ((S)XPS))
- k-resolution  $< 0.003 \text{ \AA}^{-1}$
- Energy resolution  $< 1.5 \text{ meV}$
- Motorized virtual entrance slit



SPECS-TII Inc.

T +1 (508) 618 1292  
E [usa@specs.com](mailto:usa@specs.com)  
H [www.specs-group.com](http://www.specs-group.com)

SPECS™

A member of SPECSGROUP

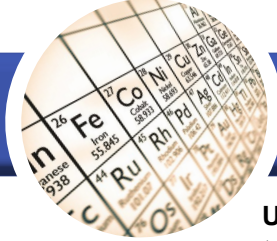


# UNITED MINERAL & CHEMICAL CORP.

160 Chubb Avenue, Suite 206, Lyndhurst, New Jersey 07071

(201) 507-3300 - [inquiry@umccorp.com](mailto:inquiry@umccorp.com)

[WWW.UMCCORP.COM](http://WWW.UMCCORP.COM)



## DEPOSITION PRODUCTS

United Mineral and Chemical Corp. has been a leading supplier of high purity source materials to the compound semiconductor industry and complimentary technologies for more than 35 years. World-wide sourcing and supply chain management enables manufacturers and researchers to efficiently purchase, with most products available for immediate shipment from local stock. Custom forms and shapes are also available for many items.

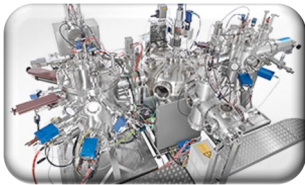
### ULTRA HIGH PURITY METALS FOR MBE

Aluminum	Antimony	Antimony Trioxide	Arsenic
Bismuth	Boron	Cadmium	Cadmium Selenide
Cadmium Telluride	Gallium	Gallium Phosphide	Gallium Telluride
Germanium	Mercury	Indium	Magnesium
Manganese	Red Phosphorus	Selenium	Silicon
Tellurium	Tin	Zinc	Zinc Selenide

UMC can also provide other MBE Grade Materials upon request.



### MOLECULAR BEAM EPITAXY [MBE] SYSTEMS AND COMPONENTS

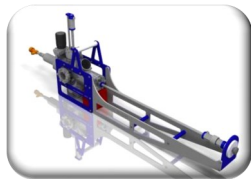


**MBE-Komponenten has more than 50 years of combined MBE industry experience in design, fabrication and use of effusion, evaporation, sublimation and gas sources. In addition, a wide range of crucibles and ancillary parts are available or can be produced for standard and modified MBE machines and equipment.**

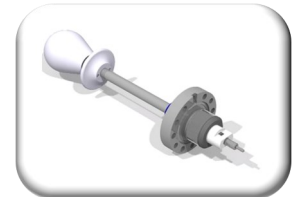


### WOBBLESTICKS AND UHV SUITCASES

**FERROVAC GMBH**  
ULTRA HIGH VACUUM TECHNOLOGY



**Ferrovac GmbH was founded in 1996 in Switzerland. Ferrovac's experts have profound knowledge of ultra high vacuum technology, experimental physics, scanning probe microscopy and are able to realize flexible solutions for various customer's requests. They set new standards for sample manipulation by the use and perpetual advancement of magnetically coupled manipulators. The systems allow reliable loading, transferring and manipulating of samples inside UHV multi chamber systems.**



### PULSED LASER DEPOSITION [PLD] SYSTEMS AND COMPONENTS



**TSST is specialized in the design and production of customized, thin film deposition equipment, with a focus on Pulsed Laser Deposition (PLD). TSST systems and components can be found at universities and research labs all over the world. With 20 years of experience and developed knowledge, TSST shares its expertise in the field of complex materials thin film growth with its customers.**



# PCSI-47 Schedule Overview

## Sunday:

- 1:00 p.m. Registration
- 2:30 p.m. Sunday Afternoon Session: *2D Heterostructure Design*
- 4:15 p.m. Coffee Break and Poster Setup
- 4:30 p.m. Sunday Afternoon Session: *Epitaxial Growth of Quantum Materials and Structures*
- 5:05 p.m. Poster Setup
- 6:00 p.m. Welcome Reception
- 7:30 p.m. Sunday Evening Session: *Single Photon Detectors*

## Monday:

- 7:30 a.m. Registration and Continental Breakfast
- 8:30 a.m. Monday Morning Session: *Oxides*
- 10:05 a.m. Coffee Break and Poster Viewing
- 11:00 a.m. Monday Morning Session: *Hybrid Materials*
- 12:00 p.m. Lunch and Poster Viewing
- 2:00 p.m. Monday Afternoon Session: *Catalysis/Nanowires*
- 3:15 p.m. Coffee Break and Poster Viewing
- 4:20 p.m. Monday Afternoon Session: *Dopants in Semiconductors*
- 6:00 p.m. Dinner
- 7:30 p.m. Monday Evening Session: *Superconductivity I*

## Tuesday:

- 7:30 a.m. Registration and Continental Breakfast
- 8:30 a.m. Tuesday Morning Session: *Magnetism*
- 10:05 a.m. Coffee Break and Poster Viewing
- 11:00 a.m. Tuesday Morning Session: *Superconductivity II*
- 12:00 p.m. Free Afternoon
- 7:00 p.m. Tuesday Evening Session: *The Future of PV*

## Wednesday:

- 7:30 a.m. Registration and Continental Breakfast
- 8:30 a.m. Wednesday Morning Session: *Optical Properties of 2D Materials*
- 9:45 a.m. Coffee Break and Poster Viewing
- 11:00 a.m. Wednesday Morning Session: *Material Modification and Self Assembly*
- 12:00 p.m. Lunch and Poster Viewing
- 2:00 p.m. Wednesday Afternoon Session: *Devices and Contacts*
- 3:25 p.m. Coffee Break and Poster Viewing
- 4:30 p.m. Wednesday Afternoon Session: *Synthesis of Materials for Devices*
- 6:30 p.m. Conference Banquet

## Thursday:

- 7:30 a.m. Registration and Continental Breakfast
- 8:30 a.m. Thursday Morning Session: *2D Materials - Strain and Heterostructures*
- 10:00 a.m. Coffee Break and Poster Viewing
- 11:00 a.m. Thursday Morning Session: *Material for Storage*
- 11:50 a.m. Conference Ends

# Sunday Afternoon, January 19, 2020

<b>Room Canyon/Sugarloaf</b>		
2:30pm	<b>PCSI-47 Opening Remarks</b>	<p style="text-align: center;"><b>PCSI-1SuA - 2D Heterostructure Design</b></p> <p><b>Moderator:</b> Edward Yu, The University of Texas at Austin</p>
2:35pm	<b>INVITED: PCSI-1SuA2</b> Optical Properties of Semiconducting Moiré Crystals, <i>Xiaoqin Elaine Li</i> , Univ of Texas at Austin	
2:40pm	Invited talk continues.	
2:45pm		
2:50pm		
2:55pm		
3:00pm		
3:05pm		
3:10pm		
3:15pm	<b>INVITED: PCSI-1SuA10</b> Berryogenesis: Spontaneous Out-of-Equilibrium Plasmonic Magnetism, <i>Justin Song</i> , Nanyang Technological University Singapore, Singapore	
3:20pm	Invited talk continues.	
3:25pm		
3:30pm		
3:35pm		
3:40pm		
3:45pm		
3:50pm		
3:55pm	<b>UPGRADED: PCSI-1SuA18</b> Investigation of Graphene/Ge(110) Interface, <i>Miriam Galbiati</i> , Technical University of Denmark, Denmark	
4:00pm	Upgraded talk continues.	
4:05pm		
4:10pm		
4:15pm	<b>Coffee Break and Poster Setup (Flagstaff/Trailridge Room)</b>	
4:20pm		
4:25pm		
4:30pm	<b>UPGRADED: PCSI-2SuA25</b> Epitaxial Growth and Electronic Characterization of GdSb, <i>Hadass Inbar</i> , <i>S. Chatterjee</i> , <i>M. Pendharkar</i> , <i>Y. Chang</i> , <i>M. Bocheff</i> , <i>T. Guo</i> , <i>T. Brown-Heft</i> , University of California, Santa Barbara; <i>A. Fedorov</i> , Lawrence Livermore National Laboratory; <i>D. Read</i> , Cardiff University; <i>C.J. Palmstrom</i> , University of California, Santa Barbara	<p style="text-align: center;"><b>PCSI-2SuA - Epitaxial Growth of Quantum Materials and Structures</b></p> <p><b>Moderator:</b> Seung Sae Hong, Stanford University</p>
4:35pm	Upgraded talk continues.	
4:40pm		
4:45pm		
4:50pm	<b>PCSI-2SuA29</b> MBE Growth of Zn <sub>x</sub> Cd <sub>1-x</sub> Te on Cd <sub>3</sub> As <sub>2</sub> , <i>Anthony Rice</i> , <i>K. Alberi</i> , National Renewable Energy Laboratory	
4:55pm	<b>PCSI-2SuA30</b> Interfaces and Growth of NbTiN-AlN Heterostructures on Sapphire as Epitaxial Josephson Junctions, <i>Chris Richardson</i> , <i>A. Thomas</i> , <i>A. Alexander</i> , <i>C. Weddle</i> , Laboratory for Physical Sciences; <i>B. Arey</i> , <i>M. Olszta</i> , PNNL	
5:00pm	<b>PCSI-2SuA31</b> Growth of AlN Barriers in Al/AlN/Al SIS Josephson Junctions by Low Temperature Atomic Layer Epitaxy, <i>Charles R. Eddy, Jr.</i> , U.S. Naval Research Laboratory; <i>D.J. Pennachio</i> , <i>J.S. Lee</i> , <i>A. McFadden</i> , University of California, Santa Barbara; <i>S.G. Rosenberg</i> , U.S. Naval Research Laboratory; <i>Y. Chang</i> , <i>C.J. Palmstrom</i> , University of California, Santa Barbara	
5:05pm	<b>Poster Setup (Flagstaff/Trailridge Room)</b>	
6:00pm	<b>Welcome Reception (Century Room)</b>	

# Sunday Evening, January 19, 2020

Room Canyon/Sugarloaf	
7:30pm	<b>INVITED: PSCI-SuE1</b> Theory of Single Photon Detection by a Photoreceptive Molecule and a Quantum Coherent Spin Center, <i>N. Harmon</i> , University of Evansville; <i>Michael Flatté</i> , University of Iowa
7:35pm	Invited talk continues.
7:40pm	
7:45pm	
7:50pm	
7:55pm	
8:00pm	
8:05pm	
8:10pm	<b>INVITED: PSCI-SuE9</b> From Dark Matter Detection to Artificial Intelligence: Uses for Superconducting Nanowire Single Photon Detectors, <i>Sae Woo Nam</i> , National Institute of Standards and Technology, USA
8:15pm	Invited talk continues.
8:20pm	
8:25pm	
8:30pm	
8:35pm	
8:40pm	
8:45pm	

## PSCI-SuE - Single Photon Detectors

**Moderator:** Christopher Palmstrom, University of California, Santa Barbara

# Monday Morning, January 20, 2020

<b>Room Canyon/Sugarloaf</b>	
8:30am	<b>INVITED: PCSI-1MoM1</b> MOCVD Epitaxy and Doping for $\beta$ -Ga <sub>2</sub> O <sub>3</sub> and (Al <sub>x</sub> Ga <sub>1-x</sub> ) <sub>2</sub> O <sub>3</sub> , <b>Hongping Zhao</b> , The Ohio State University
8:35am	Invited talk continues.
8:40am	
8:45am	
8:50am	
8:55am	
9:00am	
9:05am	
9:10am	
9:15am	<b>PCSI-1MoM10</b> Growth and Structures of Metal Dopant-Ceria Mixed Oxide Interfaces, <i>E. Ginting, L. Du, Jing Zhou</i> , University of Wyoming
9:20am	<b>INVITED: PCSI-1MoM11</b> Freestanding Crystalline Oxide Membranes and Heterostructures, <b>Seung Sae Hong</b> , Stanford University
9:25am	
9:30am	
9:35am	
9:40am	
9:45am	
9:50am	
9:55am	
10:00am	<b>PCSI-1MoM19</b> Effects of Annealing on Electronic Defects in $\beta$ -Ga <sub>2</sub> O <sub>3</sub> Revealed by Linearly-Polarized Photoluminescence (LPPL), <i>R. Sun, Y.K. Ooi, P. Ranga</i> , University of Utah; <i>M. Saleh, K.G. Lynn</i> , Washington State University; <i>S. Krishnamoorthy, Mike A. Scarpulla</i> , University of Utah
10:05am	<b>Coffee Break &amp; Poster Viewing (Flagstaff/Trailridge Room)</b>
10:10am	
10:15am	
10:20am	
10:25am	
10:30am	
10:35am	
10:40am	
10:45am	
10:50am	
10:55am	
11:00am	<b>INVITED: PCSI-2MoM31</b> Hybrid Perovskite-Based High Energy Photon Detectors, <b>Wanyi Nie</b> , Los Alamos National Laboratory
11:05am	Invited talk continues.
11:10am	
11:15am	
11:20am	
11:25am	
11:30am	
11:35am	
11:40am	
11:45am	<b>PCSI-2MoM40</b> Arrangement and Electronic Properties of Cobalt Phthalocyanine Molecules on B-Si(111)- $\sqrt{3} \times \sqrt{3} R 30^\circ$ , <b>Susi Lindner, M. Franz, M. Kubicki, S. Appelfeller, M. Dähne, H. Eisele</b> , Technische Universität Berlin, Germany
11:50am	<b>PCSI-2MoM41</b> Amino-Acids Detection with Modulation Doped and Surface Nanoengineered GaAs Schottky Diodes, <i>T. Alkhidir, M. Abi Jaoude</i> , KUST, United Arab Emirates; <i>D. Gater</i> , University College London, United Kingdom; <i>C. Alpha</i> , Cornell University; <b>Abdel Isakovic</b> , Colgate University
11:55am	<b>PCSI-2MoM42</b> Carrier Collection and Transport at Interface of Lead-Free Halide Perovskites (FA,MA)SnI <sub>3</sub> Solar Cells, <b>William Jo</b> , Ewha Womans University, Republic of Korea
12:00pm	<b>Lunch (Century/Millennium Room) and Poster Viewing (Flagstaff/Trailridge Room)</b>

## PCSI-1MoM - Oxides

**Moderator:** Tohru Honda, Kogakuin University

## PCSI-2MoM - Hybrid Materials

**Moderator:** Joseph Berry, National Renewable Energy Laboratory

# Monday Afternoon, January 20, 2020

Room Canyon/Sugarloaf		
2:00pm	<b>INVITED: PCSI-1MoA1</b> Engineering Active and Stable Semiconductor Photoelectrodes by Atomic Layer Deposition, <i>Ian Sharp</i> , Walter Schottky Institut/Technische Universität München, Germany  Invited talk continues.	<b>PCSI-1MoA - Catalysis/Nanowires</b>  <b>Moderators:</b> Charles R. Eddy, Jr., U.S. Naval Research Laboratory, Hongping Zhao, The Ohio State University
2:05pm		
2:10pm		
2:15pm		
2:20pm		
2:25pm		
2:30pm		
2:35pm		
2:40pm	<b>PCSI-1MoA9</b> Surface States Induced Catalyst-free CO Sensing at GaN and AlGa <sub>N</sub> /GaN Heterostructures, <i>Monu Mishra</i> , Indian Institute of Technology Delhi; <i>G. Gupta</i> , National Physical Laboratory, India	
2:45pm	<b>PCSI-1MoA10</b> Cu <sub>2</sub> O Nanoparticles for Enhancing Gas Phase Photocatalysis over Metal Oxide Semiconductor Nanostructures, <i>Hikaru Masegi</i> , Keio University, Japan	
2:50pm	<b>PCSI-1MoA11</b> UPGRADED: Self-Selective Formation of 1D and 2D GaBi Structures on GaAs, <i>Y. Liu</i> , Lund University, Sweden; <i>S. Benter, J. Knutsson, S. Lehmann</i> , Lund University; <i>E. Young, N. Wilson, C.J. Palmstrom</i> , University of California, Santa Barbara; <i>A. Mikkelsen, Rainer Timm</i> , Lund University, Sweden  Upgraded talk continues.	
2:55pm		
3:00pm		
3:05pm		
3:10pm	<b>PCSI-1MoA15</b> Iuliacumite: A Novel Two-Dimensional Chemical Short Range Order in a Wurtzite Single Monolayer InAs <sub>1-x</sub> Sb <sub>x</sub> Shell on InAs Nanowires, <i>Michael Schnedler</i> , Forschungszentrum Jülich, Germany; <i>T. Xu, I. Lefebvre, J.-P. Nys</i> , Université Lille, CNRS, Centrale Lille, ISEN, Université Valenciennes, France; <i>S. Plissard</i> , Université Lille, CNRS, Centrale Lille, ISEN, Université Valenciennes, Germany; <i>M. Berthe</i> , Université Lille, CNRS, Centrale Lille, ISEN, Université Valenciennes, France; <i>H. Eisele</i> , Technische Universität Berlin, Germany; <i>R. Dunin-Borkowski, P. Ebert</i> , Forschungszentrum Jülich, Germany; <i>B. Grandier</i> , Université Lille, CNRS, Centrale Lille, ISEN, Université Valenciennes, France	
3:15pm	<b>Coffee Break &amp; Poster Viewing (Flagstaff/Trailridge Room)</b>	
3:20pm		
3:25pm		
3:30pm		
3:35pm		
3:40pm		
3:45pm		
3:50pm		
3:55pm		
4:00pm		
4:05pm		
4:10pm		
4:15pm		
4:20pm	<b>INVITED: PCSI-2MoA29</b> Control of Spin-Orbit Coupling in Single Acceptor States in Silicon, <i>Sven Rogge</i> , University of New South Wales, Australia  Invited talk continues.	<b>PCSI-2MoA - Dopants in Semiconductors</b>  <b>Moderator:</b> John Robertson, University of Cambridge
4:25pm		
4:30pm		
4:35pm		
4:40pm		
4:45pm		
4:50pm		
4:55pm		

# Monday Afternoon, January 20, 2020

5:00pm	<p><b>PCSI-2MoA37 UPGRADED:</b> Low-Temperature Epitaxial Silicon Growth and Confinement of Delta Doped Si:P Nanostructures, <b>Scott Schmucker</b>, <i>E. Anderson, J. Lucero, E. Bussmann, P. Lu, A. Katzenmeyer, T. Luk, T. Beechem, L. Tracy, T.-M. Lu, A. Grine, D. Ward, D. Campbell, P. Gamache, M. Gunter, S. Misra</i>, Sandia National Laboratories</p> <p>Upgraded talk continues.</p>
5:05pm	
5:10pm	
5:15pm	
5:20pm	
5:25pm	
5:30pm	
5:35pm	
5:40pm	
5:45pm	
5:50pm	
5:55pm	
6:00pm	<p><b>Dinner (Century/Millennium Room)</b></p>

# Monday Evening, January 20, 2020

Room Canyon/Sugarloaf	
7:30pm	<b>INVITED: PCSI-MoE1</b> Fluctuating High Temperature Superconductivity in Monolayer FeSe / SrTiO <sub>3</sub> , <i>Kyle Shen, B. Faeth, S. Yang, D. Schlom</i> , Cornell University
7:35pm	Invited talk continues.
7:40pm	
7:45pm	
7:50pm	
7:55pm	
8:00pm	
8:05pm	
8:10pm	<b>PCSI-MoE9</b> Advances and Possibilities of the Materials Innovation Platform with Examples from Spin-ARPES, <i>Daniel Beaton</i> , Scienta Omicron Inc.
8:15pm	<b>INVITED: PCSI-MoE10</b> Superconductivity at Surfaces Studied by Scanning Tunneling Microscopy, <i>Yukio Hasegawa</i> , The University of Tokyo, Japan
8:20pm	Invited talk continues.
8:25pm	
8:30pm	
8:35pm	
8:40pm	
8:45pm	
8:50pm	

**PCSI-MoE - Superconductivity I**

**Moderator:** David Pappas, NIST



# Tuesday Morning, January 21, 2020

<b>Room Canyon/Sugarloaf</b>		
8:30am	<b>INVITED: PCSI-1TuM1</b> Quantum Microscopy of Nanoscale Materials and Devices, <i>Christian Degen</i> , ETH Zurich, Switzerland	<b>PCSI-1TuM - Magnetism</b>  <b>Moderator:</b> Michael Flatté, University of Iowa
8:35am	Invited talk continues.	
8:40am		
8:45am		
8:50am		
8:55am		
9:00am		
9:05am		
9:10am		
9:15am	Upgraded talk continues.	
9:20am		
9:25am		
9:30am	<b>PCSI-1TuM13</b> Room Temperature Ferromagnetic Monolayer MnGaN-2D Investigated by Spin-polarized Scanning Tunneling Microscopy/ Spectroscopy and First-principles Density Functional Theory, <i>Y. Ma, T. Erickson</i> , Nanoscale & Quantum Phenomena Institute; <i>K.Y. Meng, F.-Y. Yang</i> , The Ohio State University; <i>D. Hunt, A. Barral, V. Ferrari</i> , CAC-CNEA, Argentina; <i>A.R. Smith</i> , Nanoscale & Quantum Phenomena Institute	
9:35am	<b>UPGRADED: PCSI-1TuM14</b> Local Exchange Resonance in DC Magnetoresistance of Spin-Polarized Current Through a Dopant, <i>Stephen McMillan</i> , University of Iowa; <i>N. Harmon</i> , University of Evansville; <i>M. Flatté</i> , University of Iowa	
9:40am	Upgraded talk continues.	
9:45am		
9:50am		
9:55am	<b>PCSI-1TuM18</b> Room Temperature Ferromagnetism in GaSb Thin Films Doped with Mn, <i>A.O. Pulzara Mora, Camilo Andres Pulzara Mora</i> , Universidad Nacional de Colombia, Colombia	
10:00am	<b>PCSI-1TuM19</b> Magnetotransport Studies in Hybrid 2D/0D Nanostructures, <i>Ethel Perez-Hoyos, Y. Luo, A. Dehankar, J. Xu, D. Pharis, J. Winter, R. Kawakami, E. Johnston-Halperin</i> , The Ohio State University	
10:05am	<b>Coffee Break &amp; Poster Viewing (Flagstaff/Trailridge Room)</b>	
10:10am		
10:15am		
10:20am		
10:25am		
10:30am		
10:35am		
10:40am		
10:45am		
10:50am		
10:55am		
11:00am	<b>INVITED: PCSI-2TuM31</b> Fabrication of High Coherence Superconducting Qubits, <i>J. Long, H.S. Ku, X. Wu</i> , NIST; <i>R. Lake</i> , BlueFors; <i>David Pappas</i> , NIST	<b>PCSI-2TuM - Superconductivity II</b>  <b>Moderator:</b> Kyle Shen, Cornell University
11:05am	Invited talk continues.	
11:10am		
11:15am		
11:20am		
11:25am		
11:30am		
11:35am		
11:40am		
11:45am	Upgraded talk continues.	
11:55am		
12:00pm	<b>Free Afternoon</b>	

# Tuesday Evening, January 21, 2020

Room Canyon/Sugarloaf	
7:00pm	<p><b>INVITED: PCSI-TuE1</b> Progress in Hybrid Perovskite Photovoltaics and Optoelectronics, <i>Joseph Berry</i>, National Renewable Energy Laboratory</p> <p>Invited talk continues.</p>
7:05pm	
7:10pm	
7:15pm	
7:20pm	
7:25pm	
7:30pm	
7:35pm	
7:40pm	<p><b>INVITED: PCSI-TuE9</b> On the Path Towards Tandem Junction Nanowire Based Solar Cells, <i>Magnus Borgström</i>, Lund University, Sweden</p> <p>Invited talk continues.</p>
7:45pm	
7:50pm	
7:55pm	
8:00pm	
8:05pm	
8:10pm	
8:15pm	

## PCSI-TuE - The Future of PV

**Moderator:** Kirstin Alberi, National Renewable Energy Laboratory

# Wednesday Morning, January 22, 2020

Room Canyon/Sugarloaf		
8:30am	<b>INVITED: PCSI-1WeM1</b> Metals at the Atomic Limit, <i>Joshua Robinson</i> , Penn State University Invited talk continues.	<b>PCSI-1WeM - Optical Properties of 2D Materials</b>  <b>Moderator:</b> Wanyi Nie, Los Alamos National Laboratory
8:35am		
8:40am		
8:45am		
8:50am		
8:55am		
9:00am		
9:05am		
9:10am	<b>PCSI-1WeM9</b> Tuning the Spontaneous Emission of Monolayer Wse <sub>2</sub> by Optical Environment Control – Cavity Coupling and Substrate Manipulation, <i>Hyunseung Lee</i> , Ajou University, Republic of Korea	
9:15am	<b>PCSI-1WeM10</b> First Principles Study on Optical Properties of Monolayer Bismuthene under an Electric Field, <i>Wei-Chieh Liu, L.L. Xu, M.C. Lin</i> , Hanyang University, South Korea; <i>T.C. Leung, H.Y. Hsu</i> , National Taipei University of Technology, Republic of China	
9:20am	<b>PCSI-1WeM11</b> Formation of Coherent Phase Domain Heterojunctions in Single Layer MoS <sub>2</sub> on Au(111), <i>Fanglue Wu, Z. Liu</i> , Texas A&M University; <i>M. Chandross</i> , Sandia National Laboratories; <i>Q. Moore</i> , Texas A&M University; <i>N. Argibay, J. Curry</i> , Sandia National Laboratories; <i>J. Batteas</i> , Texas A&M University	
9:25am	<b>UPGRADED: PCSI-1WeM12</b> Effects of Electromechanical Coupling in Locally Strained Monolayer MoS <sub>2</sub> , <i>Alex De Palma, G. Cossio, K. Jones, J. Quan</i> , The University of Texas at Austin; <i>X.E. Li</i> , Univ of Texas at Austin; <i>E. Yu</i> , The University of Texas at Austin  Upgraded talk continues.	
9:30am		
9:35am		
9:40am		
9:45am	<b>Coffee Break &amp; Poster Viewing (Flagstaff/Trailridge Room)</b>	
9:50am		
9:55am		
10:00am		
10:05am		
10:10am		
10:15am		
10:20am		
10:25am		
10:30am		
10:35am		
10:40am		
10:45am		
10:50am		
10:55am		
11:00am	<b>INVITED: PCSI-2WeM31</b> Neuromorphic Computing with the Redox Transistor, <i>Alec Talin</i> , Sandia National Laboratories Invited talk continues.	<b>PCSI-2WeM - Material Modification and Self Assembly</b>  <b>Moderator:</b> Sven Rogge, UNSW
11:05am		
11:10am		
11:15am		
11:20am		
11:25am		
11:30am		
11:35am		

# Wednesday Morning, January 22, 2020

11:40am	<b>PCSI-2WeM39</b> Kinetically-Driven Assembly of TaS <sub>2</sub> -SnS Heterostructures with Flexible Stacking Architectures, <i>Dennice Roberts</i> , National Renewable Energy Laboratory; <i>D. Bardgett</i> , University of Oregon; <i>B. Gorman</i> , Colorado School of Mines; <i>J. Perkins</i> , <i>A. Zakutayev</i> , <i>S. Bauers</i> , National Renewable Energy Laboratory	
11:45am	<b>PCSI-2WeM40</b> Globally Aligned Single-Wall Carbon Nanotube Films through Electrostatic Ordering, <i>Joshua Walker</i> , University of Wyoming; <i>J. Fagan</i> , <i>A. Biacchi</i> , National Institute of Standards and Technology; <i>V. Kuehl</i> , University of Wyoming; <i>T. Searles</i> , Howard University; <i>A. Hight Walker</i> , National Institute of Standards and Technology; <i>W. Rice</i> , University of Wyoming	
11:50am	<b>PCSI-2WeM41</b> Defining Insulating Regions on TiO <sub>2</sub> Thin Films by Laser Heating, <i>S. Ahmed</i> , <i>J. Ritter</i> , <b>Matt McCluskey</b> , Washington State University	
11:55am	<b>PCSI-2WeM42</b> Towards Mask Free Direct Write fabrication of Micro- and Nanoscale Architectures on Different Substrates via Aqueous Ink Precursors and CVD Synthesis, <i>Irma Kuljanishvili</i> , <i>D. Alameri</i> , <i>D. Karbach</i> , <i>R. Dong</i> , <i>L. Moore</i> , Saint Louis University; <i>R. Divan</i> , <i>Y. Liu</i> , Argonne National Laboratory	
12:00pm	<b>Lunch (Century/Millennium Room) and Poster Viewing (Flagstaff/Trailridge Room)</b>	

# Wednesday Afternoon, January 22, 2020

Room Canyon/Sugarloaf		
2:00pm	<p><b>INVITED: PCSI-1WeA1</b> Towards Fermi Level De-pinning at Contacts, <i>John Robertson</i>, Cambridge University, UK; <i>Y. Guo</i>, Wuhan University, China; <i>Z. Zhang</i>, Cambridge University, UK</p> <p>Invited talk continues.</p>	<p><b>PCSI-1WeA - Devices and Contacts</b></p> <p><b>Moderator:</b> Alex Demkov, The University of Texas</p>
2:05pm		
2:10pm		
2:15pm		
2:20pm		
2:25pm		
2:30pm		
2:35pm		
2:40pm	<p><b>PCSI-1WeA9</b> Observation, Characterization, and Mitigation of the Internal <math>p</math>-<math>n</math> Junction in Pyrite FeS<sub>2</sub>, a Potential Low-cost Solar Absorber, <i>Bryan Voigt, W. Moore, J. Walter, B. Das, M. Maiti, M. Manno</i>, University of Minnesota; <i>E. Aydil</i>, New York University; <i>C. Leighton</i>, University of Minnesota</p>	
2:45pm	<p><b>UPGRADED: PCSI-1WeA10</b> Photo-Driven Dipole Reordering: Key to Carrier Separation in Metalorganic Halide Perovskites, <i>Philipp Ebert</i>, Forschungszentrum Jülich, Germany; <i>H.-C. Hsu</i>, National Taiwan University, Republic of China; <i>B.-C. Huang</i>, Academia Sinica, Republic of China; <i>S.-C. Chin</i>, National Taiwan University, Republic of China; <i>C.-R. Hsing, D.-L. Nguyen</i>, Academia Sinica, Republic of China; <i>M. Schnedler</i>, Forschungszentrum Jülich, Germany; <i>R. Sankar</i>, Academia Sinica, Republic of China; <i>R. Dunin-Borkowski</i>, Forschungszentrum Jülich, Germany; <i>C.-M. Wei</i>, Academia Sinica, Republic of China; <i>C.-W. Chen, Y.-P. Chiu</i>, National Taiwan University, Republic of China</p> <p>Upgraded talk continues.</p>	
2:50pm		
2:55pm		
3:00pm		
3:05pm	<p><b>PCSI-1WeA14</b> First Principles Study on Electronic Properties of Graphene Nanostructures for High Current Density Cathode, <i>Nan Zhao, L.L. Xu, M.C. Lin</i>, Hanyang University, South Korea; <i>T.C. Leung</i>, National Chung Cheng University, Republic of China; <i>H.Y. Hsu</i>, National Taipei University of Technology, Republic of China</p>	
3:10pm	<p><b>PCSI-1WeA15</b> Band Offset Modulation in Si-EuO Heterostructures <i>via</i> Controlled Interface Formation, <i>W. Li, A. Posadas</i>, The University of Texas at Austin; <i>Alex Demkov</i>, The University of Texas</p>	
3:15pm	<p><b>PCSI-1WeA16</b> First Principles Study on Electronic Properties of Magnetite for Spin Polarized Emission under an Electric Field, <i>Liang liang Xu, N. Zhao, M.C. Lin</i>, Hanyang University, South Korea; <i>T.C. Leung</i>, National Chung Cheng University, Republic of China; <i>H.Y. Hsu</i>, National Taipei University of Technology, Republic of China</p>	
3:20pm	<p><b>PCSI-1WeA17</b> Work Functions of Alkali and Alkaline Earth Metal Surfaces under Electric Fields based on First-Principles Calculations, <i>Y. Wang, L.L. Xu, Ming-Chieh Lin</i>, Hanyang University, South Korea; <i>T.C. Leung</i>, National Chung Cheng University, Republic of China; <i>H.Y. Hsu</i>, National Taipei University of Technology, Republic of China</p>	
3:25pm	<p><b>Coffee Break &amp; Poster Viewing (Flagstaff/Trailridge Room)</b></p>	
3:30pm		
3:35pm		
3:40pm		
3:45pm		
3:50pm		
3:55pm		
4:00pm		
4:05pm		
4:10pm		
4:15pm		
4:20pm		
4:25pm		

# Wednesday Afternoon, January 22, 2020

4:30pm	<b>INVITED: PCSI-2WeA31</b> Nitrogen Doping of Gallium Oxide by Ion Implantation and its Application to Vertical Transistors, <b>Masataka Higashiwaki</b> , National Institute of Information and Communications Technology, Japan; <b>M.H. Wong</b> , National Institute of Information and Communications Technology; <b>K. Goto</b> , <b>H. Murakami</b> , <b>Y. Kumagai</b> , Tokyo University of Agriculture and Technology, Japan  Invited talk continues.	<b>PCSI-2WeA - Synthesis of Materials for Devices</b>  <b>Moderator:</b> Alec Talin, Sandia National Laboratories
4:35pm		
4:40pm		
4:45pm		
4:50pm		
4:55pm		
5:00pm		
5:05pm		
5:10pm	<b>PCSI-2WeA39</b> Studying the Nucleation of GaP on v-Grooved Si for III-V/Si Device Integration, <b>Emily Warren</b> , National Renewable Energy Laboratory; <b>T. Saenz</b> , Colorado School of Mines; <b>A. Norman</b> , National Renewable Energy Laboratory; <b>J. Zimmerman</b> , Colorado School of Mines	
5:15pm	<b>PCSI-2WeA40</b> Improving Heterointerfaces in Rapidly Grown III-V Electronic Devices using Dynamic Hydride Vapor Phase Epitaxy (D-HVPE), <b>Dennice Roberts</b> , <b>J. Simon</b> , <b>K. Schulte</b> , <b>A. Ptak</b> , National Renewable Energy Laboratory	
5:20pm	<b>PCSI-2WeA41</b> Real-Time Optical Monitoring of the Epitaxial Growth of Zincblende Semiconductors, <b>Alfonso Lastras-Martinez</b> , Universidad Autónoma de San Luis Potosí, México	
5:25pm	<b>PCSI-2WeA42</b> Pulsed Laser Deposition of Epitaxial Sr <sub>3</sub> Al <sub>2</sub> O <sub>6</sub> as a Water-Soluble Sacrificial Layer for GaAs Deposition, <b>Imran Khan</b> , <b>B. McMahan</b> , <b>A. Norman</b> , <b>A. Zakutayev</b> , National Renewable Energy Laboratory	
5:30pm	<b>PCSI-2WeA43</b> On the Theory of the Energetic Spectrum of Vicinal Superlattices: The Role of Crystal Potential, <b>Victor Petrov</b> , Russian Academy of Sciences, Russian Federation	
5:35pm	<b>PCSI-2WeA44</b> Epitaxial Relationship of Cu <sub>3</sub> N Grown on YSZ(001) Substrate by Mist CVD Method, <b>Nao Wakabayashi</b> , Kogakuin University, Japan	
5:40pm	<b>UPGRADED: PCSI-2WeA45</b> Halogen Surface Chemistries for Atomically Precise Manufacturing on Si(100), <b>Kevin Dwyer</b> , <b>M. Dreyer</b> , <b>K. Gaskell</b> , University of Maryland; <b>R. Butera</b> , Laboratory for Physical Sciences  Upgraded talk continues.	
5:45pm		
5:50pm		
5:55pm		
6:00pm	<b>PCSI-2WeA49</b> Novel Growth Mechanisms in van der Waals Epitaxy: 3D Morphologies of Bi <sub>2</sub> Se <sub>3</sub> , <b>Theresa Ginley</b> , <b>S. Law</b> , University of Delaware	
6:30pm	<b>Conference Banquet (Century/Millennium Room)</b>	

# Thursday Morning, January 23, 2020

Room Canyon/Sugarloaf		
8:30am	<b>INVITED: PCSI-1ThM1</b> Electron Transport in Strain-Engineered Graphene, <i>Nadya Mason</i> , University of Illinois at Urbana Champaign	<b>PCSI-1ThM - 2D Materials - Strain and Heterostructures</b>  <b>Moderator:</b> Joshua Robinson, Penn State University
8:35am	Invited talk continues.	
8:40am		
8:45am		
8:50am		
8:55am		
9:00am		
9:05am		
9:10am		
9:15am	Upgraded talk continues.	
9:20am		
9:25am		
9:30am	<b>PCSI-1ThM13</b> Optical Determination of Ice-Induced Interfacial Strain on Single-Layer Graphene, <i>Subash Kattel, J. Murphy, S. Pasco, J. Ackerman, V. Alvarado, W.D. Rice</i> , University of Wyoming	
9:35am	<b>UPGRADED: PCSI-1ThM14</b> Electron Pairing by Remote-Phonon Scattering in Oxide-Supported Graphene, <i>D. Shin</i> , The University of Texas; <i>M. Fischetti</i> , The University of Texas at Dallas; <i>Alex Demkov</i> , The University of Texas	
9:40am	Upgraded talk continues.	
9:45am		
9:50am		
9:55am		
10:00am		<b>Coffee Break &amp; Poster Viewing (Flagstaff/Trailridge Room)</b>
10:05am		
10:10am		
10:15am		
10:20am		
10:25am		
10:30am		
10:35am		
10:40am		
10:45am		
10:50am		
10:55am		
11:00am	<b>INVITED: PCSI-2ThM31</b> Modeling of Interfaces in All-Solid-State Li-ion Batteries, <i>Yue Qi</i> , Michigan State University	<b>PCSI-2ThM - Material for Storage</b>  <b>Moderator:</b> Ian Sharp, Walter Schottky Institut/Technische Universität München
11:05am	Invited talk continues.	
11:10am		
11:15am		
11:20am		
11:25am		
11:30am		
11:35am		
11:40am		
11:45am	<b>PCSI-2ThM40</b> Properties of Two-Dimensional Titanium Carbide (Ti <sub>3</sub> C <sub>2</sub> T <sub>x</sub> ) MXene for Energy Conversion: Effects of Interlayer Spacing, Flake Size and Electrochemical Environment, <i>Sanju Gupta, W. Ringo</i> , Western Kentucky University; <i>M. Hu, X. Wang</i> , Chinese Academy of Sciences, China	
11:50am	<b>Conference Ends</b>	

**Bold page numbers indicate presenter**

— A —

Abi Jaoude, M.: PCSI-2MoM41, 11  
 Ackerman, J.: PCSI-1ThM13, 21  
 Ahmed, S.: PCSI-2WeM41, 18  
 Ahn, Y.H.: PCSI-1TuM9, 15  
 Alameri, D.: PCSI-2WeM42, 18  
 Alberi, K.: PCSI-2SuA29, 9  
 Alexander, A.: PCSI-2SuA30, 9  
 Alkhalid, T.: PCSI-2MoM41, 11  
 Alpha, C.: PCSI-2MoM41, 11  
 Altoe, V.: PCSI-2TuM39, 15  
 Alvarado, V.: PCSI-1ThM13, 21  
 Anderson, E.: PCSI-2MoA37, 13  
 Appelfeller, S.: PCSI-2MoM40, 11  
 Arey, B.: PCSI-2SuA30, 9  
 Argibay, N.: PCSI-1WeM11, 17  
 Aydil, E.: PCSI-1WeA9, 19

— B —

Bannerjee, A.: PCSI-2TuM39, 15  
 Bardgett, D.: PCSI-2WeM39, 18  
 Barral, A.: PCSI-1TuM13, 15  
 Batteas, J.: PCSI-1WeM11, 17  
 Bauers, S.: PCSI-2WeM39, 18  
 Beaton, D.: PCSI-MoE9, 14  
 Beechem, T.: PCSI-2MoA37, 13  
 Benter, S.: PCSI-1MoA11, 12  
 Berry, J.: PCSI-TuE1, 16  
 Berthe, M.: PCSI-1MoA15, 12  
 Biacchi, A.: PCSI-2WeM40, 18  
 Bocheff, M.: PCSI-2SuA25, 9  
 Borgström, M.: PCSI-TuE9, 16  
 Brown-Heft, T.: PCSI-2SuA25, 9  
 Bruckmann, C.: PCSI-1MoM9, 11  
 Bussmann, E.: PCSI-2MoA37, 13  
 Butera, R.: PCSI-2WeA45, 20

— C —

Cabrini, S.: PCSI-2TuM39, 15  
 Campbell, D.: PCSI-2MoA37, 13  
 Chandross, M.: PCSI-1WeM11, 17  
 Chang, Y.: PCSI-2SuA25, 9; PCSI-2SuA31, 9  
 Chatterjee, S.: PCSI-2SuA25, 9  
 Chen, C.-W.: PCSI-1WeA10, 19  
 Chin, S.-C.: PCSI-1WeA10, 19  
 Chiu, Y.-P.: PCSI-1WeA10, 19  
 Cossio, G.: PCSI-1WeM12, 17  
 Courtade, E.: PCSI-1ThM9, 21  
 Crooker, S.A.: PCSI-1ThM9, 21  
 Curry, J.: PCSI-1WeM11, 17

— D —

Dähne, M.: PCSI-2MoM40, 11  
 Das, B.: PCSI-1WeA9, 19  
 De Palma, A.: PCSI-1WeM12, 17  
 Degen, J.: PCSI-1TuM1, 15  
 Dehankar, A.: PCSI-1TuM19, 15  
 Demkov, A.: PCSI-1ThM14, 21; PCSI-1WeA15, 19  
 Dimakis, N.: PCSI-2ThM39, 21  
 Divan, R.: PCSI-2WeM42, 18  
 Dong, R.: PCSI-2WeM42, 18  
 Dreyer, M.: PCSI-2WeA45, 20  
 Du, L.: PCSI-1MoM10, 11  
 Dunin-Borkowski, R.: PCSI-1MoA15, 12; PCSI-1WeA10, 19  
 Dwyer, K.: PCSI-2WeA45, 20

— E —

Ebert, P.: PCSI-1MoA15, 12; PCSI-1WeA10, 19  
 Eddy, Jr., C.R.: PCSI-2SuA31, 9  
 Eisele, H.: PCSI-1MoA15, 12; PCSI-1MoM9, 11; PCSI-2MoM40, 11  
 Erickson, T.: PCSI-1TuM13, 15

— F —

Faeth, B.: PCSI-MoE1, 14  
 Fagan, J.: PCSI-2WeM40, 18

Fedorov, A.: PCSI-2SuA25, 9  
 Ferrari, V.: PCSI-1TuM13, 15  
 Fischetti, M.: PCSI-1ThM14, 21  
 Flatté, M.: PCSI-1TuM14, 15; PSCI-SuE1, 10  
 Franz, M.: PCSI-2MoM40, 11

— G —

Galazka, Z.: PCSI-1MoM9, 11  
 Galbiati, M.: PCSI-1SuA18, 9  
 Gamache, P.: PCSI-2MoA37, 13  
 Gaskell, K.: PCSI-2WeA45, 20  
 Gater, D.: PCSI-2MoM41, 11  
 Ginley, T.: PCSI-2WeA49, 20  
 Ginting, E.: PCSI-1MoM10, 11  
 Gorman, B.: PCSI-2WeM39, 18  
 Goryca, M.: PCSI-1ThM9, 21  
 Goto, K.: PCSI-2WeA31, 19  
 Grandidier, B.: PCSI-1MoA15, 12  
 Griffin, S.: PCSI-2TuM39, 15  
 Grine, A.: PCSI-2MoA37, 13  
 Gunter, M.: PCSI-2MoA37, 13  
 Guo, T.: PCSI-2SuA25, 9  
 Guo, Y.: PCSI-1WeA1, 19  
 Gupta, G.: PCSI-1MoA9, 12  
 Gupta, S.: PCSI-2ThM39, 21; PCSI-2ThM40, 21

— H —

Harmon, N.: PCSI-1TuM14, 15; PSCI-SuE1, 10  
 Hasegawa, Y.: PCSI-MoE10, 14  
 Higashiwaki, M.: PCSI-2WeA31, 20  
 Hight Walker, A.: PCSI-2WeM40, 18  
 Hofmann, J.: PCSI-1MoM9, 11  
 Hong, S.S.: PCSI-1MoM11, 11  
 Hsing, C.-R.: PCSI-1WeA10, 19  
 Hsu, H.-C.: PCSI-1WeA10, 19  
 Hsu, H.Y.: PCSI-1WeA14, 19; PCSI-1WeA16, 19; PCSI-1WeA17, 19; PCSI-1WeM10, 17  
 Hu, M.: PCSI-2ThM40, 21  
 Huang, B.-C.: PCSI-1WeA10, 19  
 Hunt, D.: PCSI-1TuM13, 15

— I —

Inbar, H.: PCSI-2SuA25, 9  
 Isakovic, A.: PCSI-2MoM41, 11

— J —

Jo, W.: PCSI-2MoM42, 11  
 Johnston-Halperin, E.: PCSI-1TuM19, 15  
 Jones, K.: PCSI-1WeM12, 17

— K —

Karbach, D.: PCSI-2WeM42, 18  
 Kattel, S.: PCSI-1ThM13, 21  
 Katzenmeyer, A.: PCSI-2MoA37, 13  
 Kawakami, R.: PCSI-1TuM19, 15  
 Khan, I.: PCSI-2WeA42, 20  
 Kim, K.H.: PCSI-1TuM9, 15  
 Knutsson, J.: PCSI-1MoA11, 12  
 Kriekebaum, J.M.: PCSI-2TuM39, 15  
 Krishnamoorthy, S.: PCSI-1MoM19, 11  
 Ku, H.S.: PCSI-2TuM31, 15  
 Kubicki, M.: PCSI-2MoM40, 11  
 Kuehl, V.: PCSI-2WeM40, 18  
 Kuljanishvili, I.: PCSI-2WeM42, 18  
 Kumagai, Y.: PCSI-2WeA31, 19

— L —

Lake, R.: PCSI-2TuM31, 15  
 Lastras-Martinez, A.: PCSI-2WeA41, 20  
 Law, S.: PCSI-2WeA49, 20  
 Lee, H.: PCSI-1WeM9, 17  
 Lee, H.W.: PCSI-1TuM9, 15  
 Lee, J.: PCSI-1TuM9, 15  
 Lee, J.S.: PCSI-2SuA31, 9  
 Lefebvre, I.: PCSI-1MoA15, 12  
 Lehmann, S.: PCSI-1MoA11, 12  
 Leighton, C.: PCSI-1WeA9, 19  
 Leung, T.C.: PCSI-1WeA14, 19; PCSI-1WeA16, 19; PCSI-1WeA17, 19; PCSI-1WeM10, 17

Li, J.: PCSI-1ThM9, 21  
 Li, W.: PCSI-1WeA15, 19  
 Li, X.E.: PCSI-1SuA2, 9; PCSI-1WeM12, 17  
 Lin, M.C.: PCSI-1WeA14, 19; PCSI-1WeA16, 19; PCSI-1WeA17, 19; PCSI-1WeM10, 17  
 Lindner, S.: PCSI-2MoM40, 11  
 Liu, W.C.: PCSI-1WeM10, 17  
 Liu, X.: PCSI-2TuM39, 15  
 Liu, Y.: PCSI-1MoA11, 12; PCSI-2WeM42, 18  
 Liu, Z.: PCSI-1WeM11, 17  
 Long, J.: PCSI-2TuM31, 15  
 Lu, P.: PCSI-2MoA37, 13  
 Lu, T.-M.: PCSI-2MoA37, 13  
 Lucero, J.: PCSI-2MoA37, 13  
 Luk, T.: PCSI-2MoA37, 13  
 Luo, Y.: PCSI-1TuM19, 15  
 Lynn, K.G.: PCSI-1MoM19, 11

— M —

Ma, Y.: PCSI-1TuM13, 15  
 Maiti, M.: PCSI-1WeA9, 19  
 Manno, M.: PCSI-1WeA9, 19  
 Marie, X.: PCSI-1ThM9, 21  
 Masegi, H.: PCSI-1MoA10, 12  
 Mason, N.: PCSI-1ThM1, 21  
 McCluskey, M.: PCSI-2WeM41, 18  
 McFadden, A.: PCSI-2SuA31, 9  
 McMahan, B.: PCSI-2WeA42, 20  
 McMillan, S.: PCSI-1TuM14, 15  
 Meng, K.Y.: PCSI-1TuM13, 15  
 Mikkelsen, A.: PCSI-1MoA11, 12  
 Minor, A.: PCSI-2TuM39, 15  
 Mishra, M.: PCSI-1MoA9, 12  
 Misra, S.: PCSI-2MoA37, 13  
 Moore, L.: PCSI-2WeM42, 18  
 Moore, Q.: PCSI-1WeM11, 17  
 Moore, W.: PCSI-1WeA9, 19  
 Murakami, H.: PCSI-2WeA31, 19  
 Murphy, J.: PCSI-1ThM13, 21

— N —

Nam, S.: PSCI-SuE9, 10  
 Nguyen, D.-L.: PCSI-1WeA10, 19  
 Nie, W.: PCSI-2MoM31, 11; PCSI-2MoM39, 11  
 Norman, A.: PCSI-2WeA39, 20; PCSI-2WeA42, 20  
 Nys, J.-P.: PCSI-1MoA15, 12

— O —

Ogletree, D.F.: PCSI-2TuM39, 15  
 Olszta, M.: PCSI-2SuA30, 9  
 Ooi, Y.K.: PCSI-1MoM19, 11

— P —

Palmstrom, C.J.: PCSI-1MoA11, 12; PCSI-2SuA25, 9; PCSI-2SuA31, 9  
 Pappas, D.: PCSI-2TuM31, 15  
 Pasco, S.: PCSI-1ThM13, 21  
 Pendharkar, M.: PCSI-2SuA25, 9  
 Pennachio, D.J.: PCSI-2SuA31, 9  
 Perez-Hoyos, E.: PCSI-1TuM19, 15  
 Perkins, J.: PCSI-2WeM39, 18  
 Petrov, V.: PCSI-2WeA43, 20  
 Pharis, D.: PCSI-1TuM19, 15  
 Plissard, S.: PCSI-1MoA15, 12  
 Posadas, A.: PCSI-1WeA15, 19  
 Ptak, A.: PCSI-2WeA40, 20  
 Pulzara Mora, A.O.: PCSI-1TuM18, 15  
 Pulzara Mora, C.A.: PCSI-1TuM18, 15

— Q —

Qi, Y.: PCSI-2ThM31, 21  
 Quan, J.: PCSI-1WeM12, 17

— R —

Ranga, P.: PCSI-1MoM19, 11  
 Read, D.: PCSI-2SuA25, 9  
 Rice, A.: PCSI-2SuA29, 9



## Author Index

- Rice, W.: PCSI-2WeM40, 18  
Rice, W.D.: PCSI-1ThM13, 21  
Richardson, C.: PCSI-2SuA30, 9  
Ringo, W.: PCSI-2ThM40, 21  
Ritter, J.: PCSI-2WeM41, 18  
Robert, C.: PCSI-1ThM9, 21  
Roberts, D.: PCSI-2WeA40, 20; PCSI-2WeM39, 18  
Robertson, J.: PCSI-1WeA1, 19  
Robinson, J.: PCSI-1WeM1, 17  
Rogge, S.: PCSI-2MoA29, 12  
Rosenberg, S.G.: PCSI-2SuA31, 9  
— S —  
Saenz, T.: PCSI-2WeA39, 20  
Saleh, M.: PCSI-1MoM19, 11  
Sankar, R.: PCSI-1WeA10, 19  
Scarpulla, M.A.: PCSI-1MoM19, 11  
Schlom, D.: PCSI-MoE1, 14  
Schmucker, S.: PCSI-2MoA37, 13  
Schnedler, M.: PCSI-1MoA15, 12; PCSI-1WeA10, 19  
Schulte, K.: PCSI-2WeA40, 20  
Schulze, C.: PCSI-1MoM9, 11  
Searles, T.: PCSI-2WeM40, 18  
Sharp, I.: PCSI-1MoA1, 12  
Shen, K.: PCSI-MoE1, 14  
Shin, D.: PCSI-1ThM14, 21  
Shree, S.: PCSI-1ThM9, 21  
Siddiqi, I.: PCSI-2TuM39, 15  
Simon, J.: PCSI-2WeA40, 20  
Smith, A.R.: PCSI-1TuM13, 15  
Son, J.: PCSI-1TuM9, 15  
Song, J.: PCSI-1SuA10, 9  
Stier, A.V.: PCSI-1ThM9, 21  
Sun, R.: PCSI-1MoM19, 11  
— T —  
Talin, A.: PCSI-2WeM31, 17  
Taniguchi, T.: PCSI-1ThM9, 21  
Thomas, A.: PCSI-2SuA30, 9  
Timm, R.: PCSI-1MoA11, 12  
Tracy, L.: PCSI-2MoA37, 13  
Tsai, H.: PCSI-2MoM39, 11  
— U —  
Urbaszek, B.: PCSI-1ThM9, 21  
— V —  
Voigt, B.: PCSI-1WeA9, 19  
— W —  
Wakabayashi, N.: PCSI-2WeA44, 20  
Walker, J.: PCSI-2WeM40, 18  
Walter, J.: PCSI-1WeA9, 19  
Wang, X.: PCSI-2ThM40, 21  
Wang, Y.: PCSI-1WeA17, 19  
Ward, D.: PCSI-2MoA37, 13  
Warren, E.: PCSI-2WeA39, 20  
Watanabe, K.: PCSI-1ThM9, 21  
Weddle, C.: PCSI-2SuA30, 9  
Wei, C.-M.: PCSI-1WeA10, 19  
Wells, J.: PCSI-2MoA41, 13  
Wilson, N.: PCSI-1MoA11, 12  
Winter, J.: PCSI-1TuM19, 15  
Wong, M.H.: PCSI-2WeA31, 19  
Wu, F.: PCSI-1WeM11, 17  
Wu, X.: PCSI-2TuM31, 15  
— X —  
Xu, J.: PCSI-1TuM19, 15  
Xu, L.L.: PCSI-1WeA14, 19; PCSI-1WeA16, 19; PCSI-1WeA17, 19; PCSI-1WeM10, 17  
Xu, T.: PCSI-1MoA15, 12  
— Y —  
Yang, F.-Y.: PCSI-1TuM13, 15  
Yang, S.: PCSI-MoE1, 14  
Young, E.: PCSI-1MoA11, 12  
Yu, E.: PCSI-1WeM12, 17  
— Z —  
Zakutayev, A.: PCSI-2WeA42, 20; PCSI-2WeM39, 18  
Zhang, Z.: PCSI-1WeA1, 19  
Zhao, H.: PCSI-1MoM1, 11  
Zhao, N.: PCSI-1WeA14, 19; PCSI-1WeA16, 19  
Zhou, J.: PCSI-1MoM10, 11  
Zielinski, R.: PCSI-1MoM9, 11  
Zimmerman, J.: PCSI-2WeA39, 20

## Optical Properties of Semiconducting Moiré Crystals

Xiaoqin Elaine Li

Physics Department, the University of Texas at Austin

In van der Waals (vdW) heterostructures formed by stacking two monolayers, lattice mismatch or rotational misalignment introduces an in-plane moiré superlattice. The periodic atomic alignment variations between the two layers impose both an energy and optical selection rule modulations as illustrated in Fig. 1A-B. Optical properties of such moiré superlattices have just begun to be investigated experimentally [1-5]. In this talk, I will discuss how the properties of the interlayer excitons in a twisted transition metal dichalcogenide (TMD) heterobilayer are modified by the moiré potential. Specifically, we studied MoSe<sub>2</sub>/WSe<sub>2</sub> bilayers with small twist angles, where electrons mostly reside in the MoSe<sub>2</sub> and holes nominally in the WSe<sub>2</sub> monolayer because of the type-II band alignment. We observe multiple interlayer exciton resonances with either positive or negative circularly polarized emission (Fig. 1C). We attribute these resonances to the ground and excited exciton states confined within the moiré potential. The twist angle dependence, recombination dynamics, and temperature dependence are consistent with this interpretation. These results highlight the versatile and tunable optical properties of semiconducting moiré crystals.

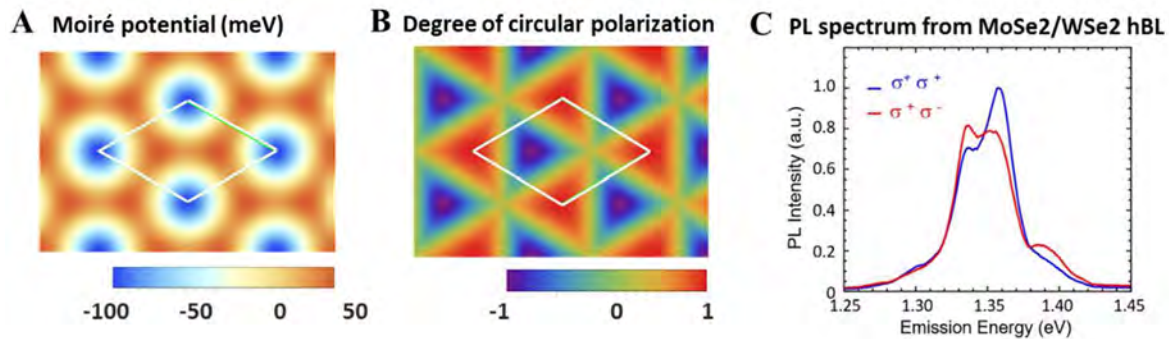


**Fig. 1:** Calculated (A) energy modulation and (B) spatially varying optical selection rules of a 2D moiré crystal in a TMD bilayer. (C) Measured PL spectra of interlayer excitons in a stacked MoSe<sub>2</sub>/WSe<sub>2</sub> bilayer with a small twist angle of 1°.

- [1] Nature **567**, 71-75 (2019);
- [2] Nature **567**, 66-70 (2019);
- [3] Nature **567**, 76-80 (2019);
- [4] Nature **567**, 81-86 (2019)
- [5] Nano Letters, 18, 7651, (2018)

# Berryogenesis: spontaneous out-of-equilibrium plasmonic magnetism

**Justin C. W. Song<sup>1,2</sup>**

<sup>1</sup> *Division of Physics and Applied Physics, Nanyang Technological University, 21 Nanyang Link, Singapore 637371*

<sup>2</sup> *Institute of High Performance Computing, A\*STAR, 1 Fusionopolis Way, Singapore 138632*

Spontaneous symmetry breaking lies at the heart of the description of interacting phases of matter. Here we argue that a driven interacting system subject to a linearly polarized (achiral) driving field can spontaneously magnetize (acquire chirality). In particular, we find when a metal is driven close to its plasmon resonance, it hosts strong internal ac fields that enable Berryogenesis: the spontaneous generation of a self-induced Bloch band Berry flux, which supports and is sustained by a circulating plasmonic motion, even for a linear polarized driving field. This non-equilibrium phase transition occurs above a critical driving amplitude, and depending on system parameters, can enter the spontaneously magnetized state in either a discontinuous or continuous fashion. Berryogenesis relies on nontrivial interband coherences for electronic states near the Fermi energy generated by ac fields readily found in a wide variety of multiband systems. We anticipate that graphene devices, in particular, which can host high quality plasmons, provide a natural and easily available platform to achieve Berryogenesis and spontaneous non-equilibrium (plasmon-mediated) magnetization in present-day devices, e.g., those based on graphene plasmonics. If we have time, we will also discuss other manifestations of non-trivial quantum geometry in Dirac systems.

<sup>+</sup> Author for correspondence: justinsong@ntu.edu.sg

## Investigation of Graphene/Ge(110) interface

**M. Galbiati<sup>1+</sup>, L. Persichetti<sup>2</sup>, M. De Seta<sup>2</sup>, L. Di Gaspare<sup>2</sup>, M. Bianchi<sup>3</sup>, P. Hofmann<sup>3</sup> and L. Camilli<sup>1</sup>**

1. Department of Physics, Technical University of Denmark, 2800 Kgs. Lyngby, Denmark

2. Department of Science, Roma Tre University, 00146 Rome, Italy

3. Department of Physics and Astronomy, Aarhus University, 8000 Aarhus, Denmark

Investigating the interfacial properties between graphene and traditional semiconductors is crucial to develop novel electronics [1]. In this framework, the Graphene/Ge(110) has received a great deal of attention over the last couple of years [2–7]. These studies focus on the structure of Graphene/Ge(110) interface and notably on the possible reconstructions of Ge surface as shown by scanning tunnelling microscopy (STM). However, no insights into the electronic properties of this interesting system are today available.

Here, we investigate the evolution of the system's interface upon annealing in vacuum at different temperatures. We use low-temperature STM to probe the surface structure with atomic precision. At each stage, images at different applied biases are collected and interestingly, graphene becomes transparent at high biases. When growing graphene by chemical vapour deposition, hydrogen that is used during growth passivates the Ge surface, stabilizing the (1x1) phase (i.e., unreconstructed surface) [5]. Annealing the sample at 350°C leads to desorption of hydrogen and STM and low energy electron diffraction (LEED) reveal that the surface of Ge(110) reconstructs into a (6x2) phase, never observed for bare Ge. Upon further annealing above 700°C, STM shows that the Ge surface modifies back into the (1x1) phase. At this point, due to the lack of hydrogen, the (1x1) is stabilized by graphene forming chemical bonds with Ge atoms underneath [2]. Indeed, the Ge surface remains in the (1x1) phase even if further annealing at temperature above 350°C is performed. To gain insights into the electronic properties, we perform angle resolved photoemission spectroscopy (ARPES) after each thermal annealing step. The ARPES data show how graphene's doping changes upon thermal annealing, signature of a different interaction with the Ge substrate (Figure 1).

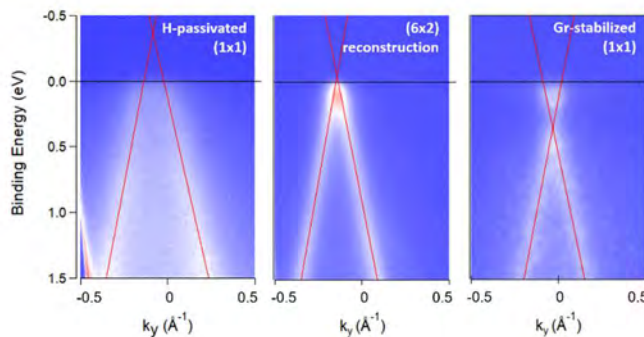


Figure 1. ARPES intensity maps of Gr/Ge(110) samples as grown (left), annealed at temperature below (middle) and above 800 °C (right). The shift of the Dirac point as a function of the annealing temperature is evident.

- [1] J. Lee, Science, 344(2014).
- [2] J. Tesch, Carbon, 122(2017).
- [3] G.P. Campbell, Phys. Rev. Mater., 2(2018).
- [4] J. Tesch, Nanoscale, 10(2018).
- [5] D. Zhou, J. Phys. Chem. C., 122(2018).
- [6] H.W. Kim, J. Phys. Chem. Lett., 9(2018).
- [7] B. Kiraly, Appl. Phys. Lett., 113(2018).

<sup>+</sup> Author for correspondence: [mirgal@dtu.dk](mailto:mirgal@dtu.dk)

## Epitaxial Growth and Electronic Characterization of GdSb

**H. S. Inbar,<sup>1</sup> S. Chatterjee,<sup>2</sup> M. Pendharkar,<sup>2</sup> Y. Chang,<sup>1</sup> M. M. Bocheff,<sup>1</sup> T. Guo,<sup>1</sup>  
T. L. Brown-Heft<sup>1</sup>, A. V. Fedorov<sup>3</sup>, D. Read<sup>4</sup>, C. J. Palmström<sup>1,2</sup>**

<sup>1</sup>Materials Dept., University of California, Santa Barbara, CA, USA

<sup>2</sup>Dept. of Electrical & Comp. Eng., University of California, Santa Barbara, CA, USA

<sup>3</sup>Advanced Light Source, Lawrence Berkeley National Laboratory, CA, USA

<sup>4</sup>School of Physics and Astronomy, Cardiff University, UK

In recent years, the class of rare-earth monpnictides (RE-Vs) has received renewed interest due to predictions of topological semimetal states<sup>[1]</sup> and observations of extremely large magnetoresistance (XMR)<sup>[2]</sup>, phenomena holding great promise in novel physics devices and magnetic sensing technologies. The wide range of lattice constants and simple rock salt structure of RE-Vs also allows to easily incorporate them epitaxially with III-V semiconductors. Coupled to III-Vs, RE-Vs have potential applications as buried ohmic contacts, THz emitters and detectors, thermoelectrics, reaction barriers, and plasmonic heterostructures.<sup>[3]</sup> In the family of RE-Vs, GdSb shares the common features of antiferromagnetic type II ordering and unusually high magneto-resistance.<sup>[4]</sup> Due to the absence of orbital momentum in the  $4f^7$  configuration of  $Gd^{3+}$  and the simple magnetic phase diagram, GdSb can serve as a model system for the study of the effect of biaxial strain on band dispersion in RE-Vs, and the interplay between magnetism and XMR.

In this talk, we will demonstrate the first epitaxial growth and characterization of GdSb thin films with thickness varied from 3-30 nm and biaxial strains ranging from -2% to +2% lattice-mismatch. We utilize molecular beam epitaxy to grow GdSb films on  $In_{1-x}Al_xSb$  and Be-doped  $In_{1-x}Ga_xSb$  buffer layers deposited on undoped and Zn-doped GaSb (001) substrates for magnetotransport and angle-resolved photoemission spectroscopy measurements, respectively. Reflection high-energy electron diffraction patterns observed during growth and *in-situ* X-ray photoelectron spectroscopy and scanning tunneling microscopy (STM) were used to determine the formation of a rock salt phase with the characteristic surface reconstruction of  $1 \times 1$ , indicating the absence of interfacial reactions between the GdSb films and underlying buffer layers. Surface morphology was examined with STM to confirm the growth of continuous films at thicknesses down to 3nm. To determine the in-plane lattice constant and strain of the GdSb thin films we have recorded reciprocal space maps on asymmetric reflections. The thickness dependence in lattice-matched buffers and the effect of biaxial strain on magnetotransport behavior and the bandstructure of GdSb will also be discussed.

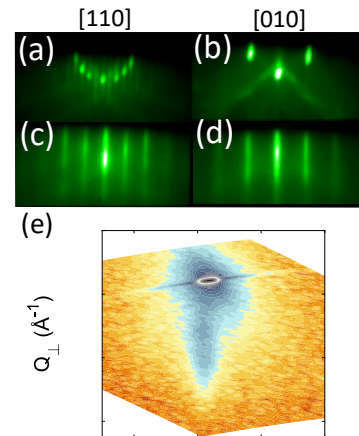


**Figure 1:** RHEED patterns: (a)-(b) c(2X6) reconstruction of the GaSb substrate and (c)-(d) (1X1) reconstruction of the GdSb film. (e) Asymmetric (226) reciprocal space map demonstrating biaxial straining and epitaxial growth of GdSb on GaSb (001)

[1] Duan, Xu, et al. Commun. Phys. 1 (1) (2018): 71.

[2] Tafti, F. F., et al. Nat. Phys. 12 (3) (2016): 272.

[3] Bomberger, Cory C., et al. JVST B 35 (3) (2017): 030801.

[4] Li, D. X., et al. Phys. Rev. B 54 (15) (1996): 10483.

<sup>+</sup> Author for correspondence: hadass@ucsb.edu

## MBE growth of $\text{Zn}_x\text{Cd}_{1-x}\text{Te}$ on $\text{Cd}_3\text{As}_2$

**A.D. Rice,<sup>1+</sup> K. Alberi<sup>1</sup>**

<sup>1</sup> National Renewable Energy Lab, Golden, CO, USA.

The Dirac semimetal  $\text{Cd}_3\text{As}_2$  has become a scientifically useful material, as it provides access to a variety of interesting phenomena ranging from topological superconductivity to massless Dirac fermions. It is also potentially useful for energy-related applications due to its high electron mobility and large phonon-phonon scattering. While thin film growth has become an increasingly popular route of synthesis, there have been no reports of epitaxial growth on  $\text{Cd}_3\text{As}_2$ , limiting the ability to develop full heterostructures. One barrier to epitaxy on  $\text{Cd}_3\text{As}_2$  is the high vapor pressure of  $\text{Cd}_3\text{As}_2$  ( $1\text{e-}7$  mbar at only  $135^\circ\text{C}$ ), which is well below the ideal growth temperature of most semiconductors [1].

The  $\text{Zn}_x\text{Cd}_{1-x}\text{Te}$  (111) system provides one promising option for overgrowth given that it can be lattice matched to the (112) surface of  $\text{Cd}_3\text{As}_2$  and has a relatively low optimal growth temperature ( $240\text{-}300^\circ\text{C}$ ). Reflective high-energy electron diffraction (RHEED) patterns of epilayers grown on  $\text{Cd}_3\text{As}_2$  exhibit a  $(2\times 1)$  reconstruction, even with a growth interruption. These patterns are consistent with As-terminated CdTe observed following high temperature annealing under As [2]. CdTe epilayers growth at  $\text{Cd}_3\text{As}_2$ -compatible substrate temperatures ( $\sim 120^\circ\text{C}$ ) are rough, but further growth at  $240^\circ\text{C}$  yields smoother surfaces, as seen in atomic force microscopy. X-ray diffraction confirms  $\text{Cd}_3\text{As}_2$  remains following the higher temperature growth step, suggesting complete coverage is achieved. Higher temperature anneals under As further smooth and passivate this surface, while similar anneals under Te result in disappearance of a RHEED pattern and loss of the  $\text{Cd}_3\text{As}_2$  layer. Introduction of moderate Zn content into CdTe results in complete surface coverage but also very large features, likely a result of very low Zn adatom mobility at these temperatures. Our results provide a starting point for incorporating  $\text{Cd}_3\text{As}_2$  into a variety of device structures.

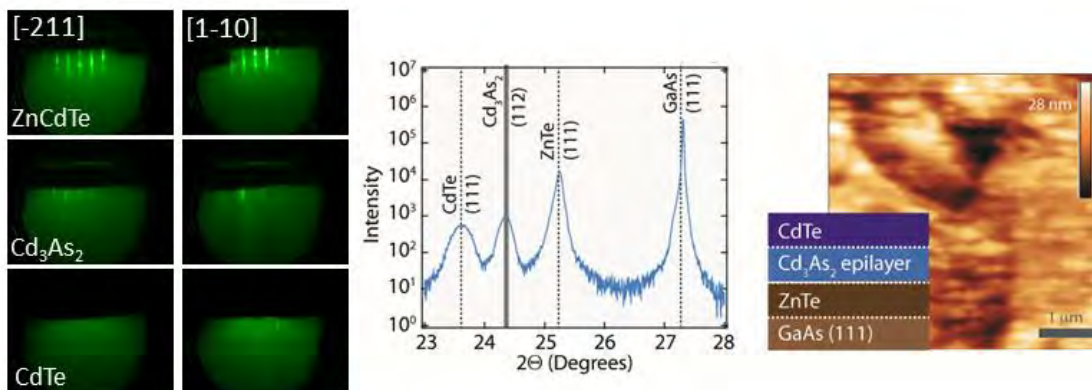


**Figure 1.** RHEED, XRD, and AFM of  $\text{CdTe}/\text{Cd}_3\text{As}_2$  structures

<sup>+</sup> Author for correspondence [Anthony.Rice@nrel.gov](mailto:Anthony.Rice@nrel.gov)

[1] V.J. Lyons and V.J. Silvestri, J. Phys. Chem. **64**, 2266 (1960)

[2] Y. Nakazawa, M. Uchida, S. Nishihaya, S. Sato, A. Nakao, J. Matsuno, and M. Kawasaki, APL Mater. **7**, 071109 (2019)

## **Interfaces and growth of NbTiN-AlN heterostructures on sapphire as epitaxial Josephson junctions**

**C. J. K. Richardson<sup>1</sup>, A. Thomas<sup>1</sup>, A. Alexander<sup>1</sup>, C. G. Weddle<sup>1</sup>, B. Arey<sup>2</sup>, M. Olszta<sup>2</sup>**

<sup>1</sup>*Laboratory for Physical Sciences, University of Maryland, 8050 Greenmead Dr., College Park MD 20740*

<sup>2</sup>*Pacific Northwest National Laboratory, Richland, Washington 99352, United States.*

Plasma assisted Molecular beam epitaxy (PAMBE) is used to grow niobium titanium nitride alloys ( $\text{Nb}_x\text{Ti}_{1-x}\text{N}$ ) and wide bandgap nitride (AlN) superconductors directly on c-plane sapphire wafers. This combination of nitride materials provides sufficient degrees of freedom that synthesis of an epitaxial Josephson junction may be possible while satisfying the device requirements for superconducting quantum circuits. Thin films of various  $\text{Nb}_x\text{Ti}_{1-x}\text{N}$  alloys are grown using the abrupt metamorphic growth paradigm and show the ability to tune the lattice parameters and critical temperatures of the superconducting films. Surface topology, degree of twinning, and superconducting loss are used to evaluate the fitness of these layers.

A prototype NbTiN/AlN/NbTiN (superconductor-insulator-superconductor) Josephson junction structure has been grown. The structural, superconducting, and current-voltage characterization of these heterostructures will be presented.

+ Author for correspondence: [richardson@lps.umd.edu](mailto:richardson@lps.umd.edu)

## Growth of AlN Barriers in Al/AlN/Al SIS Josephson Junctions by Low Temperature Atomic Layer Epitaxy

C.R. Eddy, Jr.<sup>1,+</sup>, D.J. Pennachio<sup>2</sup>, J.S. Lee<sup>2</sup>, A. McFadden<sup>2</sup>, S.G. Rosenberg<sup>3</sup>,  
Y.H. Chang<sup>2</sup>, C.J. Palmstrøm<sup>2</sup>

<sup>1</sup> U.S. Naval Research Laboratory, Washington, DC 20375

<sup>2</sup> University of California Santa Barbara, Santa Barbara, CA 93106

<sup>3</sup> American Assoc. for Engineering Education, Washington DC 20036 (residing at NRL)

Superconductor-Insulator-Superconductor (SIS) structures are of increasing interest for the creation of Josephson junctions that can serve as the basis for quantum qubit transmons, which hold significant promise for quantum computing technologies. Traditionally, these devices have been developed using amorphous AlO<sub>x</sub> in Al/AlO<sub>x</sub>/Al structures and have enabled fundamental demonstrations of transmon performance. However, improved performance may be expected with an epitaxial insulator. Even in these structures, the nature of the superconductor/substrate interface and the superconductor/ambient interface limits coherence and, consequently, qubit performance.

In an effort to address this challenge, we employ low temperature atomic layer epitaxy (ALEp) to grow crystalline AlN insulators on crystalline aluminum films. Smooth epitaxial aluminum films are grown by evaporation on cryogenically-cooled, buffered GaAs(001) substrates [1]. These epitaxial surfaces are “frozen” using a low temperature nitridation atomic layer process (ALP) before the samples are ramped to 300°C for low temperature ALE of AlN using semiconductor grade trimethylaluminum and UHP argon and nitrogen inductively coupled plasmas (ICPs). In this study, we evaluate the structural effects of variations in the initial nitridation ALP, growth conditions of ALEp AlN barriers, and SIS barrier thickness using transmission electron microscopy. We have found that at one end of the spectrum, a simple 5 cycle nitridation ALP of epitaxial aluminum at ~90°C, where each cycle is a 30 second exposure to 300W UHP argon/nitrogen (200/75 sccm) ICP, consumes a significant fraction of the aluminum to make an amorphous AlN insulator that is roughly 2 nm thick. When this surface is subjected to another low temperature Al evaporation, the top Al films are a mixture of amorphous and polycrystalline. When the same nitridation ALP is employed and followed by 5nm of ALEp AlN growth at 300°C, a similar amount of the aluminum film is consumed and an amorphous ALEp AlN layer results. Finally, when the nitridation ALP is reduced to a single cycle of nitridation, less of the aluminum film is consumed and the 5nm AlN ALEp film shows polycrystallinity with small regions demonstrating sharp, potentially epitaxial interfaces. This result suggests that proper ALP nitridation of the epitaxial aluminum can support epitaxial growth of AlN by ALE. Further studies of the influence of number of cycles, cycle duration, plasma chemistry and plasma power on both the nitridation ALP and AlN ALEp will be presented.

[1] S. Gazibegovic et al., Nature 548, 434 (2017).

<sup>+</sup>Author for correspondence: chip.eddy@nrl.navy.mil

Work at the U.S. Naval Research Laboratory is sponsored by the Office of Naval Research. This work also conducted under the Laboratory University Collaboration Initiative (LUCI) program sponsored by the Basic Research Office, Office of Undersecretary of Defense for Research & Engineering.



# Theory of Single Photon Detection by a Photoreceptive Molecule and a Quantum Coherent Spin Center

N. J. Harmon,<sup>1</sup> M. E. Flatté,<sup>2</sup>

<sup>1</sup> *Department of Physics, University of Evansville, Evansville, IN, 47722, USA*

<sup>2</sup> *Department of Physics and Astronomy, University of Iowa, Iowa City, IA 52242, USA;  
Pritzker School for Molecular Engineering, University of Chicago, Chicago, IL, 60637;  
Eindhoven University of Technology, P.O. Box 513, 5600 MB Eindhoven, The Netherlands*

The long spin coherence times in ambient conditions of color centers in solids, such as nitrogen-vacancy ( $\text{NV}^-$ ) centers in diamond, make these systems attractive candidates for quantum sensing. Quantum sensing provides remarkable sensitivity at room temperature to very small external perturbations, including magnetic fields, electric fields, and temperature changes. A photoreceptive molecule, such as those involved in vision, changes its charge state or conformation in response to the absorption of a single photon. We show the resulting change in local electric field modifies the properties of a nearby quantum coherent spin center in a detectable fashion. Using the formalism of positive operator valued measurements (POVMs), we analyze the photo-excited electric dipole field and, by extension, the arrival of a photon based on a measured readout, using a fluorescence cycle, from the spin center. We determine the jitter time of photon arrival and the probability of measurement errors. We predict that configuring multiple independent spin sensors around the photoreceptive molecule would dramatically suppresses the measurement error[1].

[1] N. J. Harmon and M. E. Flatté, arXiv:1906.01800

# From dark matter detection to artificial intelligence: uses for superconducting nanowire single photon detectors

**Sae Woo Nam**<sup>1</sup>

<sup>1</sup> *National Institute of Standards and Technology, 325 Broadway, Boulder, CO 80305 USA*

Single-photon detectors are an essential tool for a wide range of applications in physics, chemistry, biology, communications, computing, imaging, medicine, and remote sensing. Ideally, a single photon detector generates a measurable signal only when a single photon is absorbed. Furthermore, the ideal detector would have 100% detection efficiency, no false positive (dark counts), and transform-limited timing resolution. Since the first reported detection of a single photon using a superconducting nanowire in 2001[1], steady progress has been made in the development and application of superconducting nanowire single photon detectors (SNSPD or SSPD) with ideal properties. The performance of these detectors is fundamentally related to characterizing and understanding the materials used in these quasi-1D wires that are able to detect photons. I will briefly describe progress in detector developments, use of these detectors in new applications, and opportunities for future work.

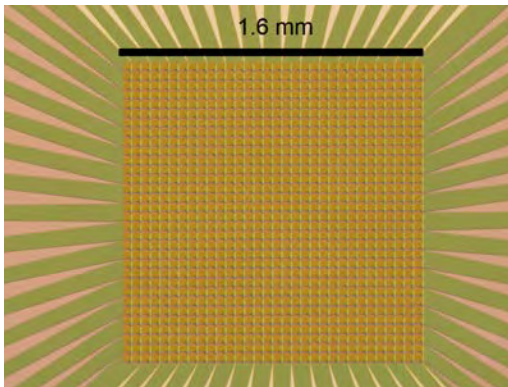


Figure 1 : Optical micrograph of a 32 x 32 array of SNSPD detectors

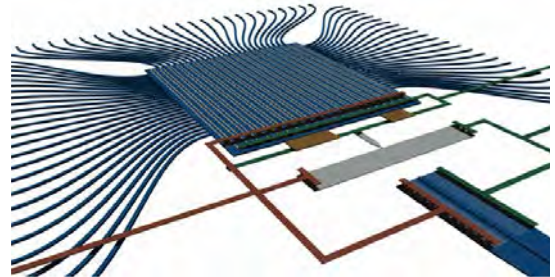


Figure 2 : Sketch of an artificial neuron using a single photon detector (SNSPD) and a weak

## References

- [1] Gol'tsman, G. N., O. Okunev, G. Chulkova, A. Lipatov, A. Semenov, K. Smirnov, B. Voronov, A. Dzardanov, C. Williams, and Roman Sobolewski. "Picosecond Superconducting Single-Photon Optical Detector." *Applied Physics Letters* 79, no. 6 (August 1, 2001): 705–7. <https://doi.org/10.1063/1.1388868>.

<sup>+</sup> Author for correspondence: saewoo.nam@nist.gov

## MOCVD Epitaxy and Doping for $\beta$ -Ga<sub>2</sub>O<sub>3</sub> and (Al<sub>x</sub>Ga<sub>1-x</sub>)<sub>2</sub>O<sub>3</sub> (Invited)

Hongping Zhao

*Department of Electrical and Computer Engineering, The Ohio State University,  
Columbus, OH 43210, USA*

*Department of Materials Science and Engineering, The Ohio State University,  
Columbus, OH 43210, USA*

*Email : [zhao.2592@osu.edu](mailto:zhao.2592@osu.edu)*

Ultrawide bandgap (UWBG) gallium oxide (Ga<sub>2</sub>O<sub>3</sub>) represents an emerging semiconductor material with excellent chemical and thermal stability. It has a band gap of 4.5-4.9 eV, much higher than that of the GaN (3.4 eV) and 4H-SiC (3.2 eV). The monoclinic  $\beta$ -phase Ga<sub>2</sub>O<sub>3</sub> represents the thermodynamically stable crystal among the known five phases ( $\alpha$ ,  $\beta$ ,  $\gamma$ ,  $\delta$ ,  $\epsilon$ ). The breakdown field of  $\beta$ -Ga<sub>2</sub>O<sub>3</sub> is estimated to be 6-8 MV/cm, which is much larger than that of the 4H-SiC and GaN. These unique properties make  $\beta$ -Ga<sub>2</sub>O<sub>3</sub> a promising candidate for high power electronic device and solar blind photodetector applications. Single crystal  $\beta$ -Ga<sub>2</sub>O<sub>3</sub> substrates can be synthesized by scalable and low cost melting based growth techniques. Metalorganic chemical vapor deposition (MOCVD) growth technique was used to develop high quality  $\beta$ -Ga<sub>2</sub>O<sub>3</sub> thin films and its ternary alloy (Al<sub>x</sub>Ga<sub>1-x</sub>)<sub>2</sub>O<sub>3</sub>. Control of background and n-type doping in  $\beta$ -Ga<sub>2</sub>O<sub>3</sub> will be discussed. Record carrier mobilities of 184 cm<sup>2</sup>/V·s at room temperature and 4984 cm<sup>2</sup>/V·s at low temperature (45 K) were measured for  $\beta$ -Ga<sub>2</sub>O<sub>3</sub> thin films with room-temperature doping concentrations of 2.5×10<sup>16</sup> and 2.75×10<sup>16</sup> cm<sup>-3</sup>, respectively [1]. Growth and fundamental understanding of (Al<sub>x</sub>Ga<sub>1-x</sub>)<sub>2</sub>O<sub>3</sub> are still lacking. The limit of Al incorporation in beta-phase Ga<sub>2</sub>O<sub>3</sub> has not been understood or experimentally verified, although it was predicted up to 60% of Al composition could be incorporated into  $\beta$ -Ga<sub>2</sub>O<sub>3</sub>. N-type doping capability as a function of Al composition in (Al<sub>x</sub>Ga<sub>1-x</sub>)<sub>2</sub>O<sub>3</sub> is another important fundamental question. Carrier transport properties in (Al<sub>x</sub>Ga<sub>1-x</sub>)<sub>2</sub>O<sub>3</sub> will be discussed.

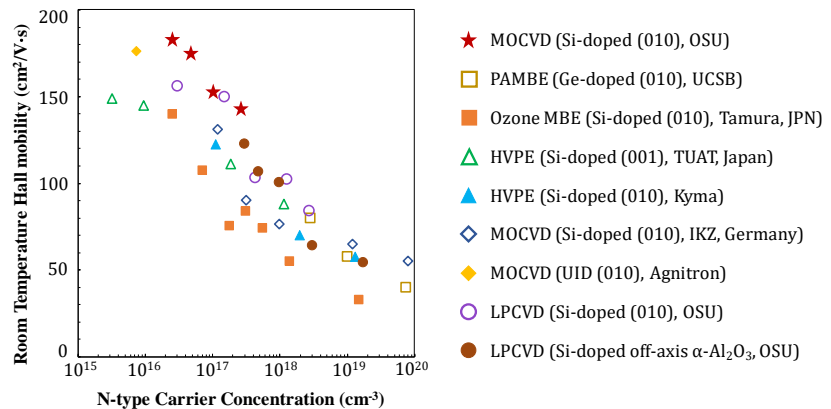


Fig. 1 Results from this work as compared to state-of-the-art: room temperature carrier mobility vs. carrier concentration for (010)  $\beta$ -Ga<sub>2</sub>O<sub>3</sub> films.

*Acknowledgement: The authors acknowledge the funding support from the Air Force Office of Scientific Research FA9550-18-1-0479 (AFOSR, Dr. Ali Sayir) and the National Science Foundation (1810041).*

[1] Z. Feng, AFM Bhuiyan, M. R. Karim, H. Zhao, Appl. Phys. Letts, 114, 250601 (2019).

## Atomic Structure and Electronic Properties of the Non-Polar $\text{In}_2\text{O}_3$ and $\beta\text{-Ga}_2\text{O}_3(100)$ surfaces

C. S. Schulze,<sup>1</sup> R. Zielinski,<sup>1</sup> J.K. Hofmann,<sup>1</sup> C. Bruckmann,<sup>1</sup> Z. Galazka,<sup>2</sup> and H. Eisele<sup>1</sup>

<sup>1</sup> Technische Universität Berlin, Institut für Festkörperphysik, Hardenbergstr. 36, 10623 Berlin, Germany

<sup>2</sup> Leibniz-Institut für Kristallzüchtung, Max-Born-Str. 2, 12489 Berlin, Germany

$\text{In}_2\text{O}_3$  and  $\beta\text{-Ga}_2\text{O}_3$  belong to the transparent conducting oxides (TCOs), being promising candidates for a wide field of applications like in solar cells, in detectors, and for high-power devices. In order to achieve high efficiency in electronic and opto-electronic devices a variety of prerequisites are necessary, as e.g., high crystal quality with low defect densities, adjustable conductivity by doping, controllable surfaces and interfaces, etc. Especially the doping mechanisms and the resulting high electron mobility are still under broad discussion for sesquioxide material: Mainly oxygen vacancies are under strong debate about their functionality [1]. We use scanning tunneling microscopy (STM) and spectroscopy (STS) in order to analyze the atomic structure of the non-polar surfaces. Since non-polar surfaces typically show no intrinsic surface states within the fundamental band gap of semiconductor materials, it is furthermore possible to study bulk and doping states using these methods [2].

Both semiconductors,  $\text{In}_2\text{O}_3(111)$  and  $\beta\text{-Ga}_2\text{O}_3(100)$  show at their respective non-polar surface a  $1\times 1$  surface unit cell without reconstruction upon *in situ* cleavage. We found the unreconstructed surface unit cell in the case of  $\text{In}_2\text{O}_3(111)$  in empty state images with atomic resolution. In respective room-temperature STS spectra we can identify the conduction band contribution, the direct and the indirect valence band as well as at least 3 intrinsic states being located within the band gap. Due to the variation of the growth parameter we can assign at least some of these states to charge transfer levels of impurities and vacancies. Since the Fermi level is located within the fundamental band gap, we can exclude an intrinsic electron accumulation for the freshly cleaved surface, while in air aged samples show a strongly different behavior, i.e. metallic appearance as in the case of a surface electron accumulation.

The  $\beta\text{-Ga}_2\text{O}_3(100)$  surface also shows atomic resolution in empty state images. Even more, we can identify single dopant atoms. In the corresponding STS spectra we can assign the conduction band contribution and again charge transfer levels, originating most likely from vacancies of the three differently coordinated oxygen atom positions within the unit cell. Even more, we can identify a charge transfer level, which we can assign to Si doping. Due to our findings from differently doped samples we conclude that the conductivity from unintentionally doped  $\beta\text{-Ga}_2\text{O}_3(100)$  can be assigned to background doping by Si.

[1] J.B. Varley, J.R. Weber, A. Janotti, and C.G. Van de Walle, Appl. Phys. Lett. **97**, 142106 (2010).

[2] Ph. Ebert, G. Cox, U. Poppe, and K. Urban, Surf. Sci. **271**, 587 (1992).

<sup>+</sup> Author for correspondence: holger.eisele@physik.tu-berlin.de

## Growth and Structures of Metal Dopant-Ceria Mixed Oxide Interfaces

E. Ginting, L. Du, J. Zhou<sup>†</sup>

Department of Chemistry, University of Wyoming, Laramie, Wyoming 82071

Ceria has been widely studied as an oxidation-reduction catalyst due to its unique redox properties and oxygen storage capacity [1]. The addition of other metal elements such as Ti and Mn into ceria could better enhance its thermal stability and improve its redox properties and oxygen storage capacity. To understand the chemistry of doped-ceria mixed oxides, it is of crucial importance to determine their surface structures at the fundamental level. We present our study on the growth of ceria thin films with Ti and Mn dopants and the understanding of their structures using X-ray photoelectron spectroscopy, low-energy electron diffraction, as well as scanning tunneling microscopy. Well-ordered CeO<sub>x</sub>(111) with controlled degree of Ce reduction and atomic structures can be prepared on a Ru(0001) single crystal substrate [2]. Metal-doped ceria mixed oxide interfaces were prepared by depositing Ti or Mn over CeO<sub>x</sub>(111) thin films. Co-deposition of Ce with metal dopants can produce well-ordered Ce<sub>1-x</sub>M<sub>x</sub>O<sub>2-δ</sub>(111) mixed oxide films (M=Ti, Mn) [3]. Dopant types and compositions can influence the surface structures, electronic structures, and redox properties of ceria. Effects of Mn and Ti dopants in ceria were investigated for Ni as steam reforming of ethanol catalysts for energy production. Compared to pure ceria, addition of metal dopants in ceria can provide unique anchoring sites and interaction for deposited Ni, which can significantly stabilize Ni as small metal nanoparticles upon heating. Additionally, modified structures and electronic properties of ceria by dopants offer alternative adsorption and reaction sites and provide promotional effects in the resistance of the coke formation over deposited Ni nanoparticles in the adsorption and reaction of ethanol. The research is sponsored by the National Science Foundation (Award Number: CHE1151846).

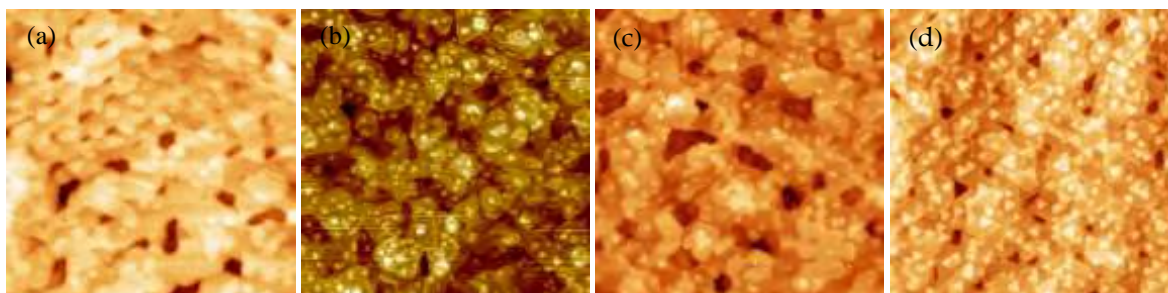


Figure 1 STM images of (a) Ce<sub>0.94</sub>Mn<sub>0.06</sub>O<sub>1.91</sub> and (b) MnO-CeO<sub>x</sub>, (c) and (d) Ce<sub>0.94</sub>Mn<sub>0.06</sub>O<sub>1.91</sub> and MnO-CeO<sub>x</sub> upon deposition of 0.25 ML Ni at 300 K and heating to 800 K. Image sizes are 100 nm × 100 nm.

- [1] A. Trovarelli, *Catalysis by Ceria and Related Materials*, Imperial College Press: London (2002).  
 [2] Y. H. Zhou, J. M. Perket, A. B. Crooks, J. Zhou, *J. Phys. Chem. Lett.* **1**, (9), 1447-1453 (2010).  
 [3] Y. H. Zhou, J. Zhou, *J. Phys. Chem. Lett.* **1**, (11), 1714-1720 (2010).

<sup>†</sup> Author for correspondence: jzhou2@uwyo.edu

# Freestanding crystalline oxide membranes and heterostructures

**S. S. Hong**<sup>1,2</sup>

<sup>1</sup>*Department of Materials Science and Engineering, University of California, Davis, CA, USA*

<sup>2</sup>*Department of Applied Physics, Stanford University, Stanford, CA, USA*

The ability to create and manipulate materials in two-dimensional (2D) form has repeatedly had transformative impact on science and technology. In parallel with the exfoliation and stacking of intrinsically layered crystals, the atomic-scale thin film growth of complex materials has enabled the creation of artificial 2D heterostructures with novel functionality and emergent phenomena, as seen in perovskite oxides. We present a general method to create freestanding complex oxide membranes and heterostructures with millimeter-scale lateral dimensions and nanometer-scale thickness [1]. This facilitates many new opportunities we are beginning to explore, and here we focus on probing the nanomechanical response and the application of extreme strain states [2].

[1] D. Lu, D. J. Baek, S. S. Hong, L. F. Kourkoutis, Y. Hikita, and H. Y. Hwang, *Nat. Mater.* **15**, 1255 (2016).

[2] S. S. Hong, M. Gu, M. Verma, V. Harbola, B. Y. Wang, D. Lu, A. Vailionis, Y. Hikita, R. Pentcheva, J. M. Rondinelli, and H. Y. Hwang, *in revision*.

+ Author for correspondence: seungsae@stanford.edu

## Effects of Annealing on Electronic Defects in $\beta$ -Ga<sub>2</sub>O<sub>3</sub> Revealed by Linearly-Polarized Photoluminescence (LPPL)

R. Sun<sup>1,2</sup>, Y.K. Ooi<sup>2</sup>, P. Ranga<sup>2</sup>, M. Saleh<sup>3,4</sup>, K.G. Lynn<sup>3,4</sup>, S. Krishnamoorthy<sup>2</sup>  
and M.A. Scarpulla<sup>1,2</sup>

<sup>1</sup> Materials Science & Engineering, University of Utah, Salt Lake City, UT 84112

<sup>2</sup> Electrical & Computer Engineering, University of Utah, Salt Lake City, UT 84112

<sup>3</sup> Materials Science & Engineering Program, Washington State University, Pullman, WA, 99164

<sup>4</sup> Center for Materials Research, Washington State University, Pullman, WA, 99164

$\beta$ -Ga<sub>2</sub>O<sub>3</sub> is of high interest for high voltage and high-power DC and microwave applications. Annealing in different ambient environments can be used to manipulate the point defect populations as a function of depth, both to understand populations induced by growth processes and then to use this understanding to optimize properties for applications. Here, we report on our studies of electronic defects using unique linearly-polarized photoluminescence (LP-PL). We utilize annealing in different atmospheres to manipulate defects. We find intriguing differences between responses of bulk crystals and epilayers grown on various substrates, elucidating the unanticipated confounding effects of substrates. We use these comparisons to help to sort out the myriad possible hypotheses for which combinations of defects produce the observed changes. We attempt to unify our results with prior literature and interpretations.

+ Author for correspondence: [scarpulla@eng.utah.edu](mailto:scarpulla@eng.utah.edu)

## Hybrid perovskite-based high energy photon detectors

Fangze Liu<sup>1</sup>, Michael Yoho<sup>2</sup>, Hsinhan Tsai<sup>1</sup>, Kasun Fernando<sup>1</sup>, Jeremy Tisdale<sup>1</sup>, Shreetu Shrestha<sup>1</sup>, Kevin Baldwin<sup>3</sup>, Aditya Mohite<sup>4</sup>, Sergei Tretiak<sup>3,5</sup>, Duc T. Vo<sup>2</sup>, and Wanyi Nie<sup>1</sup>

<sup>1</sup>*Material Physics and Application Division, Los Alamos National Laboratory, Los Alamos, NM*

<sup>2</sup>*Nuclear Engineering and Nonproliferation Division, Los Alamos National Laboratory, Los Alamos, NM*

<sup>3</sup>*Center for Integrated Nanotechnology, Los Alamos National Laboratory, Los Alamos, NM*

<sup>4</sup>*Chemical and Biomolecular Engineering, Rice University, Houston, TX*

<sup>5</sup>*Theory Division, Los Alamos National Laboratory, Los Alamos, NM*

Radiation spectroscopy is widely needed in security, medical treatment, nuclear material monitoring as well as space science. It quantifies the gamma-ray energies by single radiation photon counting devices. The key is to precisely count gamma-ray photons using highly sensitive detectors. Solid-state detectors employing high density semiconductors to convert gamma-ray photon signal directly into electrical pulses offers promising solution. It outperforms scintillator technologies in count rate and sensitivities with high energy resolutions.

In this talk, I will introduce our recent progress on methylammonium lead halide perovskite single crystal detectors. We show that the single crystal detectors can efficiently count single gamma-ray photon events with electrical pulses. We further investigate the operational principles of the bromide-perovskite solid-state detectors and find using high work function contacts can block out the dark noise from thermally injected electrons and thus allow for efficient pulse collection at higher electrical fields. As a result, we observe strong and reproducible electrical pulses when exposing the detector under several radioactive sources corresponding to gamma-rays at various energies. However, we also discover that the bromide-perovskite detector suffers from voltage instability and slow response which cannot generate reliable energy resolved spectrum. Replacing the bromide by iodide in the crystal, we are able to operate the detector at much higher voltage and deliver sharp electrical pulses at room temperature. By counting the pulses under gamma-ray photons, we constructed the spectrum for <sup>137</sup>Cs that clearly shows the expected Compton scatter structure along with signals from photo-electric effect. Our results lay the foundation towards the robust operation of efficient perovskite- detector.



# Pb-Based Metal-Organic Frameworks for Efficient Perovskites Light-emitting Diodes Applications

**Hsinhan Tsai,<sup>1</sup> Wanyi Nie<sup>1+</sup>**

<sup>1</sup> *Materials Physics and Application Division, Los Alamos National Laboratory  
P.O. Box 1663, Los Alamos, NM 87545, USA*

Hybrid perovskites materials have demonstrated an extraordinary potential for clean, sustainable energy technologies and low-cost optoelectronic devices. In spite of the unprecedented progress in photovoltaics over the past decay, perovskites light-emitting diodes (PeLEDs) emergent as one of the most promising light emitters with performances exceeded 20% EQE efficient and low energy consumption devices. One of the key challenges that exists in the field today is the stability and reliability of devices under operation conditions. This vulnerability remains an open question, which might determine the fate of this remarkable material despite excellent properties.

A fundamental requirement for achieving highly efficient light emission and stability operation used in PeLEDs is to design molecular structures that facilitate recombination of the electrically or optically generated electron and hole pair to emit photons. Here, we demonstrate a new type Pb-based metal-organic frameworks (MOFs) perovskites as LED emitter with naturally formed quantum and dielectric confinement, where efficient radiative recombination is expected. We show that the Pb-based MOFs have a PeLEDs performance with over 5% EQE and extended charge localization due to the structure confinement and consequently improved the carrier transport and radiative recombination.

[1] Zhao et al, *Nat. Photonics*, **12**, 783–789 (2018).

[2] Xu et al, *Nat. Photonics*, **13**, 418–424 (2019)

[3] Tsai et al, *Adv.Mater.*, **30**, 1704217 (2018).

<sup>+</sup> Author for correspondence: wanyi@lanl.gov

## Arrangement and electronic properties of cobalt phthalocyanine molecules on B-Si(111)- $\sqrt{3} \times \sqrt{3} R 30^\circ$

**S. Lindner,<sup>1</sup> M. Franz,<sup>1</sup> M. Kubicki,<sup>1</sup> S. Appelfeller,<sup>1</sup> M. Dähne,<sup>1</sup> and H. Eisele<sup>1</sup>**

<sup>1</sup> *Institut für Festkörperphysik, Technische Universität Berlin, Hardenbergstraße 36, 10623 Berlin, Germany*

The formation of self-assembled monolayers of organic molecular materials on solid surfaces is an important subject, both from the viewpoint of basic science and in regard of applications. Transition metal phthalocyanines represent a family of organic semiconductors, which are based on a  $\pi$ -conjugated macrocycle ring. Cobalt phthalocyanine (CoPc) is an interesting candidate for interface research, due to its partially filled  $d_{z^2}$  orbital.

However, the combination of transition metal phthalocyanines with the existing microelectronics technology, being predominantly silicon based, has the potential of novel applications as semiconductor devices. Moreover, semiconductor substrates offer the possibility to tune the molecule substrate interaction by a passivation of the surface. A prominent example in this case is the B-Si(111)- $\sqrt{3} \times \sqrt{3} R30^\circ$  (Si:B) surface. The incorporation of B atoms in the subsurface layer leads to a removal of the dangling bonds of the Si(111) surface. This results in an empty  $p_z$  orbital of the Si adatom and a chemical deactivation of the surface.

In this talk we demonstrate the molecular arrangement and electronic properties of CoPc on the deactivated Si:B surface in detail by means of scanning tunneling microscopy (STM) as well as spectroscopy (STS). Our data clearly show that submonolayers of CoPc lie flat on the surface and that a selective orbital hybridization occurs. Furthermore, our photoemission spectroscopy (PES) data support the model of the formation of local hybrid state between the partially filled  $d_{z^2}$  orbital of the CoPc molecule and the empty  $p_z$  orbital of the Si adatom. For high CoPc coverages, in contrast, CoPc molecules are tilted with respect to the Si:B surface establishing exceedingly ordered molecular arrangements. The spectroscopic data show clearly that several monolayers of CoPc feature identical electronic properties as pure CoPc.

Financial support by the Deutsche Forschungsgemeinschaft of Project No. LI 3068/2-1 is gratefully acknowledged.

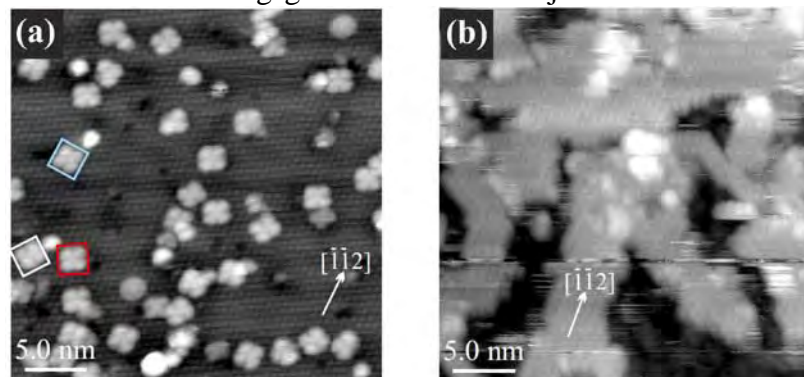


**Figure 1.** (a) Empty states STM image of a passivated Si:B substrate with a CoPc coverage of 0.2 ML (sample voltage  $V_S = +1.8$  V, tunneling current  $I_T = 50$  pA). The different molecular orientations are indicated by colored squares. (b) Empty states STM image of a Si:B surface with a CoPc coverage of 3.2ML ( $V_S = +2.5$  V,  $I_T = 20$  pA)

# Amino-Acids Detection With Modulation Doped and Surface Nanoengineered GaAs Schottky Diodes

**T. Alkhidir<sup>1</sup>, M. Abi-Jaoude<sup>1</sup>, D. L. Gater<sup>2</sup>, C. Alpha<sup>3</sup> and A. F. Isakovic<sup>1,3,4</sup>**

<sup>1</sup>KUST, Chemistry Dept., Abu Dhabi, 127788, United Arab Emirates

<sup>2</sup>University College London, London, WC1E 6BT, UK

<sup>3</sup>Cornell University, CNF, Ithaca, NY, 14850, USA

<sup>4</sup>Colgate University, Physics and Astronomy Dept., Hamilton, NY, 13346, USA

Most current techniques for analyzing amino acids require substantial instrumentation and significant sample pre-processing. With this problem in mind, we designed, fabricated and tested scalable diode-based microdevice that allows for direct sensing and quantification of amino acids. The device is based on a modulation doped GaAs heterostructure with a Schottky contact. While relatively high mobility and small dielectric constant of GaAs are naturally helpful in this problem [1][2], we additionally present how etching procedure allows for substantial modification of the surface properties, thereby further boosting the sensing performance. Data for several qualitatively different amino acids (e.g. belonging to different classes, such as non-polar with aliphatic R-group, polar uncharged R- and charged R-group) with specific examples of Glycine, Cysteine and Histidine, respectively, are presented.

The conductance for the GaAs-amino acid interface measured using scanning tunneling microscope (STM) was previously reported to have distinct spectral features [3][4]. In this talk, we show that measuring differential conductance of GaAs diode whose surface is in a direct contact with an amino acid, can still lead to a useful (and easier to obtain) information, previously available only via effective but cumbersome STM and molecular electronics type of inquiries. We employ standard multivariate data analysis techniques to extract reliably distinct (> 97%) single amino acid specific features. We also present how sensitivity of detection can be achieved within broadly varied pH levels (pH from 4 to 9, so far). Density functional theory (DFT) was used to examine which adsorption processes were likely responsible for surface conductance modification.

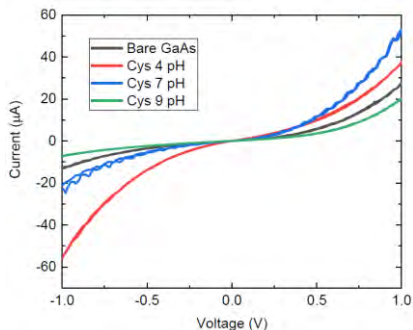


Figure 1 I-V curves of GaAs-Cysteine interface for varied pH factor.

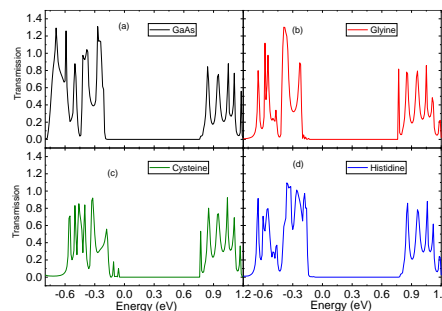


Figure 2 The simulated conductance for the different amino acids adsorbed at GaAs surface

[1] M. Matmor and N. Ashkenasy, J. Am. Chem. Soc. **50**, 132 (2012).

[2] D. Bavli *et al.*, Langmuir. **28**,1020 (2012).

[3] W. Shinwari *et al.*, Adv. Funct. Mater. **20**, 1865 (2010).

[4] F. Piguet *et al.*, Nat. Commun. **9**, 966 (2018).

+ Author for correspondence: [aisakovic@colgate.edu](mailto:aisakovic@colgate.edu)

# Carrier Collection and Transport at *Interface* of Lead-Free Halide Perovskites (FA,MA)SnI<sub>3</sub> Solar Cells

Bich Phuong Nguyen<sup>1</sup>, Hye Ri Jung<sup>1</sup>, Ka Yeon Ryu<sup>2</sup>, KyungKon Kyungkon Kim<sup>2</sup> and William Jo<sup>1\*</sup>

<sup>1</sup>Department of Physics and New and Renewable Energy Research Center (NREC), Ewha Womans University, Seoul 03760, Republic of Korea

<sup>2</sup>Department of Chemistry and Nanoscience, Ewha Womans University, Seoul 03760, Republic of Korea

\*Corresponding author:

Charge extraction at carrier transport layers adjacent to perovskites is crucial for the optimization of perovskite solar cells. In particular, Sn-perovskites with no lead elements are known to struggle from charge extraction. Here, we report effects of organic ligands like FA and MA (FA = HC(NH<sub>2</sub>)<sub>2</sub><sup>+</sup>; MA = CH<sub>3</sub>NH<sub>3</sub><sup>+</sup>) on charge separation at the interface between electron transport layers and perovskites. TiO<sub>2</sub> mesoporous covering the tin-perovskites show significant changes in electronic structure and built-in potentials according to the ratio of FA to MA. Through a local probe with potential and current mapping, charge transport has been intensively examined. The best cell in this study is obtained as 5.37% at FA : MA = 3 : 1 with only iodine at the halide sites. Even though the value itself is not comparable with lead halides but it could pave a new direction to improve lead-free perovskite solar cells.

<sup>+</sup> Author for correspondence: William Jo (wmjo@ewha.ac.kr).

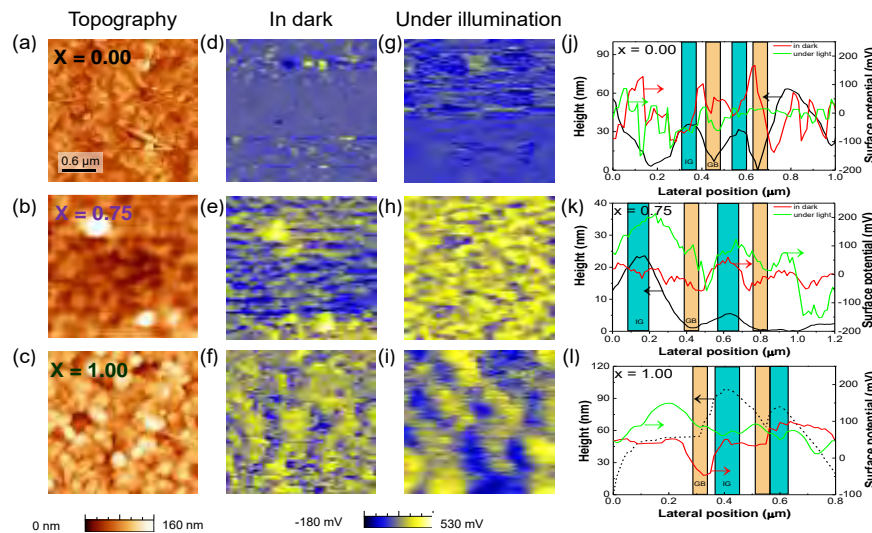


Figure 1. (a)–(c) Topography of the FA<sub>x</sub>MA<sub>1-x</sub>SnI<sub>3</sub>/mesoporous TiO<sub>2</sub>/blocking TiO<sub>2</sub>/FTO substrate. (d)–(f) Surface potential of FA<sub>x</sub>MA<sub>1-x</sub>SnI<sub>3</sub> corresponding to the topography measured in the dark. (g)–(i) Surface potential of FA<sub>x</sub>MA<sub>1-x</sub>SnI<sub>3</sub> corresponding to the topography measured under illumination. (j)–(l) Surface potential profiles of FA<sub>x</sub>MA<sub>1-x</sub>SnI<sub>3</sub> corresponding to the topography measured in dark and under illumination.

# Engineering Active and Stable Semiconductor Photoelectrodes by Atomic Layer Deposition

**Ian D. Sharp<sup>1</sup>**

<sup>1</sup> *Walter Schottky Institute and Physics Department, Technical University of Munich, Am Coulombwall 4, 85748 Garching, Germany*

The capture of solar energy and its direct conversion to chemical fuel in artificial photosystems provides a promising route to sustainably meet global energy demands and to overcome our current reliance on fossil fuels. However, development of practical photosystems has been impeded by a lack of semiconductor light absorbers that are simultaneously efficient and stable under the reactive conditions required for driving desired chemical transformations. To address this issue, new strategies based on atomic layer deposition (ALD) of conformal corrosion protection layers onto photoelectrode surfaces have recently been developed and yield highly robust systems. Here, we provide an overview of such approaches, discuss outstanding challenges that must be addressed, and highlight a multi-functional water splitting catalyst that is specifically engineered to be interfaced with semiconductor light absorbers. In particular, plasma-enhanced ALD is used to create biphasic cobalt oxide composites that strike a careful balance of necessary chemical, optical, and electrical properties [1]. This coating consists of nanocrystalline  $\text{Co}_3\text{O}_4$  spinel that is physically robust and provides a stable interface with the chemically sensitive light absorber. This is combined with a chemically labile and disordered  $\text{Co}(\text{OH})_2$  surface layer that can be easily activated to provide high catalytic activity (Fig. 1). Functional characteristics of the working interface are probed by advanced *in situ* electrochemical X-ray photoelectron spectroscopy, which reveals how the interface transforms from the resting to the active state [2]. Application of the protective catalyst to Si photoanodes results in long-term stable operation with high photochemical activity. These results demonstrate that PE-ALD is a powerful method for synthesizing multi-functional catalysts that support desired chemical transformations, permit efficient interfacial charge transport, and minimize parasitic light absorption due to their conformal nature even at very low thicknesses.

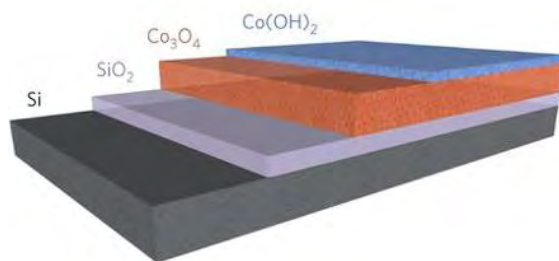


Figure 1: Schematic illustration of the biphasic  $\text{Co}_3\text{O}_4/\text{Co}(\text{OH})_2$  coating formed by PE-ALD that provides high stability and catalytic activity when coupled to a Si photoanode.

[1] J. Yang, et al., *Nature Mater.* **16**, 335 (2017).

[2] M. Favaro, et al., *J. Am. Chem. Soc.* **139**, 8960 (2017).

<sup>+</sup> Author for correspondence: sharp@wsi.tum.de

## Surface states induced catalyst-free CO sensing at GaN and AlGa<sub>N</sub>/GaN heterostructures

Monu Mishra<sup>1,2</sup> and Govind Gupta<sup>2</sup>

<sup>1</sup>*Department of Physics, Indian Institute of Technology Delhi, Hauz Khas, New Delhi - 110016, India.*

<sup>2</sup>*Sensor Devices Metrology, National Physical Laboratory (NPL), New Delhi - 110012, India.*

Email: [monumishra.phy@gmail.com](mailto:monumishra.phy@gmail.com)

### Abstract:

III-Nitride semiconductors owing unique material properties have proven their potential in the detection of light, chemical, biomolecules and toxic/explosive gases. Despite of numerous advantages *viz.* biocompatibility, high temperature/frequency tolerance and harsh/adverse environmental condition sustainability, the use of expensive catalysts (e.g. platinum) and higher operation temperature for gas sensing (>250°C) has plagued the development of GaN based cost-effective sensor technology. Upto the best of our knowledge, literature lacks research articles on the development of catalyst-free CO sensors operating at room-temperature using GaN or AlGa<sub>N</sub>/GaN structures which indicates the necessity of dedicated scientific attention in this area. Therefore, we report the fabrication of nanoflowers-decorated GaN and AlGa<sub>N</sub>/GaN heterostructure based catalyst-free CO sensors operating at lower (including room) temperature. A set of planar as well as nanostructured GaN & AlGa<sub>N</sub>/GaN thin films were employed for sensors fabrication which exhibited significant CO sensing associated with its superior surface and interface properties. For in-depth understanding, the obtained results were thoroughly analyzed and correlated to investigate the underlying science/phenomenon which revealed that CO sensing on GaN (and AlGa<sub>N</sub>/GaN) is governed by the chemical nature of ambient-oxidation induced amorphous oxide (O<sub>2</sub><sup>-</sup>, O<sup>2-</sup> or OH<sup>-</sup> species) layer grown on the surface. These surface state act as donor/acceptor states and perturbed the CO adsorption and charge transfer mechanism significantly. Besides, electron accumulation at AlGa<sub>N</sub>/GaN interface also influenced the critical parameters like schottky barrier height, ideality factor etc. which govern the effective carrier transport and ultimately the device performance. In conclusion, we have observed that the surface and interface states has a strong impact on the efficiency of GaN and AlGa<sub>N</sub>/GaN based fabricated CO sensors. However, being a first study of its kind, further research is required to explore to uncover the scientific phenomenon and optimization of device performance.

### References:

1. M. Mishra, N. K. Bhalla, A. Dash and G. Gupta, Nanostructure GaN and AlGa<sub>N</sub>/GaN heterostructure for catalyst-free low-temperature CO sensing, *Appl. Surf. Sci.* 481, 379 (2019).

## **Cu<sub>2</sub>O Nanoparticles for Enhancing Gas Phase Photocatalysis over Metal Oxide Semiconductor Nanostructures**

**Hikaru (H.) Masegi, Keio University, Japan**

Gas phase photocatalysis over metal oxide (widegap) semiconductor materials has been attracting attention as one of the environmentally friendly technologies such as air purification and clean and renewable energy conversion. In addition, monitoring gas phase photocatalysis is of great use for discussing the basic reaction mechanisms [1]. Since a large part of the metal oxide semiconductor materials are n-type, the development and utilization of p-type materials are quite promising in order to facilitate charge separation and enhance photocatalytic activities via pn-heterojunctions. In this work, we focused on p-type Cu<sub>2</sub>O nanoparticles (CNPs) and performed electrochemical fabrication of composites of CNPs and anodized n-type nanotubular arrays such as hematite ( $\alpha$ -Fe<sub>2</sub>O<sub>3</sub>) and TiO<sub>2</sub>. Then, the gas phase photocatalysis over the prepared nanocomposites was examined to understand roles of CNPs for the enhanced photocatalytic functions.

As an example, hematite nanotubular arrays (FNTs) were fabricated by anodizing pure iron foils in ethylene glycol containing NH<sub>4</sub>F, and crystallized by annealing in oxygen atmosphere. After that, CNPs were deposited onto the anodized samples by pulse electrodeposition in a deposition bath containing CuSO<sub>4</sub> and lactic acid. The CNPs were deposited by applying a potential of -0.6 V<sub>Ag/AgCl</sub> for 0.5 s (on pulse) and 0 V<sub>Ag/AgCl</sub> for 5 s (off pulse). Then, the H<sub>2</sub> amount from decomposition of gas phase water/methanol mixture was evaluated by gas chromatography.

CNPs with an average diameter of 200 nm were deposited on the FNT surface with a pore diameter of 20 nm (See Fig.1). As for their photocatalytic properties, the H<sub>2</sub> amount produced with the CNP/FNT sample increased monotonically with longer time of the visible light irradiation (380-800 nm), and the maximal H<sub>2</sub> yield was 0.08  $\mu$ mol/cm<sup>2</sup> after 6 hours of visible light irradiation (See Fig.2). In addition, H<sub>2</sub> was not detected either with only FNT or only CNP. H<sub>2</sub> production with the FNT/CNP sample may be attributed to Z-scheme mechanism. Besides, we also confirmed that CNPs can work as cocatalysts for photocatalytic TiO<sub>2</sub> nanotubular arrays.

## Self-Selective Formation of 1D and 2D GaBi Structures on GaAs

Y. Liu,<sup>1</sup> S. Benter,<sup>1</sup> J. V. Knutsson,<sup>1</sup> S. Lehmann,<sup>1</sup> E. Young,<sup>2</sup> N. Wilson,<sup>2</sup>  
C. J. Palmstrøm,<sup>2,3</sup> A. Mikkelsen,<sup>1</sup> and R. Timm<sup>1\*</sup>

<sup>1</sup> Department of Physics and NanoLund, Lund University, Box 118, 221 00 Lund, Sweden

<sup>2</sup> Materials Department, University of California – Santa Barbara, CA 93106, USA

<sup>3</sup> Dept. of Elect. & Comp. Eng., University of California – Santa Barbara, CA 93106, USA

Bismuth (Bi) incorporation and alloying in III-V semiconductors such as InAsBi and GaAsBi has become a popular topic during recent years, due to a number of promising properties including band gap engineering, a large spin-orbit splitting, and predicted band inversion and topological behavior in the case of high Bi concentrations [1,2]. However, the realization of alloys with high Bi content by epitaxial growth has remained challenging [3].

We follow a different approach and deposit Bi onto the surfaces of GaAs and InAs planar substrates and nanowires (NWs), aiming for a surface layer of high Bi content. We use scanning tunneling microscopy and spectroscopy (STM/S) for systematically studying Bi adsorption and incorporation for different Bi deposition temperatures and post-deposition annealing parameters. Nanowires give us an extra degree of freedom, since they can be grown containing both segments of cubic zincblende (Zb) and of hexagonal wurtzite (Wz) crystal phase, resulting in a variety of surface facets. Previously, we studied the deposition of Sb on GaAs NWs with STM/S and observed a preferential incorporation of Sb atoms into Zb {110} surface facets as compared to {11-20} Wz facets [4].

Here, we observe the incorporation of Bi atoms in the topmost layer of the GaAs surface through group-V exchange, replacing As atoms, upon Bi deposition on GaAs NWs at a temperature of 250°C. The NWs had been cleaned before by annealing in atomic hydrogen, which has been shown previously to remove the native oxide layer [4]. On the NW Zb segments, Bi atoms are scattered at random positions (though generally on As lattice sites), with an increase in density towards step edges of the surface terraces. On the Wz segments, however, the incorporated Bi tends to form one-dimensional GaBi chains and extended two-dimensional GaBi islands along the <0001> edges of surface terraces. A model for the incorporation of Bi through the step edges will be discussed, including differences observed between {11-20} and {10-10} Wz facets and for different densities of surface steps. Importantly, the ordered 1D and 2D GaBi structures are exclusively found on the Wz segments, which can be tailored in size through NW growth conditions, forming atomically sharp interfaces to Zb segments [5]. This lays the path towards the formation of ordered GaBi structures with atomic-scale precision.

- [1] M. Ferhat, A. Zaoui, *Structural & electronic properties of III-V Bi compounds*, Phys. Rev. B **73**, 1 (2006).
- [2] F.-C. Chuang et al., *Prediction of Large-Gap Two-Dimensional Topological Insulators Consisting of Bilayers of Group III Elements with Bi*, Nano Lett. **14**, 2505 (2014).
- [3] L. Wang et al., *Novel Dilute Bismide, Epitaxy, Physical Properties & Device Appl.*, Crystals **7**, 63 (2017).
- [4] M. Hjort et al., *Crystal Structure Induced Preferential Surface Alloying of Sb on Wurtzite/Zinc Blende GaAs Nanowires*, Nano Lett. **17**, 3634 (2017).
- [5] J.V. Knutsson et al., *Electronic Structure Changes due to Crystal Phase Switching at the Atomic Scale Limit*, ACS Nano **11**, 10519 (2017)

\* Author for correspondence: Rainer.Timm@sljus.lu.se



# Iuliacumite: a novel two-dimensional chemical short range order in a wurtzite single monolayer $\text{InAs}_{1-x}\text{Sb}_x$ shell on InAs nanowires

**M. Schnedler,<sup>1</sup> T. Xu,<sup>2,3</sup> I. Lefebvre,<sup>2</sup> J.-P. Nys,<sup>2</sup> S. R. Plissard,<sup>2,4</sup> M. Berthe,<sup>2</sup> H. Eisele,<sup>5</sup> R. E. Dunin-Borkowski,<sup>1</sup> Ph. Ebert,<sup>1</sup> and B. Grandidier<sup>2</sup>**

<sup>1</sup>Peter Grünberg Institut, Forschungszentrum Jülich GmbH, 52425 Jülich, Germany

<sup>2</sup>Université Lille, CNRS, Centrale Lille, ISEN, Université Valenciennes, UMR 8520 - IEMN, F-59000 Lille, France

<sup>3</sup>Key Laboratory of Advanced Display and System Application, Shanghai University, 149 Yanchang Road, Shanghai 200072, People's Republic of China

<sup>4</sup>CNRS-Laboratoire d'Analyse et d'Architecture des Systèmes (LAAS), Université de Toulouse, 7 Avenue du Colonel Roche, 31400 Toulouse, France

<sup>5</sup>Institut für Festkörperphysik, Technische Universität Berlin, Hardenbergstr. 36, 10623 Berlin

The reduced dimensionality of semiconductor nanowires (NWs) offers the unique opportunity to grow materials with crystal structures, which are otherwise unstable. One of the most prominent example is the growth of wurtzite (WZ) structure InAs NWs, although stable InAs bulk material prefers the zincblende (ZB) structure. In contrast, other III-V materials, notably  $\text{InAs}_{1-x}\text{Sb}_x$ , prefer to keep their ZB bulk structure even in NWs or nanostructures with reduced dimensionality. However, lateral overgrowth of these ternary III-V semiconductor alloys on sidewall facets of WZ structure III-V nanowires offers the prospect to nevertheless obtain reliably a WZ structure shell, despite being unstable. Thereby new polytype structures of ternary III-V semiconductor alloys can be achieved, offering additional degrees of freedom for adjusting the band structure in, e.g., core-shell nanowires. Therefore, we designed a two-dimensional single monolayer  $\text{InAs}_{1-x}\text{Sb}_x$  WZ structure shell on sidewall facets of InAs nanowires and investigated the chemical ordering using atomically resolved scanning tunneling microscopy. We identify the existence of a short-range chemical ordering in this WZ structure single monolayer shell. The new type of two-dimensional ordering, called Iuliacumite, is characterized by an ordering vector in  $[0001]$  and an anti-ordering vector in  $\langle 11-20 \rangle$  direction. The ordering is driven by a strong repulsive interaction of neighboring Sb atoms along the  $\langle 11-20 \rangle$ -oriented atomic chains on the  $m$  plane sidewall facets.

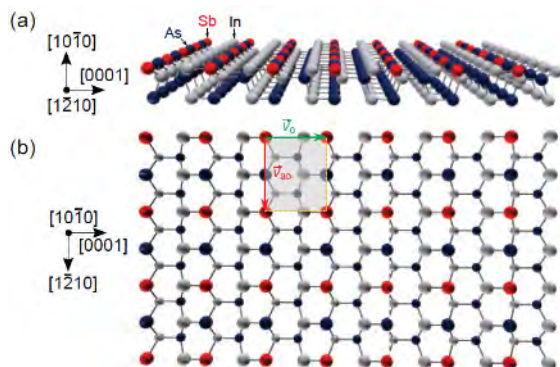


Figure 1 Perspective view of a ball model of the two-dimensional idealized (long range) chemical ordering of the monolayer shell on the InAs sidewall facet, based on the ordering and antiordering vectors extracted from pair correlation function. (a) Side and (b) top view with surface unit cell.

<sup>+</sup> Author for correspondence: m.schnedler@fz-juelich.de, bruno.grandidier@isen.iemn.univ-lille1.fr

## Control of spin-orbit coupling in single acceptor states in silicon

S. Rogge<sup>+</sup>

*Centre for Quantum Computation and Communication Technology,  
School of Physics, University of New South Wales Sydney, NSW 2052, Australia*

Spins in silicon are suitable candidates for scalable quantum information devices, because of their long coherence times and inherent compatibility with current CMOS processing techniques. While quantum information devices in donor-based systems have been shown to be promising [1], the small dipole moment of donor spins make interaction of multiple qubits challenging to implement. The presence of spin-orbit coupling in acceptors however, could allow for fast quantum-gate manipulations [2] and effective long-range inter-qubit coupling [3]. Recent acceptor qubit proposals [4] suggest the possibility of maintaining the dipole moment between the spin-orbit states, without suffering from short coherence times.

In the first part of the presentation we show that long coherence times can be achieved for acceptor spins in bulk isotopically purified strained  $^{28}\text{Si}$ . By coupling the bulk  $^{28}\text{Si}$  crystal to a superconducting coplanar waveguide (CPW) resonator, we measured a coherence time ( $T_2$ ) of 0.7 ms for the acceptor spin ensemble in bulk  $^{28}\text{Si}$  crystal under strain, in contrast to 0.04 ms for the same crystal without externally applied strain. The coherence time for the strained  $^{28}\text{Si}$  crystal was extended to 8.5 ms with the Carr-Purcell-Meiboom-Gill (CPMG) sequence [5]. This value for this coherence time is over 4 orders of magnitude higher than previously found in boron-doped silicon devices [6] and demonstrates the potential of boron-based acceptor spins in silicon as a candidate for scalable, electrically-driven qubits with long coherence times.

In the second part of the talk we focus on addressing single acceptors [7]. In general,  $J = 3/2$  systems are much less studied than  $S = 1/2$  electrons, and spin readout had not yet been demonstrated for acceptors in silicon. We present acceptor hole spin dynamics by dispersive readout of single-hole tunneling between two coupled acceptors in a nanowire transistor [8]. We identify  $mJ = \pm 1/2$  and  $mJ = \pm 3/2$  levels, and we use a magnetic field to overcome the initial heavy-light hole splitting and to tune the  $J = 3/2$  energy spectrum. We find regimes of spin-like ( $+3/2$  to  $-3/2$ ) and charge-like ( $\pm 1/2$  to  $\pm 3/2$ ) relaxations, separated by a regime of enhanced relaxation induced by mixing of light and heavy holes. The demonstrated control over the energy level ordering and hybridization are new tools in the  $J = 3/2$  system that are crucial to optimize single-atom spin lifetime and electrical coupling.

[1] J. T. Muhonen, et al., Nat. Nanotechnol. 9, 986-991 (2014)

[2] E. Kawakami, et al., Nat. Nanotechnol. 9, 666-670 (2014)

[3] J. J. Viennot, et al., Science 349, 408-411 (2015)

[4] R. Ruskov, et al., Phys. Rev. B 88, 064308 (2013); J. Salfi, et al., Phys. Rev. Lett. 116, 246801 (2016); Abadillo-Uriel, et al., New J. Phys. 19, 4 (2017)

[5] T. Kobayashi et al., arXiv:1809.10859v2 (2018)

[6] Y. P. Song & B. Golding, Europhys. Lett. 95, 47004 (2011)

[7] J. van der Heijden et al., Nanoletter Nano Lett 14, 1492-1496 (2014)

[8] J. van der Heijden et al., Sci. Adv. 4, eaat9199 (2018)

<sup>+</sup> Author for correspondence: [s.rogge@unsw.edu.au](mailto:s.rogge@unsw.edu.au)

## Low-Temperature Epitaxial Silicon Growth and Confinement of Delta Doped Si:P Nanostructures

S.W. Schmucker<sup>+</sup>, E.M. Anderson, J. Lucero, E. Bussmann, P. Lu, A.M. Katzenmeyer, T.S. Luk, T.E. Beechem, L.A. Tracy, T.-M. Lu, A.D. Grine, D.R. Ward, D. Campbell, P. Gamache, M. Gunter, S. Misra

*Sandia National Laboratories, 1515 Eubank Blvd SE, Albuquerque, NM 87123*

Atomically precise placement of phosphorus dopants using scanning tunneling microscopy-based hydrogen depassivation lithography (Figure 1) on silicon (Si:P) has implications for both high-performance digital electronics and quantum devices. Devices are fabricated by dissociative chemisorption of donor precursor molecules into patterned reactive areas in a hydrogen resist. A silicon capping layer, needed to encapsulate the device, is deposited at temperatures low enough to prevent dopant movement, but high enough to minimize defect generation.

Here, we explore the origin and influence of atomic defects in both the dopant layer and Si overgrowth, techniques available for characterization of these defects, and the relationship between surface passivation and device fidelity. Using a combination of optical spectroscopy, electrical transport, and transmission electron microscopy (TEM) (Figure 2), we relate P confinement and defect density in Si epitaxy to parameters of the fabrication process, surface chemistry, and the electronic characteristics of the resulting devices.

This work was supported by the Laboratory Directed Research and Development Program at Sandia National Laboratories, and was performed, in part, at the Center for Integrated Nanotechnologies, a U.S. DOE, Office of Basic Energy Sciences user facility. Sandia National Laboratories is managed and operated by National Technology and Engineering Solutions of Sandia, LLC., a wholly owned subsidiary of Honeywell International, Inc., for the U.S. Department of Energy under contract DE-NA-0003525. The views expressed do not necessary represent the views of the U.S. DOE or the United States Government.



Figure 1 Lithographically defined device on Si(100) 2×1:H

<sup>+</sup> Author for correspondence: [swschmu@sandia.gov](mailto:swschmu@sandia.gov)

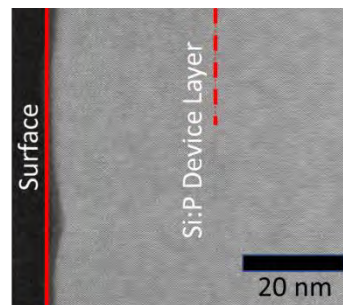


Figure 2 TEM cross-section of Si:P device after Si epitaxy

# The Electronic Bandstructure of Atomically Sharp Dopant Structures in Silicon

Justin W. Wells<sup>+</sup>

*Center for Quantum Spintronics, Department of Physics, Norwegian University of Science and Technology, NO-7491 Trondheim, Norway*

Recently, it has become possible to control the placement of dopants in silicon with atomic precision, and this has given rise to a plethora of atomic scale and quantum proto-devices [1-3]. In this talk, I will present our ongoing work on understanding the electronic bandstructure of these dopant profiles in silicon.

Angle Resolved Photo-Electron Spectroscopy (ARPES) is the method of choice for observing the bandstructure, however observing the bandstructure of buried structures is extremely challenging. We have demonstrated that it is nonetheless possible to use ARPES to measure the bandstructure of dopant structures which have been created several nm beneath the surface [4]. It is also possible to see electron-phonon and electron-impurity interactions [5], quantum confinement of both the valence band and conduction band [6] and more. I will present these findings together with an overview of the current in understanding and controlling the electronic structure of dopant assemblies in semiconductors.

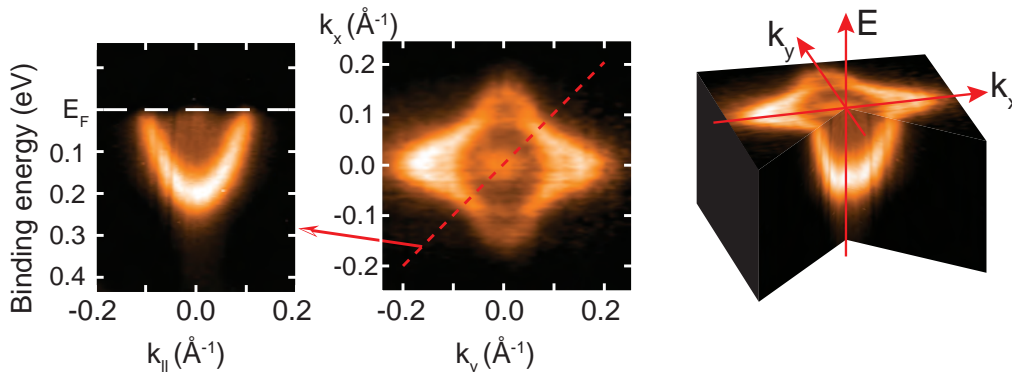


**Figure:** The measured electronic bandstructure of a 2D plane of dopants within a silicon host (so-called “delta-layer”) located several nm beneath the sample surface.

- [1] Weber *et al.*, Science 335, 64 (2012)
- [2] Zwanenburg *et al.*, Rev. Mod. Phys. 85:961 (2013).
- [3] Watson *et al.*, Nature 555, 633 EP (2018)
- [4] Miwa *et al.*, Phys. Rev. Lett. 110:136801 (2013)
- [5] Mazzola *et al.*, Appl. Phys. Lett. 104: 173108 (2014)
- [6] Mazzola *et al.*, Phys. Rev. Lett. 120:046403 (2018)

<sup>+</sup> Author for correspondence: justin.wells@ntnu.no

## Fluctuating high temperature superconductivity in monolayer FeSe / SrTiO<sub>3</sub>

Kyle M. Shen<sup>1</sup>, Brendan D. Faeth<sup>1</sup>, Shuolong Yang<sup>1,2</sup>, Darrell G. Schlom<sup>2</sup>

<sup>1</sup> Department of Physics, Cornell University, Ithaca NY 14853

<sup>2</sup> Department of Materials Science & Engineering, Cornell University, Ithaca NY 14853

The nature and origin of the enhanced superconductivity in monolayer FeSe / SrTiO<sub>3</sub> has been attracted tremendous interest due to its unique character as an interfacially enhanced high-T<sub>c</sub> superconductor. FeSe / SrTiO<sub>3</sub> exhibits a spectroscopic gap opening temperature ( $T_{\text{gap}}$ ) between 60 to 70 K, nearly one order of magnitude higher than that of bulk FeSe ( $T_c = 8\text{K}$ ), and in excess of related electron-doped FeSe-based bulk compounds. This dramatic enhancement remains the largest amongst known superconductors, positioning monolayer FeSe / SrTiO<sub>3</sub> as an ideal platform for investigating fundamental questions about interfacial superconductivity. In particular, the combination of its high-T<sub>c</sub> and inherently two-dimensional (2D) nature makes FeSe / SrTiO<sub>3</sub> suited for exploring the interplay between 2D phase fluctuations and the interfacial enhancement of superconductivity, a better understanding of which could enable the future design and engineering of artificial higher-T<sub>c</sub> superconductors. In this work, we employ a combination of *in situ* electrical resistivity and angle-resolved photoemission spectroscopy (ARPES) measurements of monolayer FeSe / SrTiO<sub>3</sub> to reveal an unprecedentedly large pseudogap regime between the initial formation of incoherent Cooper pairs ( $T_{\text{gap}} \sim 70\text{K}$ ) and the onset of a zero resistance state ( $T_0 \sim 30\text{K}$ ). Through measurements of the V(I) characteristics, we identify this large pseudogap regime as originating from two-dimensional superconducting fluctuations, establishing the critical role that reduced dimensionality plays in the superconductivity of monolayer FeSe / SrTiO<sub>3</sub>.

<sup>+</sup> Author for correspondence: kmshen@cornell.edu

## Advances and possibilities of the Materials Innovation Platform with examples from Spin-ARPES

**Daniel A Beaton<sup>1</sup>, M. Lundwall<sup>1</sup>, T. Wiell<sup>1</sup>, R. G. Moore<sup>2</sup>, M. Brahlek<sup>2</sup>, Ho Nyung Lee<sup>2</sup>**

<sup>1</sup> Scienta Omicron Inc., 3222 E. 1st Ave., Suite 512, Denver CO 80206

<sup>2</sup> Materials Science and Technology Division, Oak Ridge National Laboratory, Oak Ridge, TN 37831, USA

The quest for device applications based on quantum materials, such as topological insulators, density wave systems, or superconductors, requires strict control of the environments these materials are exposed to during production and also while under investigation. It is most straightforward to gather all parts of the experiment, from sample growth to state-of-the-art analysis, in one connected UHV system. This approach in creating a so-called Materials Innovation Platform (MIP) has proven to be extraordinarily valuable in recent years.

In this presentation, I will focus on one such configuration; a combination Molecular Beam Epitaxy (MBE) system and Angle Resolved PhotoEmission Spectroscopy with spin detection capability (Spin-ARPES). The advantages of this set-up will be explored, as well as highlighting some of the very recent electronic band structure research performed with such a system. Two specific examples will be reviewed: Yang *et al.*[1] investigation of the impact of photogenerated carriers on the superconducting transition temperature; and advances high efficiency spin-ARPES[2]. The work by Yang *et al.*, enabled by the *in-situ* growth and analysis possibility, shows rapid, reliable, reproducible switching between normal and superconducting states, which demonstrates the possibility of making energy-efficient quantum optoelectronics devices. Future possibilities of Spin-ARPES and laser-ARPES in combination with MIP will also be discussed in relation to how this approach can allow more complete and precise studies of quantum materials.

[1] Yang et al., Nature Communications (2019)10:85, <https://doi.org/10.1038/s41467-018-08024-w>

[2] Data courtesy: Prof. Dengsung Lin, Dept. of Physics, NTHU, Taiwan

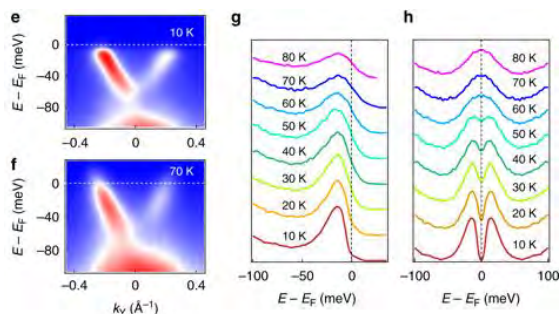


Figure 1: Taken from Yang *et al.*, ARPES Lab spectra across M-point measured at 10K (e) and 70K (f). Temperature-dependent energy distribution curves (EDCs) (g) and symmetrized EDCs (h) at the Fermi crossing, showing the superconducting gap opening between 50 K and 60 K.

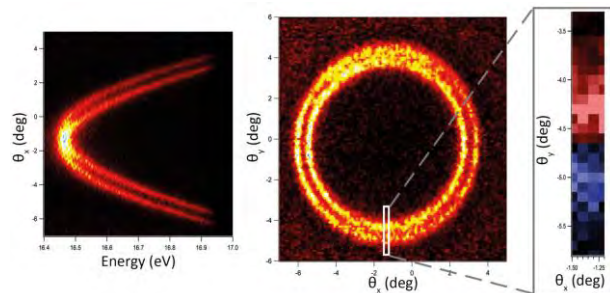


Figure 2: Overview ARPES and spin-ARPES data from [2] exemplifying high quality, high efficiency spin resolved measurements with the DA30L and VUV5k He lamp.

<sup>+</sup> Author for correspondence: [Daniel.Beaton@scientaomicron.com](mailto:Daniel.Beaton@scientaomicron.com)

# Superconductivity at Surfaces studied by Scanning Tunneling Microscopy

**Y. Hasegawa**<sup>1+</sup>

<sup>1</sup> *The Institute for Solid State Physics, The University of Tokyo*

Superconductivity that emerges in metallic surface states is one of the ultimately thin two-dimensional (2D) superconductors. One of the advantages, if compared with other 2D superconductors, is that atomically well-ordered structures can be easily formed in macroscopic dimensions because of the thermal stability through the self-organized structural reconstruction. Basic properties such as atomic structure and electronic states are well characterized by standard surface science techniques including scanning tunneling microscopy (STM), and can be modified in a controlled manner through the deposition and adsorption of additional materials.

One ubiquitous feature of the 2D atomically-thin electronic systems is the natural presence of atomic steps on its substrate. Atomic steps are considered to strongly affect electron transport as they decouple neighboring surface terraces [1]. We have demonstrated that the steps of the  $\sqrt{3}\times\sqrt{3}$ -In/Si(111) surface superconductor behave as a Josephson junction and hold elongated vortices called Josephson vortices along the steps [2]. On striped incommensurate (SIC) phase of Pb/Si(111) the steps are found to block the propagation of the superconducting proximity effect and enhance it when they are located within the coherence length [3].

In two-dimensional superconductors usual orbital pair breaking of the superconductivity by in-plane magnetic field can be suppressed, allowing the Zeeman pair breaking to determine the critical magnetic field. There is however no protection against perpendicular magnetic fields. Using STM, we found that in narrow terraces of the Pb/Si(111) surface whose width is less than the coherence length superconductivity is protected against perpendicular magnetic fields. It is presumably due to the suppression of orbital pair breaking by the step confinement. Since the density and the coupling strength of the steps can be controlled, our study opens a way to design 2D superconductors that maintain the pair correlation under magnetic field in all directions.

[1] M. Hamada and Y. Hasegawa, Phys. Rev. B 99, 125402 1-5 (2019)

[2] S. Yoshizawa, H. Kim, T. Kawakami, Y. Nagai, T. Nakayama, Xiao Hu, Y. Hasegawa, T. Uchihashi, Phys. Rev. Lett. 113, 247004 1-5 (2014).

[3] H. Kim, S.-Z. Lin, M. J. Graf, Y. Miyata, Y. Nagai, T. Kato, and Y. Hasegawa, Phys. Rev. Lett., 117, 116802 1-5 (2016)

<sup>+</sup>Author for correspondence: hasegawa@issp.u-tokyo.ac.jp

# Quantum Microscopy of Nanoscale Materials and Devices

**Christian Degen**<sup>1</sup>

<sup>1</sup> *Department of Physics, Otto Stern Weg 1, ETH Zurich, Zurich, Switzerland;  
www.spin.ethz.ch*

Diamond nanoprobe with single engineered NV centers allow enhancing scanning probe microscopy with quantum metrology. In this talk, I will introduce the basic concepts and technology of diamond nanoprobe, and give illustrative examples of applications in nanoscale imaging of magnetism and currents.

<sup>+</sup> Author for correspondence: [degenc@ethz.ch](mailto:degenc@ethz.ch)



# Mechanical control of valley magnetization and Berry curvature dipole in monolayer MoS<sub>2</sub>

**Joolee Son,<sup>1</sup> Kyung-Han Kim,<sup>2</sup> Yeong Hwan Ahn,<sup>1</sup> Hyun-Woo Lee,<sup>2</sup> Jieun Lee<sup>1</sup>**

<sup>1</sup> *Department of Physics and Department of Energy Systems Research, Ajou University, Suwon, 16499, Korea*

<sup>2</sup> *Department of Physics, Pohang University of Science and Technology, Pohang, 37673, Korea*

Atomically thin honeycomb crystals have recently emerged as promising platforms to investigate electron's valley degree of freedom for the development of functional valley-based devices. Electron control by valley index has been demonstrated using electrical, optical and magnetic means, owing to the opposite signs of the Berry curvature between two valley centers. Here we report a different kind of valley-based electron control that is based on the Berry curvature dipole. We demonstrate the generation of net valley magnetization under an in-plane electric field, regulated by the strain-induced modification of the Berry curvature distribution, which produces the Berry curvature dipole [1]. The generation of valley magnetization is optically detected by using the Kerr rotation microscopy on monolayer MoS<sub>2</sub> embedded in flexible van der Waals heterostructures as functions of tunable strain. The measured valley magnetization is well explained by the calculated values of the strain-induced Berry curvature dipole. Our work demonstrates strain as a new functionality for potential novel flexomagnetic and valley information processing devices using monolayer TMD materials.

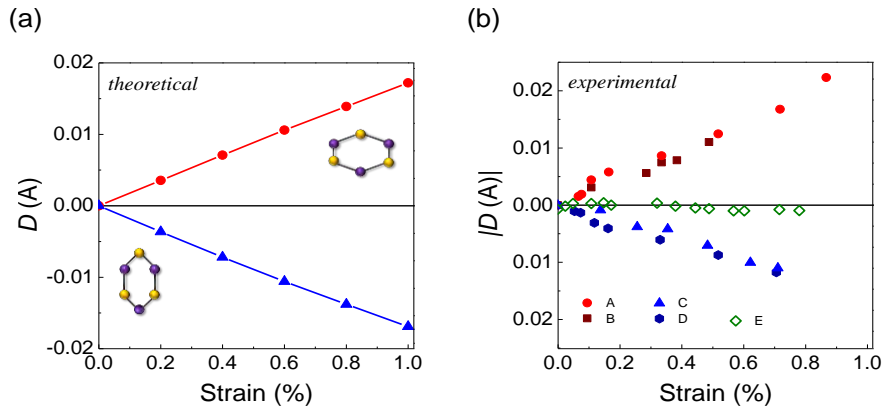


Figure 1. (a) Theoretically calculated and (b) experimentally measured Berry curvature dipole as a function of strain for two different strain directions.

[1] J. Son, et al. Phys. Rev. Lett. **123**, 036806 (2019).

<sup>+</sup> Author for correspondence: jelee@ajou.ac.kr

# Room Temperature Ferromagnetic Monolayer MnGaN-2D Investigated by Spin-polarized Scanning Tunneling Microscopy/ Spectroscopy and First-principles Density Functional Theory

Y. Ma,<sup>1</sup> T. Erickson,<sup>1</sup> K.-Y. Meng,<sup>2</sup> F.-Y. Yang,<sup>2</sup> D. Hunt,<sup>3</sup> A. Barral,<sup>3</sup> V. Ferrari,<sup>3</sup> and A. R. Smith<sup>1+</sup>

<sup>1</sup> *Nanoscale & Quantum Phenomena Institute, Department of Physics & Astronomy, Athens, OH 45701*

<sup>2</sup> *Department of Physics, The Ohio State University, Columbus, OH 43210*

<sup>3</sup> *Departamento de Fisica de la Materia Condensada, GIyA, CAC-CNEA, Buenos Aires, Argentina*

Development of spintronic applications based on semiconductor materials combined with magnetic dopants has been a topic of great interest for many years. More recently has been the rapid growth of interest in 2-dimensional materials with both semi-conductive and/or magnetic properties. We have reported the direct observation of the room-temperature ferromagnetism for MnGaN-2D using spin-polarized scanning tunneling microscopy and spectroscopy combined with first-principles calculations.[1] This 2D material is directly grown on the surface of N-polar GaN(000 $\bar{1}$ ) using molecular beam epitaxy and consists of 1/3 ML of Mn atoms incorporated into the surface Ga adlayer and forming a  $\sqrt{3} \times \sqrt{3} - R30^\circ$  structure as seen in Fig. 1.

Density functional theory shows that this monolayer structure has *perpendicular* magnetic anisotropy with a highly spin-polarized and spin-split manganese density of states. We verify the magnetic properties using SQUID magnetometry. In addition, we explore changes in the energy of the Mn peak DOS as seen in tunneling spectroscopy and discover theoretically that it is caused by surface strain. Different models, including isotropic, anisotropic, and defect-induced strain models are explored, and it is concluded that the Mn-N bond length is the critical parameter. The local strain is then directly observed in atomic scale STM images as a non-Gaussian distribution of lattice parameters, and disordering is seen in the 2D pair correlation as well. This strain may be the effect of the manner in which the surface is prepared, thus opening the possibility of atomic-scale engineering of magnetic anisotropy.

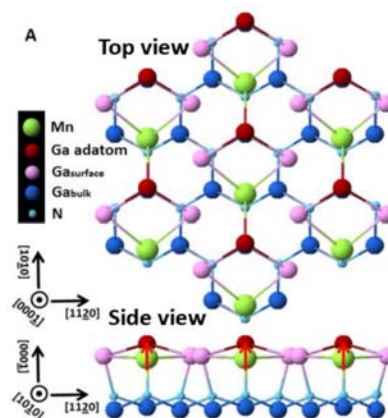


Figure 1. Top and Side views of MnGaN-2D structural model based on First-principles Density Functional Theory.

[1] Y. Ma, A.V. Chinchore, A.R. Smith, M.A. Barral, and V. Ferrari, *Nano Letters* **18**, 158 (2018).

<sup>+</sup> Author for correspondence: smitha2@ohio.edu

# Local Exchange Resonance in DC Magnetoresistance of Spin-Polarized Current Through a Dopant

**S. R. McMillan<sup>1,2</sup>, N. J. Harmon<sup>1,3</sup>, M. E. Flatté<sup>1,3,4</sup>**

<sup>1</sup> *Optical Science and Technology Center, and Department of Physics and Astronomy, University of Iowa, Iowa City, Iowa 52242, USA*

<sup>2</sup> *Pritzker School of Molecular Engineering, University of Chicago, Chicago, Illinois 60637, USA*

<sup>3</sup> *Department of Physics, University of Evansville, Evansville, Indiana 47722, USA*

<sup>4</sup> *Department of Applied Physics, Eindhoven University of Technology, P. O. Box 513, 5600 MB, Eindhoven, The Netherlands*

Components for quantum information processing and quantum sensing require localized spin-coherent states. These states can be realized in isolated magnetic dopants embedded in a non-magnetic semiconducting host. A critical requirement for utilizing a dopant-based system is an understanding of how the complex host environment influences the coherent spin dynamics at an individual site. In this work we consider the dc magnetoresistance through a spin-1/2 dopant that is addressed by a spin-polarized scanning tunneling microscope (SP-STM) and exchange coupled to an inert spin-1/2 center [1]. The stochastic Liouville formalism is employed to calculate the current through the individual dopant. We predict a substantial increase in resistance at finite magnetic fields due to the formation of a non-trivial bottleneck in the spin-correlated transport. Resonance between the Zeeman and exchange coupling leads to a cancellation in the coherent evolution of the dopant spin resulting in an on-site polarization opposing that of the SP-STM. This feature provides a precise method for measuring the dopant exchange coupling to a nearby electronic spin and by direct analog hyperfine coupling in the presence of nuclear spins. This technique does not require the use of ac electric or magnetic fields and is sensitive to exchange or hyperfine energies well below the thermal energy of the system.

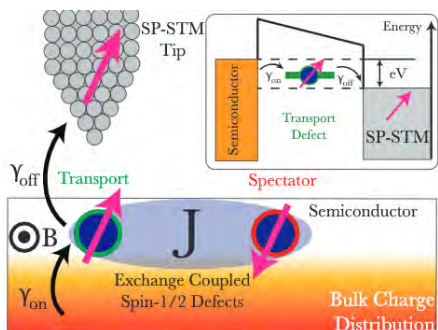


Figure 1: Schematic current path for an electron through a spin-1/2 dopant exchange coupled to a spin-1/2 center.

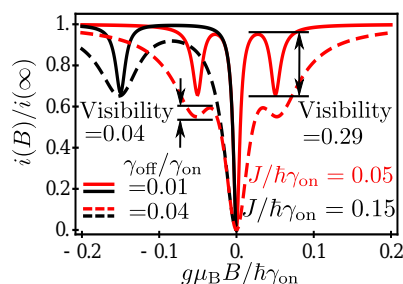


Figure 2: Magnetoresistance of current through spin-1/2 dopant. Features broaden for moderate extraction (dashed) compared to slow extraction (solid).

[1] S.R. McMillan, N.J. Harmon, M.E. Flatté, [arXiv:1907.05509](https://arxiv.org/abs/1907.05509) [cond-mat.mes-hall]

+ Author for correspondence: Stephen.mcmillan7@gmail.com

## Room temperature ferromagnetism in GaSb thin films doped with Mn

**C.A Pulzara Mora,<sup>1</sup> A.O Pulzara Mora<sup>1</sup>, R. Sáez Puche<sup>2</sup>,  
N. M. Nemes<sup>2</sup>, A. Asenjo Barahona<sup>3</sup>**

<sup>1</sup> *Department of Physics and Chemistry, Universidad Nacional de Colombia, 170001-Manizales, Colombia*

<sup>2</sup> *Universidad Complutense de Madrid, 28040 Madrid, Spain*

<sup>3</sup> *Instituto de Ciencia de Materiales de Madrid, CSIC, 28049, Spain*

The design and development of Hall Effect magnetic field sensors with III-V semiconductor materials and magnetic alloys (Mn) is a current topic - due to its applications in different branches of physics like spintronics. Semiconductor materials such as GaSb are important because of their applications in modern Nano-electronics, infrared emitting lasers with a 0.7 eV bandgap and especially in photovoltaic systems and their optical response to wavelengths longer than silicon-based solar cells [1][2]. When the Mn is introduced in the matrix of these semiconductors, we have new opportunities in the context of spintronics, owing that in the alloys the spatial distribution of electrons and holes can be controlled easily, resulting in the magnetic properties of these materials.

The structural, electrical and magnetic properties of GaSbMn thin films were studied. The samples were grown by Magnetron Sputtering on heated Si (111) substrates. In order to incorporate Mn in low concentrations in the GaSb matrix, the substrate temperatures were varied from 300°C to 400°C. X-ray diffraction patterns show that they have a polycrystalline structure. We find that at 300°C GaSbMn grows as a smooth, phase-pure film, whereas at higher temperatures (400°C) the films become increasingly rough, but more crystalline with segregated MnSb and Mn impurities, shown also by Scanning Electron Microscopy. High temperature SQUID magnetometry measures Curie temperatures of 350 K for the film grown at 300°C, and above 500K for 400°C. The GaSbMn exhibits a well-defined magnetic hysteresis loop above room temperature. These loops show that the superparamagnetic (or weak ferromagnetic) behavior of the GaSbMn layers depends on the Mn content. Magnetotransport measurements show well developed anomalous Hall effect (AHE) hysteresis loops that persist up to room temperature. This result shows that the magnetic properties are very sensitive to experimental parameters such as working pressure and growth temperature [3][4].

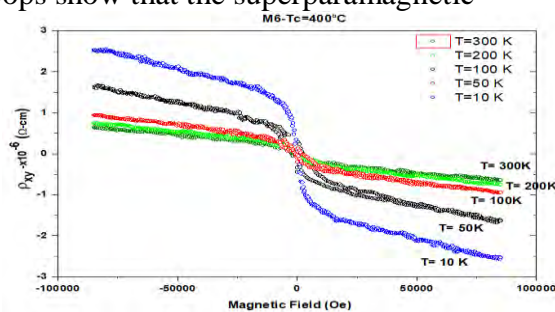


Figure 1. Resistivity Vs Magnetic field

[1] H. Luo, *Elsevier*, vol. 20, no. 3-4, pp. 338-345, 2004.

[2] R. Bernal-correa, *Momento*, no. 51, pp. 31-44, 2015

[3] M. R. Islam, *Cryst. Res. Technol.* 43, No. 10, 1091 - 1096 (2008).

[4] Z.C. Feng, *J. Appl. Phys.* 68, 5363 (1990).

+ [capulzaram@unal.edu.co](mailto:capulzaram@unal.edu.co)

## Magnetotransport studies in hybrid 2D/0D nanostructures

**Ethel Perez-Hoyos,<sup>1</sup> Yunqiu (Kelly) Luo,<sup>1</sup> Abhilasha Dehankar,<sup>2</sup> Jinsong Xu,<sup>1</sup> Daniel Pharis,<sup>1</sup> Roland Kawakami,<sup>1</sup> Jessica Winter,<sup>2</sup> Ezekiel Johnston-Halperin,<sup>1</sup>**

<sup>1</sup> Department of Physics, The Ohio State University, Columbus, OH, USA

<sup>2</sup> Department of Chemical and Biomolecular Engineering, The Ohio State University, Columbus, OH, USA

We introduce a device fabrication strategy that takes advantage of stacking techniques developed for van der Waals heterostructures to construct hybrid 2D/0D composite magnetic nanostructures, with potential application in the study of spin and charge disorder as well as magnetic-proximity effects. The structures in this study are comprised of superparamagnetic iron oxide nanoparticles (SPIONs) and monolayer graphene. The SPIONs are deposited first using a Langmuir-Blodgett technique, yielding rafts of highly ordered nanoparticles (Fig. 1b). Characterization via magnetic force microscopy (MFM) reveals magnetic order at multiple length scales and SQUID magnetometry identifies both glassy antiferromagnetic and ferromagnetic response. Single graphene monolayers are mechanically stacked on the SPIONs layer, and characterized via low temperature magneto-transport. Initial measurements show good electron mobility in the graphene layer and indications of exchange coupling between the graphene and the SPIONs layer.

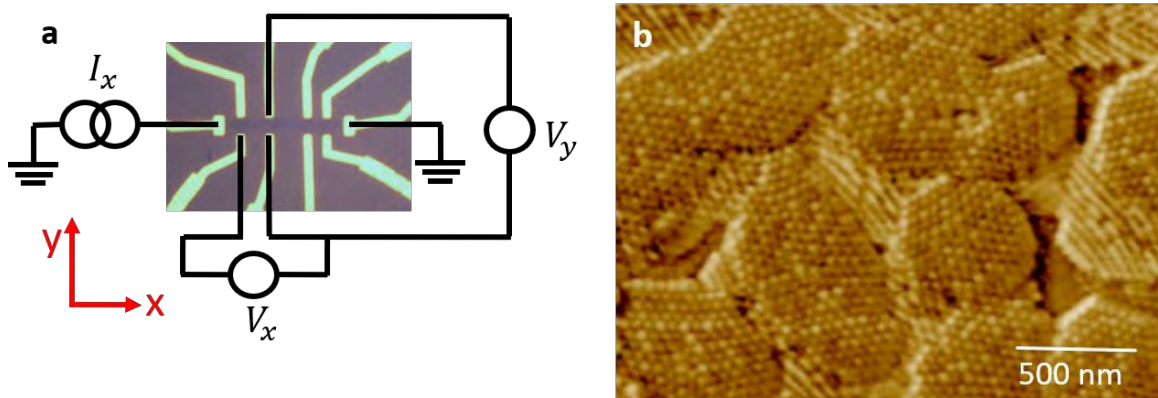


Figure 1 (a) geometry of the measurement. (b) MFM showing the SPIONs rafts.

## Fabrication of high coherence superconducting qubits

J. Long<sup>1</sup>, H. S. Ku<sup>1,2</sup>, X. Wu<sup>1,3</sup>, R. E. Lake<sup>1,4</sup>, D. P. Pappas<sup>1</sup>

<sup>1</sup>NIST, 325 Broadway, Boulder, CO 80305

<sup>2</sup>Alibaba, China 699 Wangshang Rd, Binjiang, Hangzhou, Zhejiang, China

<sup>3</sup>7000 East Avenue • Livermore, CA 94550

<sup>4</sup>Arinatie 10, 00370 Helsinki Finland

Scaling up qubit circuits and achieving high coherence relative to gate speed is imperative to realizing the full power of quantum computing. In this work we demonstrate superconducting transmons with coherence times ranging from 25 to 90  $\mu$ s, significantly longer than typical gate speeds, from 10 to 200 ns for single and two-qubit interactions.

The circuits were fabricated on intrinsic Si(001) substrates (Fig. 1). The NBTiN metallization (gold color) was patterned optically. The CPW meander feedline (from Port 1 to Port 2), capacitively couples to readout resonators (R1-R6, only R1 labeled for clarity) which are then capacitively coupled to a large, concentric capacitor shunt. The capacitor plates are connected together with a small Josephson junction that was fabricated using a two-step e-beam overlap process [1] to form transmon qubits, Q1-Q6. Some of the methods used to enhance the coherence include using a nitride pre-treatment of the substrate prior to metallization, post-treatment of the circuit with buffered oxide etch, and extensive wire-bonding. Variations of coherence between qubits was about a factor of 2, and can be understood in, for example, one case (the shortest) as being due to damage during wire-bonding. Fluctuations are hypothesized to be due to coupling of the qubits to two-level systems around the junctions [2].

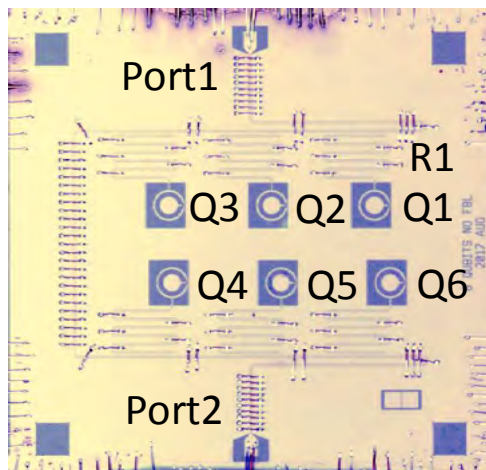


Figure 1: Six qubit test chip, 7.5x7.5 mm<sup>2</sup>.

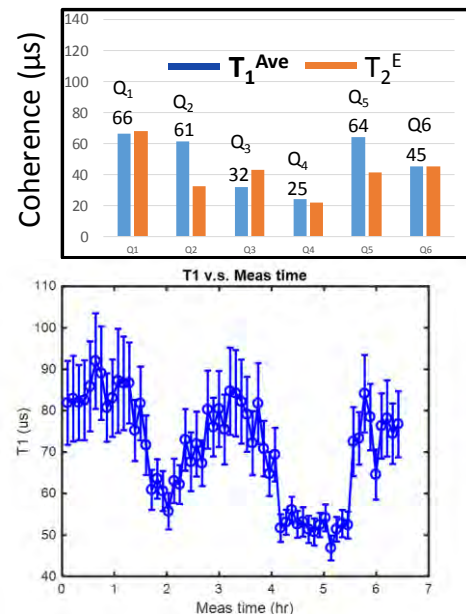


Figure 1: Top-Average coherence of qubits measured over 6 hours. Bottom- Variation of Q1 coherence.

[1] X. Wu, et al., Applied Physics Letters 111 (3), 032602.

[2] S. Schlor, et al., arXiv:1901.05352

+ Author for correspondence: David. [Pappas@NIST.gov](mailto:Pappas@NIST.gov)

## Interface Chemistry and Decoherence Processes in Superconducting Quantum Circuits

**D. Frank Ogletree,<sup>1</sup> Virginia Altoe,<sup>1</sup> Xiaotao Liu,<sup>1</sup> Andrew Minor,<sup>1</sup> Stefano Cabrini,<sup>1</sup> Sinéad Griffin,<sup>1</sup> Archan Banerjee,<sup>2</sup> John-Mark Kriekebaum,<sup>3</sup> Irfan Siddiqi<sup>2,3</sup>**

<sup>1</sup> *Molecular Foundry LBNL, Berkeley CA USA*

<sup>2</sup> *Materials Sciences Division LBNL, Berkeley CA USA*

<sup>3</sup> *Physics Department, University of California, Berkeley CA USA*

Artificial atoms based on superconducting circuit elements including Josephson tunnel junctions and strip-line resonators can be used as “qubits” for quantum computation and simulations, and as platforms for studying quantum cavity electrodynamics and other quantum phenomena. The performance of these systems depends critically on achieving coherent lifetimes that are significantly longer than initialization and readout times. Significant progress has been made in increasing coherence over the last decade or two by better electromagnetic circuit design to control losses and cross-talk, by improved radio-frequency electronics [1], and by advances in shielding and measurement techniques [2]. Further progress can come from improvements in materials and fabrication and better control of interface chemistry [3].

We will report initial results on interfacial studies combining SEM, analytical STEM, and x-ray spectroscopy to understand substrate, vacuum and internal interfaces in both Al Josephson junctions and Nb resonator structures.

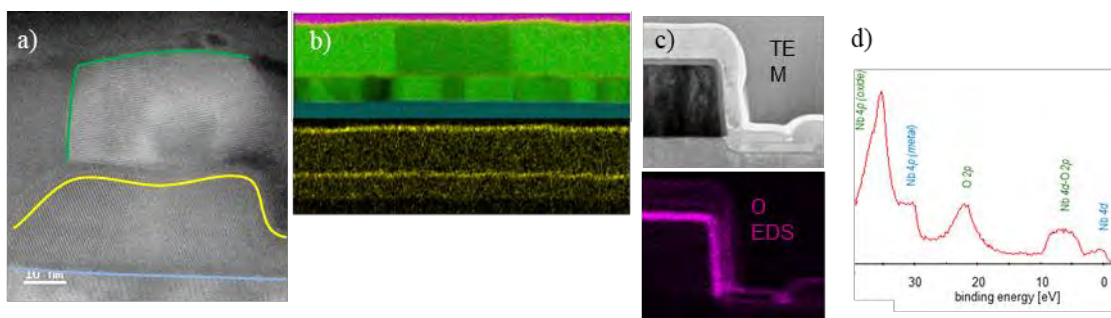


Figure 1 (a) STEM cross-section through polycrystalline Al/AIO<sub>x</sub>/AlO Josephson junction. The yellow line indicates the tunnel junction, the blue line the Al/Si interface, and the green line an Al grain boundary in the top contact. (b) TEM/EDS cross section of a different junction. The Al grain structure (green) can be seen in the two Al layers, and the oxide distribution (yellow) from EDS is shown below. (c) TEM/EDS on an Nb strip-line resonator cross section showing surface oxide. (d) Valence band XPS of Nb surface showing hybridization of the Nb 4d levels with O 2p.

[1] C. Macklin, K. O’Brien, D. Hover et al., *Science* **350**, 307 (2015).

[2] J.M. Kriekebaum, A. Dove, W. Livingston et al., *Superconducting Sci. Tech.* **29**, 104002 (2016)

[3] C. Müller, J.H. Cole, J. Lisenfeld, arXiv 1705.01108v2 (2018)

<sup>+</sup> Author for correspondence: DFOgletree@lbl.gov

## Progress in Hybrid Perovskite Photovoltaics and Optoelectronics

Joseph J. Berry<sup>1</sup>

<sup>1</sup> *National Renewable Energy Laboratory, 15013 Denver West Parkway Golden CO 80401*

Photovoltaic devices based on hybrid organic-inorganic perovskite absorbers have reached outstanding performance over the past few years, surpassing power conversion efficiency of over 25% for single junction and present multiple paths to tandems with efficiencies beyond 30%. These efficiencies have been achieved largely via the use of solution processing of the active layer coupled to more traditional vacuum processing for contacts and interface layers. This talk will start with recent progress and challenges in hybrid perovskite solar cells (HPSCs) with an emphasis on the role of materials integration challenges needed to enable device performance, tandem processing and stability. While, this talk will highlight recent progress at NREL, the challenges of tandems based on HPSC devices, work to develop hybrid materials for other applications and to understand their basic physical properties will also be discussed. Details of material structure, synthesis, the resulting interfaces and the role of processing in creating controlling material properties will be discussed. Data on the optoelectronic, spintronic and ferroelectric properties as characterized by an array of analytical tools including time resolved spectroscopy, structural studies and device level evaluation will be presented. Links from these fundamental materials properties to technologically relevant advances and suggestions for overarching research themes will be touched upon.



## On the path towards tandem junction nanowire based solar cells

M. T. Borgström

<sup>1</sup> Solid State Physics and NanoLund, Lund University, Box 118, SE-22100 Lund, Sweden.

Semiconducting nanowires have been recognized as promising materials for high-performance electronics and optics where optical and electrical properties can be tuned individual. Especially, nanowires have been identified as a means to high efficiency solar cells [1, 2] using significantly reduced materials consumption due to strong geometrically enhanced light absorbing properties [3].

In order to further optimize the performance of NWPV, and integrate them on Si in a tandem junction configuration, nanowires with dimensions corresponding to optimal light harvesting capability are necessary. We developed nano imprint lithography for patterning of catalytic metal particles with a diameter of 200 nm in a hexagonal pitch of 500 nm. We found that a pre anneal and nucleation step was necessary to keep the particles in place during high temperature annealing to remove surface oxides. We intend to transfer these grown nanowires to a Si platform (existing PV), either by direct growth on Si PV, or by nanowire peel off in polymer, followed by transfer and electrical contacting, or by aerotaxy and alignment for transfer to Si. We used electron beam induced current measurements as a tool to optimize the electrostatic potential profile in nanowires, leading to 15 % efficient InP nanowire solar cells, even though only covering about 10 % of the substrate surface. The optimal band gap in combination with Si is about 1.7 eV, where we identify GaInP and GaAsP as materials for development of nanowire *pn* junctions, the heart in a solar cell.

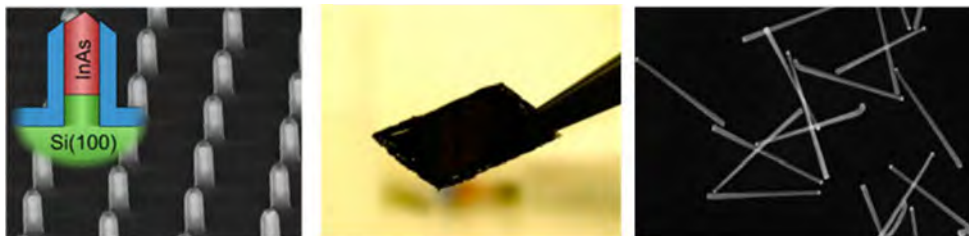


Figure 1 Simple sketch of the three different approaches. Left- template-assisted epitaxy, TASE, middle- SEM image of epitaxially grown nanowires, peeled off and held with a tweezer, intended for transfer to a Si cell. The membrane is black due to efficient light absorption in the nanowire membrane. Right- substrate-free growth by Aerotaxy, alignment and contacting

1. N. Anttu et al., Phys. Rev. B **83**, 165431 (2011)
2. J. Kupec et al., Opt. Express **18**, 27589 (2010)
3. J. Wallentin et al. Science, **339**, 1057 (2013)
4. Åberg et al, IEEE J. of Photov, **6**, 185 (2016)

<sup>+</sup> Author for correspondence: magnus.borgstrom@ftf.lth.se

## Metals at the Atomic Limit

**Joshua A. Robinson**

Materials Science and Engineering, Center for 2D and Layered Materials, NSF 2D Crystal Consortium, NSF Center for Atomically Thin Multifunctional Coatings;  
*The Pennsylvania State University; University Park, PA, USA*

The last decade has seen an exponential growth in the science and technology of two-dimensional materials. Beyond graphene, there is a huge variety of layered materials that range in properties from insulating to superconducting that can be grown over large scales for a variety of electronic devices and quantum technologies, such as topological quantum computing, quantum sensing, and neuromorphic computing. In this talk I will discuss our pioneering work in confinement heteroepitaxy (CHet) that enables the creation of 2D forms of 3D materials (e.g. 2D-Ga, In, Sn) and *decouples* the growth of the metals from other 2D layers, thereby enabling a new platform for creating artificial quantum lattices (AQLs) with atomically sharp interfaces and designed properties. As a specific example, we synthesize plasmonic layers that exhibit >2000x improvement in nonlinear optical properties, and 2D-superconductors combined with topological insulators as the building block of next generation “2D” topological superconductors. Confinement heteroepitaxy opens up avenues for enabling a virtual “legoland” of hybrid quantum materials.

# Tuning the spontaneous emission of monolayer WSe<sub>2</sub> by optical environment control – cavity coupling and substrate manipulation

**Hyunseung Lee<sup>1</sup> and Jieun Lee<sup>1</sup>**

<sup>1</sup> *Department of Physics and Department of Energy Systems Research, Ajou University, Suwon, 16449, Korea.*

Atomically thin layer of transition metal dichalcogenides (TMDs) such as monolayer WSe<sub>2</sub> exhibit direct bandgaps ranging from visible to near-infrared with strong excitonic effect [1]. Thanks to its optical characteristics, these materials can be used for integrated functional devices such as light emitting devices, photodetectors and optical modulators. In these applications, device performances can be improved by engineering the material thicknesses and doping levels, applying external fields, or modulating optical environment. In particular, tailoring the optical environment has been demonstrated by coupling monolayer TMDs to various types of optical microcavities such as Bragg reflectors or photonic crystals [2-4].

In this work, we utilize microspheres on planar substrates to manipulate the emission properties of monolayer WSe<sub>2</sub>. First, we show the enhancement of the photoluminescence (PL) emission which is controlled by the size of the coupled microsphere which ranges from 2 to 7  $\mu\text{m}$ . Time-resolved PL measurement supports the cavity-induced emission rate enhancement of monolayer WSe<sub>2</sub> coupled to a microsphere. The PL enhancement is further increased by increasing the thickness of the oxide layer between the microsphere and silicon substrate, which is supported by finite-time domain method (FDTD) simulations. Both microsphere coupling and substrate manipulation provide convenient pathways to modulate 2D material-based photonic devices.

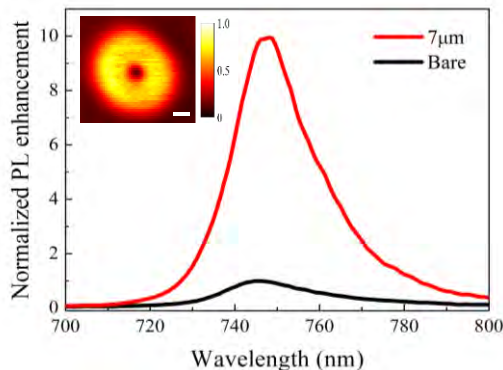


Figure 1 PL enhancement of monolayer WSe<sub>2</sub> coupled to a 7  $\mu\text{m}$  diameter microsphere. Inset scale bar : 2  $\mu\text{m}$  .

- [1] A. Ramasubramaniam, et al., Phys. Rev. B **86**, 115409 (2012).
- [2] K. F. Mak and J. Shan, Nat. Photon. **10**, 216 (2016).
- [3] L. C. Andreani, et al., Phys. Rev. B **60**, 13276 (1999).
- [4] X. Gan, et al., Appl. Phys. Lett. **103**, 181119 (2013).

<sup>+</sup> Author for correspondence: jelee@ajou.ac.kr

# First Principles Study on Optical Properties of Monolayer Bismuthene under an Electric Field

W. C. Liu,<sup>1</sup> L. L. Xu,<sup>1</sup> M. C. Lin,<sup>1</sup> T. C. Leung,<sup>2</sup> H. Y. Hsu,<sup>3</sup>

<sup>1</sup> *Multidisciplinary Computational Laboratory, Department of Electrical and Biomedical Engineering, Hanyang University Seoul 04763, South Korea*

<sup>2</sup> *Department of Physics, National Chung Cheng University, Chia-Yi 62101, Taiwan, Republic of China*

<sup>3</sup> *Department of Mechanical Engineering, National Taipei University of Technology, Taipei 10608, Taiwan, Republic of China*

Monolayer bismuthene has extraordinary optoelectronics, catalytic and biocompatible properties, and potential as a 2D topological insulator. When monolayer bismuthene is deposited in a sufficiently thin layer on an object, it possesses a stable low-buckled hexagonal structure and it has the property of semiconducting, which could be a promising low-dimensional thermoelectric material. Monolayers bismuthene is p-type semiconductors, but the hole concentration arising from the intrinsic defects is very low and hard to control. In this work, the band structure, density of states and optical constant of monolayer bismuthene have been calculated using first-principle calculations based on density functional theory (DFT). The results are compared to those calculated from the tight-binding model. With an applied external electric field, it is found that the electric and optical properties will be dramatically changed. Monolayer bismuthene can be calculated may generate some applications in optoelectronics, either combined with other 2D materials or topological materials.

[1] R. B. Chen, D. J. Jang, M. C. Lin, and M. F. Lin, *Opt. Lett.* **43**, 6089 (2018).

[2] F. F. Xia, S. Y. Xiong, Y. Y. He, Z. B. Shao, X. J. Zhang, and J. S. Jie, *J. Phys. Chem. C* 2017, **121**, 19530-19537.

<sup>+</sup> Author for correspondence: [mclin@hanyang.ac.kr](mailto:mclin@hanyang.ac.kr)

## Formation of Coherent Phase Domain Heterojunctions in Single Layer MoS<sub>2</sub> on Au(111)

F. Wu,<sup>1,2</sup> Z. Liu,<sup>1</sup> N. Hawthorne,<sup>1</sup> M. Chandross,<sup>3</sup> Q. Moore,<sup>1</sup> N. Argibay,<sup>3</sup>  
J.F. Curry<sup>3</sup> and J.D. Batteas<sup>1</sup>

<sup>1</sup> Department of Chemistry, Texas A&M University, College Station, TX 77843

<sup>2</sup> Department of Materials Science and Engineering, Texas A&M University,  
College Station, TX 77843

<sup>3</sup> Material, Physical, and Chemical Sciences Center, Sandia National Laboratories,  
Albuquerque, NM 87123

Two-dimensional (2D) transition metal dichalcogenides (TMDs) have attracted tremendous attention over the past decade due to their exciting mechanical, electronic and frictional properties [1-5]. Heterojunctions of semiconductors and metals are the fundamental building blocks of modern electronics. Coherent heterostructures between dissimilar materials can be achieved by composition, doping or heteroepitaxy of chemically different elements. Here we report, the formation of coherent single-layer MoS<sub>2</sub> heterostructures

(Figure 1), which are chemically homogenous with matched lattices, but show electronically distinct semiconducting (1H phase) and metallic (1T phase) character, when deposited by mechanical exfoliation on Au(111). The facile exfoliation technique here eliminates tape residues usually found in many exfoliation methods, and yields single-layer MoS<sub>2</sub> with millimeter (mm) size. Raman spectroscopy, X-ray photoelectron spectroscopy (XPS), scanning tunneling microscopy (STM) and scanning tunneling spectroscopy (STS) have collectively been employed to elucidate the structural and electronic properties of MoS<sub>2</sub> monolayers on Au substrates. Our work provides a basis to produce macroscale two-dimensional heterostructures, which represent unique candidates for future electronic devices and applications.

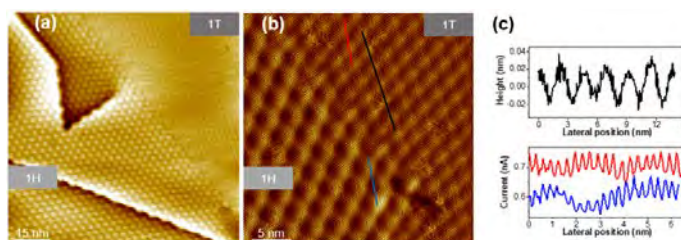


**Figure 1.** STM of the coherent heterostructures of MoS<sub>2</sub> monolayers. (a) Large-scale STM image of single-layer MoS<sub>2</sub> with two different Moiré patterns from the 1H and 1T phases. (b) Corresponding high resolution STM current image of single-layer MoS<sub>2</sub> on Au(111). (c) Line profile (black) showing the periodicity and the corrugation of the 1T-MoS<sub>2</sub> Moiré pattern in (b) and line profiles (blue and red) presenting the atomic distances for the two different phases.

[1] K. Novoselov, D. Jiang, F. Schedin, T. Booth, V. Khotkevich, S. Morozov and A. Geim, *Proc. Natl. Acad. Sci. U.S.A.* **2005**, *102*, 10451-10453.

[2] R. Ma and T. Sasaki, *Adv Mater* **2010**, *22*, 5082-5104.

[3] C. Lee, Q. Li, W. Kalb, X.-Z. Liu, H. Berger, R.W. Carpick and J. Hone, *Science* **2010**, *328*, 76-80.

[4] I. Song, C. Park and H.C. Choi, *RSC Adv.* **2015**, *5*, 7495-7514.

[5] X. Huang, Z. Zeng and H. Zhang, *Chem Soc Rev* **2013**, *42*, 1934-1946.

# Effects of Electromechanical Coupling in Locally Strained Monolayer MoS<sub>2</sub>

**A. C. De Palma,<sup>1</sup> G. Cossio,<sup>2</sup> K. Jones,<sup>3</sup> J. Quan,<sup>3</sup> X. Li,<sup>1,3</sup> E. T. Yu<sup>1,2</sup>**

<sup>1</sup> *Materials Science and Engineering Program, Texas Materials Institute, The University of Texas at Austin, Austin, TX, USA*

<sup>2</sup> *Department of Electrical and Computer Engineering, The University of Texas at Austin, Austin, TX, USA*

<sup>3</sup> *Department of Physics, The University of Texas at Austin, Austin, TX, USA*

Strain in atomically thin transition metal dichalcogenides (TMDs) has a broad range of consequences, and can be used for tuning of their optical and electronic properties [1, 2]. In particular, the use of localized strain to engineer these effects, such as in exciton funneling, has been demonstrated [3]. Additionally, TMDs exhibit intrinsic piezoelectricity in monolayer and few layer form originating from a lack of centrosymmetry [4]. The presence of piezoelectricity in TMD systems with strain and strain gradients can also have appreciable effects, which have only begun to be explored. Understanding these effects is necessary for engineering of TMD-based structures in which strain is present.

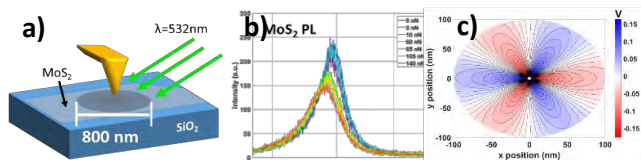


Figure 1: (a) Schematic depicting indentation and PL characterization. (b) PL measurement of MoS<sub>2</sub> during indentation. (c) Calculated electrostatic potential from piezoelectricity in indented MoS<sub>2</sub>

In this work, we examine the effects of piezoelectricity on MoS<sub>2</sub> in the presence of strain and strain gradients.

Samples consisting of monolayer MoS<sub>2</sub> suspended over 800nm-diameter cavities were fabricated by exfoliation and transfer of MoS<sub>2</sub> onto a patterned substrate. Suspended MoS<sub>2</sub> was deformed via atomic force microscope (AFM) indentation, and Photoluminescence (PL) measurements were simultaneously performed as a function of indentation force to determine the effects of the strain gradient on exciton bandgap and exciton diffusion (Fig. 1a, b). Additionally, we show through calculations that spatially varying strain, can be a source of electrostatic potentials due to the piezoelectric effect. According to a mechanical model for indentation [5], the charge density can be as high as  $10^{12}$  e/cm<sup>2</sup> at the points of highest strain gradient - significant enough to generate electrostatic potential variations on the order of  $\pm 0.1$ V over the MoS<sub>2</sub> (Fig. 1c). The relationship between strain and the potential generated by piezoelectricity, and the impact of this effect on excitons, will be discussed.

[1] H. Conley, B. Wang, J. Ziegler, R. Haglund Jr., S. Pantelides, K. Bolotin, *Nano Lett.* **12**, 8 (2013)

[2] T. Shen, A. V. Penumatcha, and J. Appenzeller, *ACS Nano* **10**, 4, 4712-4718 (2016).

[3] A. Castellanos-Gomez, R. Roldán, E. Cappelluti, M. Buscema, F. Guinea, H. S. J. van der Zant, and G. A. Steele, *Nano Lett.* **13**, 11, 5361-5366 (2013).

[4] Duerloo, K. A. N., Ong, M. T. & Reed, E. J., *J. Phys. Chem. Lett.* **3**, 2871–2876 (2012).

[5] N. M. Bhatia, W. Nachbar, *Int. J. Non-Linear Mechanics*, **3**, 307-324 (1968).

<sup>+</sup> Author for correspondence: Edward T. Yu: ety@ece.utexas.edu

## Neuromorphic Computing with the Redox Transistor

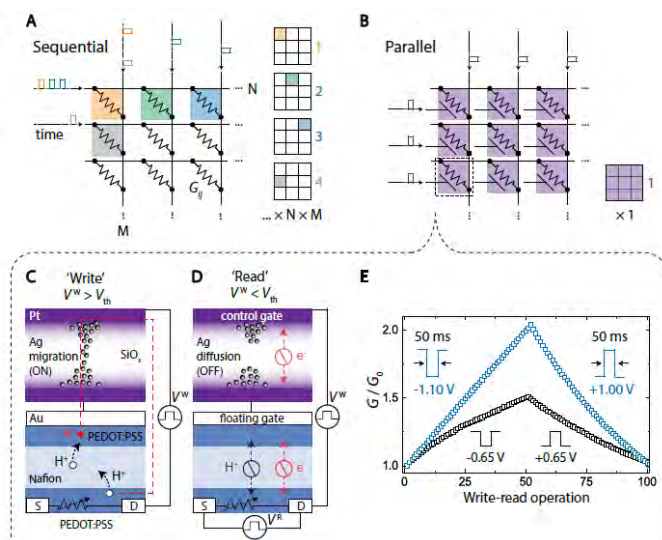
A. Alec Talin

Sandia National Laboratory

Livermore, CA 94551

aatalin@sandia.gov

Efficiency bottlenecks inherent to conventional computing in executing neural algorithms have spurred the development of novel devices capable of ‘in-memory’ computing. Commonly known as ‘memristors’, a variety of device concepts including conducting bridge, vacancy filament, phase change and other types have been proposed as promising elements in artificial neural networks for executing inference and learning algorithms. In my talk, I will review the recent advances in memristor technology for neuromorphic computing and discuss strategies for addressing the most significant performance challenges, including non-linearity, high read/write currents, and endurance. As an alternative to two-terminal memristors, I will introduce the three-terminal electrochemical memory based on the redox transistor (RT) which uses a gate to tune the redox state of the channel.<sup>1</sup> Decoupling the ‘read’ and ‘write’ operations using a third terminal and storage of that information as a charge-compensated redox reaction in the bulk of the transistor enables high-density information storage. These properties enable low-energy operation without compromising analog performance and non-volatility. I will discuss the RT operating mechanisms using organic and inorganic materials, approaches for array integration, and prospects for achieving the device density and switching speeds necessary to make electrochemical memory competitive with established digital technology.



1. Fuller, E. J.; Keene, S. T.; Melianas, A.; Wang, Z. R.; Agarwal, S.; Li, Y. Y.; Tuchman, Y.; James, C. D.; Marinella, M. J.; Yang, J. J.; Salleo, A.; Talin, A. A., Parallel programming of an ionic floating-gate memory array for scalable neuromorphic computing. *Science* **2019**, *364* (6440), 570.

# Kinetically-driven assembly of TaS<sub>2</sub>-SnS heterostructures with flexible stacking architectures

**D. M. Roberts,<sup>1</sup> D. Bardgett,<sup>1,2</sup> B. Gorman,<sup>3</sup> J.D. Perkins,<sup>1</sup> A. Zakutayev,<sup>1</sup> S. R. Bauers<sup>1</sup>**

<sup>1</sup> National Renewable Energy Laboratory, 15013 Denver West Pkwy, Golden, CO 80401

<sup>2</sup> University of Oregon, 1253 University of Oregon, Eugene, OR 97403

<sup>3</sup> Colorado School of Mines, 1500 Illinois St, Golden, CO 80401

Chalcogenide heterostructures enable access to a remarkable range of materials properties by virtue of structural flexibility at the nanoscale. An interesting approach to the preparation of such heterostructures utilizes layered amorphous precursor films designed to mimic a desired superlattice heterostructure product, and has been successful in creating a wide range of metastable selenide heterostructures. An example of such tunable properties is seen in the SnSe-VSe<sub>2</sub> system, where changing layer sequencing can both enhance and quench charge density wave (CDW) transitions, as well as modify their onset temperatures.[1] Such CDWs in TaS<sub>2</sub> are hysteretic and have been proposed for phase change memory applications,[2] and so incorporating TaS<sub>2</sub> into superlattice structures known to enhance CDW transitions might further enhance this material towards these applications.

Previous work from our group developed a framework for preparing amorphous sulfide precursor films by RF sputtering.[3] Here we present the first crystalline sulfide heterostructures prepared using this precursor approach, composed of tunable numbers of SnS sandwiched between monolayers of TaS<sub>2</sub> in a superlattice. We also demonstrate the utility of combinatorial synthesis for creating precursors of several different stacking sequences in a single deposition. Structural measurements confirm smooth films with superlattice ordering as well as the presence of constituent TaS<sub>2</sub> and SnS layers. Superlattice architecture is confirmed by high resolution transmission electron microscopy (TEM) and EDS, resolving atomically precise sequencing of SnS and TaS<sub>2</sub> monolayers in the arrangement experimentally instilled into the precursors. Electronic behavior as a function of number of SnS layers is measured.

[1] R. Atkins, Chem. Mater. **26** (2014) [2] M. Yoshida, Sci. Rep. **4** (2014) [3] D. M. Roberts, JVST B **37** (2019)

<sup>+</sup> Author for correspondence: dennice.roberts@nrel.gov

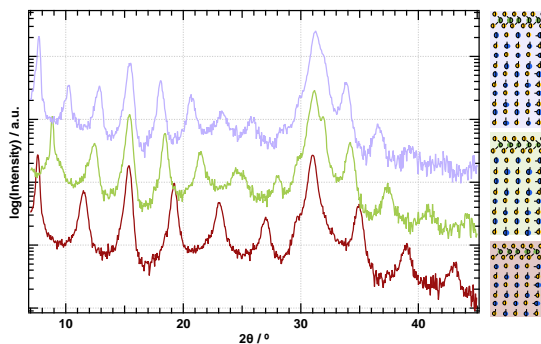


**Figure 1** X-ray diffraction pattern of films with varied number of SnS layers between TaS<sub>2</sub> layers. Structure schematic shown at right.

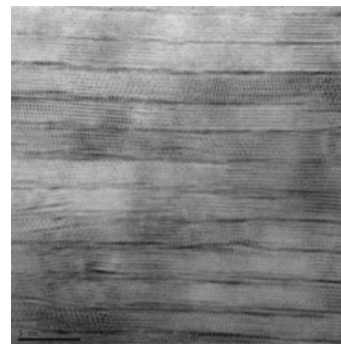


**Figure 2** Hall coefficient and resistivity of heterostructures as a function of number of SnS layers.



# Globally Aligned Single-Wall Carbon Nanotube Films through Electrostatic Ordering

**J. S. Walker,<sup>1</sup> J. A. Fagan<sup>2</sup>, A. J. Biacchi,<sup>3</sup> V. A. Kuehl,<sup>4</sup> T. A. Searles,<sup>5</sup>  
A. R. Hight Walker,<sup>3</sup> W. D. Rice<sup>1</sup>**

<sup>1</sup> Department of Physics, University of Wyoming, Laramie, WY, 82071

<sup>2</sup> National Institute of Standards and Technology, Materials Science and Engineering Division, Gaithersburg, MD, 20899

<sup>3</sup> National Institute of Standards and Technology, Nanoscale Device Characterization Division, Gaithersburg, MD, 20899

<sup>4</sup> Department of Chemistry, University of Wyoming, Laramie, WY, 82071

<sup>5</sup> Department of Physics & Astronomy, Howard University, Washington D.C., 20059

The one-dimensional nature of single-wall carbon nanotubes (SWCNTs) creates unique, anisotropic optical, electrical, and thermal characteristics. To utilize these anisotropic properties, researchers must be able to easily and reproducibly fabricate aligned SWCNT structures. To be most useful, SWCNT alignment protocols must incorporate solution-based nanotubes, as they provide the highest quality (chiral enrichment, length sorting, tube filling, etc.) nanotubes [1] which are necessary for applications.

We expanded [3] upon the slow-filtration SWCNT alignment technique [2] through automation and parallelization. Such advances not only provided increased film reproducibility and throughput, but also enabled a rapid optimization of the complex parameter space to produce the highest aligned films to date. Furthermore, this work provides researchers with a new capability to investigate the underlying physics driving alignment. We find that by controlling flow rate, flattening the meniscus, and membrane buffing, we can repeatably and automatically produce globally aligned SWCNT films. Using polarized spectroscopy, we show that high, two-dimensional nematic ordering ( $S_{2D} \approx 0.9$ ) of SWCNTs can be achieved [3]. Experiments altering the ionic strength and membrane surface charging suggest that this ordered SWCNT phase is driven by linear charging on the membrane and inter-nanotube electrostatic interactions.

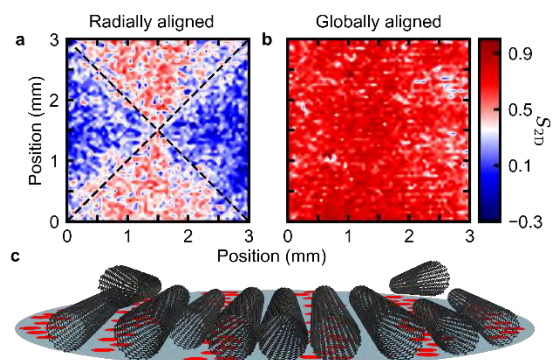


**Figure 1.** a) Spatial map of nematicity ( $S_{2D}$ ), showing radial nanotube alignment. b) Spatial map of nematicity indicating global SWCNT alignment after meniscus flattening and membrane charging. c) Depiction of the membrane surface/SWCNT-dispersion interface showing quasi-linear charging.

[1] Fagan, J., “Aqueous two-polymer phase extraction of single-wall carbon nanotubes using surfactants”. *Nanoscale Adv.* **2019**, 1, 3307.

[2] He, X., et al., “Wafer-scale monodomain films of spontaneously aligned single-walled carbon nanotubes”. *Nature Nanotechnol.* **2016**, 11, 633.

[3] Walker, J., et al., “Global alignment of solution-based single-wall carbon nanotube films via machine-vision controlled filtration”. *Nano Lett.*, **2019**, Article ASAP.

## Defining insulating regions on TiO<sub>2</sub> thin films by laser heating

S.E. Ahmed,<sup>1,2</sup> J.R. Ritter,<sup>2</sup> M.D. McCluskey<sup>1,2,3+</sup>

<sup>1</sup> Materials Science Program, Washington State University, Pullman, WA, USA 99164

<sup>2</sup> Dept. of Physics and Astronomy, Washington State University, Pullman, WA, USA 99164

<sup>3</sup> Klar Scientific, 1615 NE Eastgate Blvd., Unit G, Ste. 3E, Pullman, WA, USA 99163

Optically defining conducting and insulating regions on an oxide thin film could provide a means for writing and rewriting transparent electronic circuits. Titania (TiO<sub>2</sub>) films are straightforward to deposit and exhibit *n*-type conductivity that depends strongly on the concentration of oxygen vacancies, which act as shallow donors [1,2]. Heating in a reducing atmosphere, such as vacuum or hydrogen, increases the density of oxygen donors and hence the conductivity [3]. Conversely, heating in an oxygen atmosphere reduces the oxygen vacancy concentration and makes the sample insulating. While electrons in the rutile phase are small polarons, those in anatase TiO<sub>2</sub> behave as free electrons [4]. This property makes the anatase structure preferable for applications requiring high electrical conductivity.

In the present work, 300 nm thick anatase TiO<sub>2</sub> films were sputtered on fused silica substrates. Heating under a rough vacuum (30 mTorr) produced conducting films with free-carrier absorption in the visible and IR. A green laser (532 nm wavelength, 1-5 W power) was then focused on regions of the sample, in the open air. Localized laser heating resulted in a 7 order-of-magnitude increase in resistance, from 10 kΩ to >100 GΩ. The heated area became transparent due to the loss of free-carrier absorption (Fig. 1). Scanning electron microscopy (SEM, Fig. 2) and optical transmission spectroscopy indicate that laser heating does not degrade the films. The process is reversible – conductivity is restored after annealing in vacuum again. The effect of interface heat conduction will be discussed.

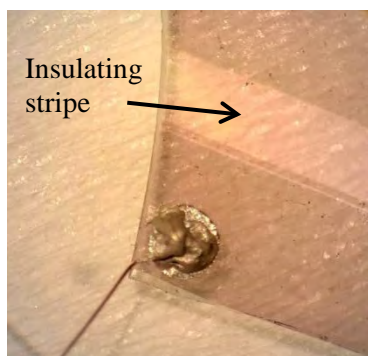


Figure 1. Sample with a laser annealed stripe (~1.5 mm wide) and pressed In contact.

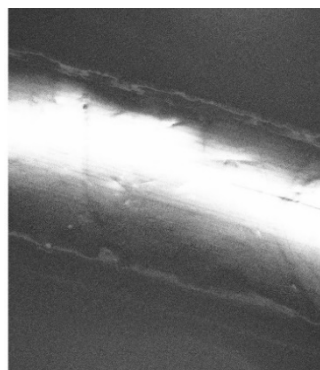


Figure 2. SEM image of the insulating stripe; the bright region is due to electrical charging.

[1] G. Mattioli, P. Alippi, F. Filippone, R. Caminiti, and A.A. Bonapasta, *J. Phys. Chem. C* **114**, 21694 (2010).

[2] P. Deák, B. Aradi, T. Frauenheim, *Phys. Rev. B* **86**, 195206 (2012).

[3] D.C Cronemeyer, *Phys. Rev.* **87**, 876 (1952).

[4] L. Forro, O. Chauvet, D. Emin, L. Zuppiroli, H. Berger, and F. Lévy, *J. Appl. Phys.* **75**, 633 (1993).

+ Author for correspondence: mattmcc@wsu.edu

## Supplementary Pages (Optional)

### **Towards Mask Free Fabrication of Micro- and Nanoscale Architectures on Different Substrates via Aqueous-Ink Precursors and CVD Synthesis**

I. Kuljanishvili<sup>1,\*</sup>, D. Alameri<sup>1</sup>, D. Karbach<sup>1</sup>, R. Dong<sup>1</sup>, L. Moore<sup>1</sup>, R. Divan<sup>2</sup>, Y. Liu<sup>2</sup>

<sup>1</sup> Saint Louis University, Department of Physics, 3511 Laclede Ave, St. Louis, MO, 63146

<sup>2</sup> Argonne National Laboratory, Center for Nanoscale Materials, Lemont, IL

Large scale implementation of nanoscale materials and nanostructures into various architectures and device platforms has become a critical necessity in nanotechnology. It is now become essential to be able to prepare, engineer materials in a controlled and scalable fashion and develop new methodologies for the implementation of nanomaterials into practical applications.

With the discovery of graphene and other layered van der Waals materials the field of engineered layered materials and nano-architectures has exploded in recent years. However, the discovery and development of newer and simpler, less expensive techniques, which will allow for reliable fabrication and materials assembly into custom architectures and device platforms has lagging. Newer materials with exotic opto-electronic, chemical and mechanical properties emerge everyday which bring the urgency for new methods to be developed to help streamline the characterization/testing of these complex heterogeneous nanomaterials and stacked architectures. In order to keep pace with the emerging number of new heterostructure materials (stacked vertically or laterally), and be able to vacillate their implementation into future practical applications, it is important to employ flexible and preferably scalable methods of fabrication and rapid testing methods suitable for nondestructive interface probing in heterostructures and devices.

Fabrication tools and methods used to prepare heterostructures- nanomaterials rely largely on conventional methods of patterning; majority of those methods are mask-assisted technologies that have been developed for traditional Si based industry, such as convention optical lithographic methods. Very few mask-free methods have been demonstrated which could deliver resolution and control of materials placement, morphology and other design parameters comparable to those of optical lithography.

We have developed methodology that allows for simple and potentially scalable technology which can bridge the gap and conveniently deliver fabricating protocols to design and produce materials (via scalable, and location specific CVD synthesis) with controlled geometry and morphology with the resolution within range of 0.1  $\mu\text{m}$ - to-10  $\mu\text{m}$ . Custom aqueous inks which are used as precursors for selective growth of specific nanomaterials, on a substrate of the choice such as Si/SiO<sub>2</sub>, Graphene, BN and other, ensure clean interfaces between material-substrate and at the heterojunction between two different nanomaterials MoS<sub>2</sub>/WS<sub>2</sub>, ZnO/Gr or ZnO/BN etc. <sup>[1,2,3,4]</sup>

## Towards Fermi level De-pinning at Contacts

**J. Robertson\***,<sup>1</sup> **Y Guo**,<sup>1,2</sup> **Z Zhang**<sup>1</sup>

<sup>1</sup> Cambridge University, Engineering, Cambridge, CB2 1PZ, UK

<sup>2</sup> School of Electrical Engineering, Wuhan University, Wuhan, China.

Fermi level pinning at Schottky barriers (SB) strongly limits the reduction of contact resistances and thus scaling of modern electronic devices and future 2D semiconductor devices. We find that some complex semiconductor-metal interfaces with bonding configurations parallel to the interface create a type of localized interface or ‘defect state’ beyond the metal induced gap state (MIGS) model. Examples are interfaces between Si and metal disilicides and between Si and Sb. These defect states do not easily match to conventional MIGS and this mixes states of metal character into the surface pinning level. This creates Fermi level de-pinning and a variation of SB height with interface orientation.

The MIGS model [1] has successfully described many aspects of Schottky barrier behavior, including the slope of barrier height (SBH) with metal work function,  $S = \partial\phi / \partial\Phi_M$  and the charge neutrality level. However, it does not include several factors like interface bonding [2]. The MIGS model would say the  $S$  factor should depend only on metal work function, not type of metal (elemental or silicide/TiN) or on the face orientation, despite these being seen experimentally [2,3] and found in DFT supercell calculations [4]. We show that both metal silicides and Sb break the MIGS due to the presence of ‘defect-like’ states [5] at their interfaces, due to states which cannot be easily captured by the limited MIGS basis set of bulk semiconductor states. A metal-like character enters the effective CNL pinning energy, which also gives the orientation dependence. The chemically different case of Si:Sb behaves similarly to the silicides. These two factors are signifiers of Fermi level de-pinning, to find other examples.

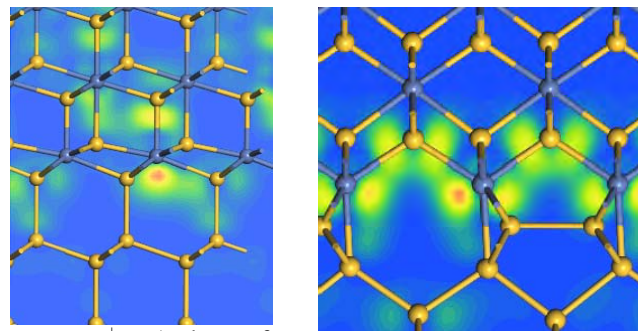
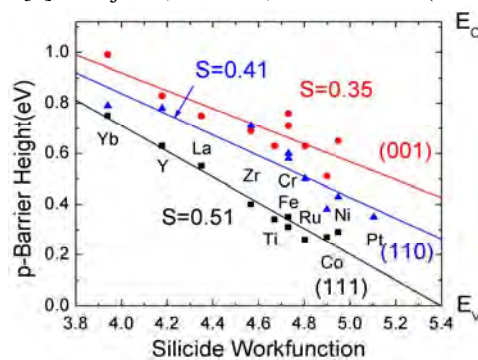
[1] J Tersoff, PRL **52** 465 (1984)

[2] R T Tung, PRL **84** 6078 (2000); APR 1 011304 (2014); PRL. **52**, 461 (1984); JVST. *B* **11**, 1546 (1993)

[3] T Nishimura, et al, APX 9 081201 (2016)

[4] L Lin, et al, APL **101** 052110 (2012); H Li, et al, Sci Report **7** 16669 (2017); J Robertson, SSDM (2018)

[5] H Fujitani, S Asano, PRB **50** 8681 (1994)



Author for  
correspondence: jr214@cam.ac.uk

Figure 1 Showing Fermi level depinning and face dependence in Si: silicide interfaces

Figure 2 Showing ‘defect state at Si:silicide (111), (100) interfaces causing the de-pinning and orientation dependence

## Observation, Characterization, and Mitigation of the Internal $p$ - $n$ Junction in Pyrite $\text{FeS}_2$ , a Potential Low-cost Solar Absorber

**B. Voigt,<sup>1+</sup> W. Moore,<sup>1</sup> J. Walter,<sup>1</sup> B. Das,<sup>1</sup> M. Maiti,<sup>1</sup> M. Manno,<sup>1</sup>  
E. S. Aydil,<sup>1,2</sup> C. Leighton<sup>1</sup>**

<sup>1</sup> Department of Chemical Engineering and Materials Science, University of Minnesota,  
421 Washington Ave SE, Minneapolis, MN 55455, USA

<sup>2</sup> Department of Chemical and Biomolecular Engineering, New York University Tandon  
School of Engineering, 6 MetroTech Center, Brooklyn, NY 11201, USA

Pyrite  $\text{FeS}_2$  is widely acknowledged as an ideal semiconductor for thin film solar cells due to its earth-abundance, low toxicity, low cost, suitable band gap (0.95 eV) and minority carrier diffusion length, and high visible light absorptivity. Power conversion efficiencies of  $\text{FeS}_2$  heterojunction solar cells, however, have never exceeded 3% due to low open-circuit voltages ( $V_{\text{OC}} < 0.3$  V). One hypothesis emerging from recent temperature ( $T$ )-dependent transport measurements of high quality single crystals is that this low  $V_{\text{OC}}$  is due to a conductive pyrite surface with a carrier type ( $p$ -type) inverted from bulk ( $n$ -type) [1,2]. This could create a leaky (*i.e.*, low- $V_{\text{OC}}$ ) internal  $p$ - $n$  junction, thus limiting heterojunction solar cell efficiencies. These studies established conduction through a 1-3 nm-thick,  $p$ -type surface upon freeze-out of  $n$ -type bulk carriers [1,2]. Two parallel resistors representing surface and bulk conduction can describe the  $T$ -dependence of resistivity across a wide  $T$  range (50-500 K) [1] and the non-linear Hall effect observed near the crossover between bulk- and surface-dominated conduction upon cooling below 300 K [2]. Notably, what has neither been observed nor characterized, however, is the internal  $p$ - $n$  junction implied by this  $p$ -type surface and  $n$ -type bulk. Here, we directly observe this internal junction for the first time. In-plane sheet resistance ( $R_S$ ) measurements of polished crystals doped heavily  $n$ -type *via* sulfur vacancies are shown to display an effect where metallic-like transport abruptly transitions to rapidly increasing  $R_S$  below  $\sim 175$  K, eventually transitioning to surface conduction at lower  $T$  ( $< 100$  K). We show that this very unusual  $T$ -dependence can be well described by incorporating an exponentially- $T$ -dependent junction resistance into the parallel resistor model. Junction barrier heights extracted from the model are typically 0.15 – 0.30 eV, in good agreement with typical  $V_{\text{OC}}$  values in past heterojunction solar cells, suggesting that this internal junction may, in fact, be limiting conversion efficiencies. Interestingly, while junction influence in  $R_S(T)$  is independent of contact materials such as In, Ag, Fe, Co, and Ni,  $\text{CoS}_2$  contacts mitigate this junction, allowing the first characterization of bulk properties to low  $T$ . Access to bulk properties at low  $T$  unveils rich phenomena, such as the onset of a smaller donor activation energy below 175 K, non-linear Hall effect near 100 K, and an unusual resistivity anomaly at  $T \leq 10$  K, showcasing  $\text{CoS}_2$  contacts as a way to both mitigate this junction and advance understanding of electronic transport in  $\text{FeS}_2$ . This work was supported by the customers of Xcel Energy through a grant from the Renewables Development Fund.

[1] M. Limpinsel *et al.*, Energy Environ. Sci. **7**, 1974 (2014).

[2] J. Walter, *et al.*, Phys. Rev. Mater. **1**, 065403 (2017).

<sup>+</sup> Author for correspondence: voigt132@umn.edu

## Photo-driven dipole reordering: key to carrier separation in metalorganic halide perovskites

H.-C. Hsu<sup>1</sup>, B.-C. Huang<sup>2</sup>, S.-C. Chin<sup>1</sup>, C.-R. Hsing<sup>2</sup>, D.-L. Nguyen<sup>2,6,7</sup>, M. Schnedler<sup>3</sup>, R. Sankar<sup>4,8</sup>, R. E. Dunin-Borkowski<sup>3</sup>, C.-M. Wei<sup>2,6</sup>, C.-W. Chen<sup>5,9,10</sup>, Ph. Ebert<sup>3</sup>, and Ya-Ping Chiu<sup>1,9</sup>

<sup>1</sup> Dept. of Physics, National Taiwan University, Taipei 10617, Taiwan

<sup>2</sup> Institute of Atomic and Molecular Sciences, Academia Sinica, Taipei 10617, Taiwan

<sup>3</sup> Peter Grünberg Institut, Forschungszentrum Jülich GmbH, 52425 Jülich, Germany

<sup>4</sup> Institute of Physics, Academia Sinica, Taipei 11529, Taiwan

<sup>5</sup> Dept. of Mat. Sci. and Eng., National Taiwan University, Taipei 10617, Taiwan

<sup>6</sup> Molecular Sci. and Technol. Program, TIGP, Academia Sinica, Taipei 10617, Taiwan

<sup>7</sup> Dept. of Physics, National Central University, Taoyuan City 32001, Taiwan

<sup>8</sup> Center for Condensed Matter Sci., National Taiwan University, Taipei 10617, Taiwan

<sup>9</sup> Center of Atomic Initiative for New Materials, National Taiwan University, Taipei 10617, Taiwan

<sup>10</sup> Taiwan Consortium of Emergent Crystalline Materials (TCECM), Ministry of Science and Technology, Taipei 10617, Taiwan

Photo-driven dipole reordering of the intercalated organic molecules in halide perovskites has been suggested to be a critical degree of freedom, potentially affecting physical properties, device performance, and stability of hybrid perovskite-based optoelectronic devices. However, thus far a direct atomically-resolved dipole mapping under device operation condition, i.e. illumination, is lacking. Here, we map simultaneously the molecule dipole orientation pattern and the electrostatic potential with atomic resolution using light-illuminated cross-sectional scanning tunneling microscopy and spectroscopy.

Our experimental observations demonstrate that a photo-driven dipole reordering, initiated by a photo-excited separation of electron-hole pairs in spatially displaced orbitals, leads to a fundamental reshaping of the potential landscape in halide perovskites, creating separate one-dimensional transport channels for holes and electrons. We anticipate that analogous light-induced polarization order transitions occur in bulk and are at the origin of the extraordinary efficiencies of organometal halide perovskite-based solar cells as well as could reconcile apparently contradictory materials' properties.

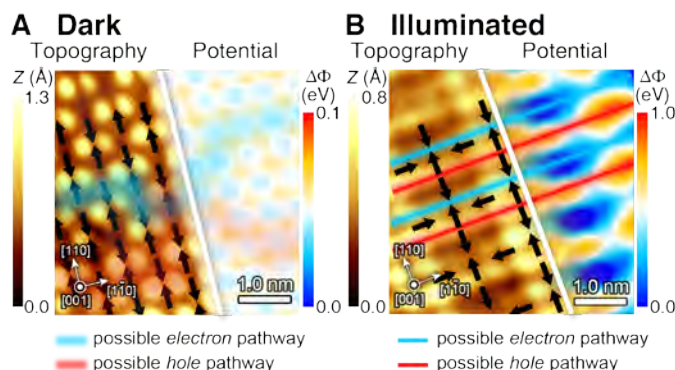


Figure 1 Illustration of light-induced structure and potential changes at  $\text{CH}_3\text{NH}_3\text{PbBr}_3$  surfaces. (A)  $2\times 2$  phase in dark and (B) illumination-induced  $4\times 2$  phase. Superimposed are the constant-current STM images (left side) and electrostatic potential energy landscapes (right).

<sup>+</sup> Author for correspondence: p.ebert@fz-juelich.de

# First principles study on electronic properties of graphene nanostructures for high current density cathode

N. Zhao,<sup>1</sup> L. L. Xu,<sup>1</sup> M. C. Lin,<sup>1</sup> T. C. Leung,<sup>2</sup> H. Y. Hsu,<sup>3</sup>

<sup>1</sup> *Multidisciplinary Computational Laboratory, Department of Electrical and Biomedical Engineering, Hanyang University Seoul 04763, South Korea*

<sup>2</sup> *Department of Physics, National Chung Cheng University, Chia-Yi 62101, Taiwan, Republic of China*

<sup>3</sup> *Department of Mechanical Engineering, National Taipei University of Technology, Taipei 10608, Taiwan, Republic of China*

Graphene is a crystalline allotrope of carbon with two-dimensional properties. Its carbon atoms are densely packed in a nano-scale hexagonal pattern. Graphene has many unusual properties. It is about 200 times stronger than the strongest steel. It can efficiently conduct heat and electricity and is nearly transparent. In this work, we study the electronic properties of graphene using first principles or *ab initio* calculations based on density functional theory (DFT) in order to explore its applications in field emission devices. The change of work function due to the lattice deformation of graphene is investigated using a supercell including a vacuum layer which is thick enough so that the layer interaction is negligible. It is found that the work function is very sensitive to the lattice size. As the lattice site increases, the work function increases proportionally. However, the work function is reduced doubly while the lattice site is reduced. The local work function of graphene has also been determined and this can be used to predict field emission current from Fowler-Nordheim equation more accurately. For realistic applications, this approach has been used to calculate the work function of carbon nanoribbons with different widths and terminating edges with and without passivation.

- [1] D. W. Boukhvalov, M. I. Katsnelson, and A. I. Lichtenstein, "Hydrogen on graphene: Electronic structure, total energy, structural distortions and magnetism from first-principles calculations", *Phys. Rev. B* 77, 035427 (2008)
- [2] D. R. Cooper, B. D'Anjou, N. Ghattamaneni, B. Harack, M. Hilke, A. Horth, N. Majlis, M. Massicotte, L. Vandsburger, E. Whiteway, and V. Yu, "Experimental Review of Graphene", *ISRN Phys. Condens. Matter.* 2012, 501686 (2012).
- [3] V. Meunier, A. G. Souza Filho, E. B. Barros, and M. S. Dresselhaus, "Physical properties of low-dimensional sp<sup>2</sup>-based carbon nanostructures", *Rev. Mod. Phys.* 88, 025005 (2016).
- [4] D. G. Kvashnin, P. B. Sorokin, J. W. Brünig, and L. A. Chernozatonskii, "The impact of edges and dopants on the work function of graphene nanostructures: The way to high electronic emission from pure carbon medium", *Appl. Phys. Lett.* 102, 183112 (2013).
- [5] T. C. Leung, C. L. Kao, W. S. Su, Y. J. Feng and C. T. Chan, "Relationship between surface dipole, work function and charge transfer: to an established rule" , *Phys. Rev. B* 68, 195408 (2003).

<sup>+</sup> Author for correspondence: [mclin@hanyang.ac.kr](mailto:mclin@hanyang.ac.kr)

## Band offset modulation in Si-EuO heterostructures via controlled interface formation

W. Li, A. Posadas, and A. A. Demkov

Department of Physics, The University of Texas at Austin, Austin, TX, 78712, USA

In a Si-based spintronic device, Si serves as the spin channel material. Owing to its small spin-orbit coupling, Si has a long spin relaxation lifetime and long spin coherence length, making it an excellent choice. Because the rock salt lattice of EuO is compatible with the *fcc* lattice of Si (see Fig. 1), and EuO is thermodynamically stable on Si, Si/EuO heterostructures have a real potential for use in Si-based spin-FETs. Combining first principles calculations and experiment, we investigate the atomic and electronic structure of the Si/EuO interface. We consider the thermodynamic stability of interface structures with different levels of oxidation to identify the most probable configuration. By comparing the calculated band alignment and core level shifts with measured values, we validate the theoretically constructed interface model. EuO has unusual electronic properties in that its charge neutrality level appears to be inside the conduction band [1,2]. In Fig. 2 we show a contour plot of the partial density of states (PDOS) as a function of energy and position along the  $z$  direction normal to the plane of the interface. In the contour plot one can clearly see the band edges of Si and EuO and read off the VBO, which is +0.19 eV. We find that the band offset can be tuned by altering the relative energy positions of the Si and EuO conduction bands via interface oxidation, which can be used to tune this materials system for specific applications in spintronics [3].

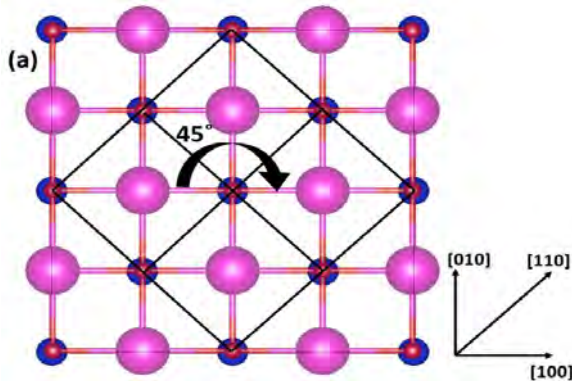


Figure 1. Top view of rock salt EuO and face centered silicon lattices. Purple ball represents Eu, red O and blue Si. It can be seen that rocksalt and face centered lattices match well. It can also be rotated by  $45^\circ$ .

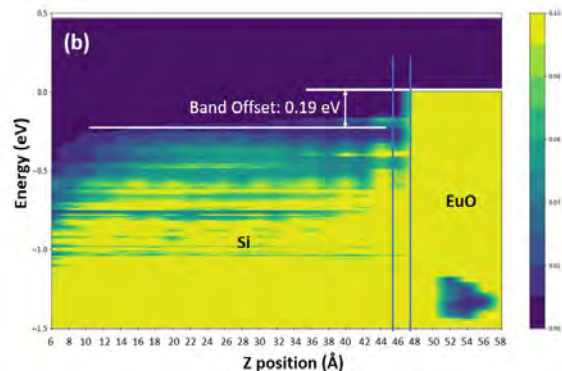


Figure 2. Contour plot of PDOS for spin-up channel in the valence band and band gap regions. The dark blue region is the band gap and the yellow region is the valence band top.

- [1] N. Jutong, I. Rungger, C. Schuster, U. Eckern, S. Sanvito, and U. Schwingenschlögl, *Phys. Rev. B* **86**, 205310 (2012).  
 [2] L. Gao, W. Guo, A. B. Posadas and A. A. Demkov, *Phys. Rev. Materials* **3**, 094403 (2019).  
 [3] W. Li, A. B. Posadas, and A. A. Demkov, *in press*, *Phys. Rev. B* (2019).

+ Author for correspondence: demkov@physics.utexas.edu



# First Principles Study on Electronic Properties of Magnetite for Spin Polarized Emission under an Electric Field

**L. L. Xu,<sup>1</sup> N. Zhao,<sup>1</sup> M. C. Lin,<sup>1</sup> T. C. Leung,<sup>2</sup> H. Y. Hsu,<sup>3</sup>**

<sup>1</sup> *Multidisciplinary Computational Laboratory, Department of Electrical and Biomedical Engineering, Hanyang University Seoul 04763, South Korea*

<sup>2</sup> *Department of Physics, National Chung Cheng University, Chia-Yi 62101, Taiwan, Republic of China*

<sup>3</sup> *Department of Mechanical Engineering, National Taipei University of Technology, Taipei 10608, Taiwan, Republic of China*

Abstract- Magnetite is a mineral and one of the main iron ores. With the chemical formula  $\text{Fe}_3\text{O}_4$ , it is one of the oxides of iron. Magnetite is the earliest discovered magnet, around 1500 B.C. It crystallizes in the inverse cubic spinel structure (Fd3m) above the so-called Verwey transition temperature, which is about 120 K. In this work, we study the electronic properties of magnetite (100), (110), and (111) surfaces under external electric fields using first principles or *ab initio* calculations based on density functional theory. With an electric field applied, the surface properties could be modified. For example, the (111) surface with an  $\text{O}_2$  termination, the half-metal behavior becomes metal behavior under a critical electric field. With a +U calculation, most of the surfaces with different terminations show half-metallic, different from those predicted by a without +U calculation. We can use an electric field to control the metallic properties to be metallic or half-metallic. Un addition, the effective work function changes under different field strength. By calculating the local work function, we can know the distribution of work function on a certain surface. The effective work functions of magnetite  $\text{Fe}_3\text{O}_4$  on different surfaces have been determined. The local work function has been found to have the correspondences with the atoms' positions and charge densities. It is proposed that the magnetite as a half-metal can possibly be used as a spin-polarized electron source.

- [1] H. T. Jeng, and G. Y. Guo, Phys. Rev. B **65**, 094429 (2002).
- [2] T. C. Leung, C. L. Kao, W. S. Su, Y. J. Feng, and C.T. Chan, Phys. Rev. B **68**, 195408 (2003).
- [3] J. Noh, O. I. Osman, S. G. Aziz, P. Winget, and J.-L. Brédas, Chem. Mater. **27**, 5856-5867 (2015).
- [4] M. Friák, A. Schindlmayr, and M. Scheffler, New J. Phys. **9**, 5 (2007).
- [5] M. C. Lin, R. F. Jao, and W. C. Lin, J. Vac. Sci. Technol. B, 2008, **26**, 821-825.
- [6] A. Pratt, M. Kurahashi, X. Sun, D. Gilks, and Y. Yamauchi, Phys. Rev. B, 2012, **85**, 180409(R).
- [7] A. Kiejna, T. Ossowski, and T. Pabisiak, Phys. Rev. B, 2012, **85**, 125414.

<sup>+</sup> Author for correspondence: [mclin@hanyang.ac.kr](mailto:mclin@hanyang.ac.kr)

## Work Functions of Alkali and Alkaline Earth Metal Surfaces under Electric Fields based on First-principles Calculations

Y. Wang,<sup>1</sup> L. L. Xu,<sup>1</sup> M. C. Lin,<sup>1</sup> T. C. Leung,<sup>2</sup> H. Y. Hsu,<sup>3</sup>

<sup>1</sup> *A Multidisciplinary Computational Laboratory, Department of Electrical and Biomedical Engineering, Hanyang University, Seoul 04763, Korea*

<sup>2</sup> *Department of Physics, National Chung Cheng University, Chia-Yi 62101, Taiwan*

<sup>3</sup> *Department of Mechanical Engineering, National Taipei University of Technology, Taipei 10608, Taiwan, Republic of China*

Alkali (Li, Na, K, Rb, Cs) and alkaline earth metal (Be, Mg, Ca, Sr, Ba) are widely used in various fields. In the field emission, the adsorption of alkali metals and alkaline earth metals to tungsten (W) will greatly change the work function. In this work, we study the work functions and local work functions of alkali and alkaline earth metal (100) (110) (111) surfaces under different electric fields using the first-principles or *ab initio* calculations. The convergence of density-functional-theory (DFT) calculations in the local-density approximation (LDA) and generalized-gradient approximation (GGA) with a plane-wave basis set the projector-augmented wave method as implemented in the Vienna ab-initio simulation package (VASP) has been carefully and systematically tested. For a comparison, the work functions have been calculated with five different pseudo potentials. By applying an electric field on the alkali and alkaline earth metals, we can calculate the effective work function, local work function and investigate the dependence of the effective work function and the local work function on the field strength.

[1] M. C. Lin, R. F. Jao, and W. C. Lin, *J. Vac. Sci. Technol. B* **26**, 821 (2008).

[2] T. C. Leung, C. L. Kao, and W. S. Su, *Phys. Rev. B* **68**, 195408 (2003)

[3] T. W. Pi, I. H. Hong, and C. P. Cheng, *Phys. Rev. B* **58**, 4149 (1998).

<sup>+</sup> Author for correspondence: mclin@hanyang.ac.kr

# Nitrogen Doping of Gallium Oxide by Ion Implantation and Its Application to Vertical Transistors

**M. Higashiwaki,<sup>1</sup> M. H. Wong,<sup>1\*</sup> K. Goto,<sup>2</sup> H. Murakami,<sup>2</sup> and Y. Kumagai<sup>2</sup>**

<sup>1</sup> National Institute of Information and Communications Technology, Koganei, Tokyo 184-8795, Japan

<sup>2</sup> Department of Applied Chemistry, Tokyo University of Agriculture and Technology, Koganei, Tokyo 184-8588, Japan

\* Currently with Department of Electrical and Computer Engineering, University of Massachusetts, Lowell, MA 01854, USA

$\beta$ -gallium oxide ( $\beta$ -Ga<sub>2</sub>O<sub>3</sub>) has a very large bandgap (~4.5 eV) and a breakdown electric field exceeding 6 MV/cm, making it an attractive candidate for next-generation power electronics. However, Ga<sub>2</sub>O<sub>3</sub> has a fundamental physical drawback, namely a lack of hole-conductive *p*-type material, because of unavailability of shallow acceptors, a valence band structure mostly formed by O 2*p* orbitals, and a self-trapping effect of free holes. Recently, we succeeded in developing a nitrogen (N)-ion-implantation doping process for Ga<sub>2</sub>O<sub>3</sub> to form an energy barrier in a device structure [1] and then fabricating vertical Ga<sub>2</sub>O<sub>3</sub> transistors by using a device process based on the N-ion implantation doping [2, 3].

N atoms are theoretically expected to be a deep acceptor in Ga<sub>2</sub>O<sub>3</sub>. We performed N-ion implantation doping into an *n*-Ga<sub>2</sub>O<sub>3</sub> layer to fabricate a current blocking layer by forming a Si-doped–N-doped–Si-doped Ga<sub>2</sub>O<sub>3</sub> *n-p-n* junction. Note that Si is a shallow donor with an activation energy of about 50 meV in Ga<sub>2</sub>O<sub>3</sub>. Then, depletion-mode (D-mode) and enhancement-mode (E-mode) vertical Ga<sub>2</sub>O<sub>3</sub> transistors with a current aperture were fabricated by using a manufacturable all-ion-implanted process, which is similar to commercial Si and SiC power device technologies, with Si and N doping. Both the D-mode and E-mode devices demonstrated successful transistor action and decent device characteristics. A schematic cross section and DC current–voltage (*I*–*V*) output characteristics of a typical D-mode transistor are shown in Figs. 1 and 2, respectively.

This work was partially supported by Council for Science, Technology and Innovation (CSTI), Cross-ministerial Strategic Innovation Promotion Program (SIP), “Next-generation power electronics” (funding agency: NEDO).

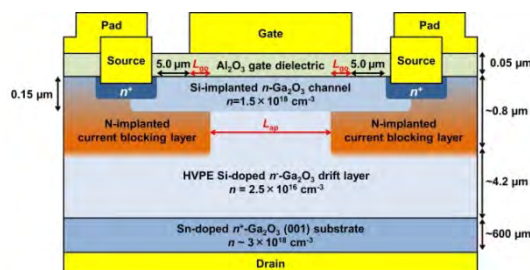


Figure 1. Cross-sectional schematic of D-mode vertical Ga<sub>2</sub>O<sub>3</sub> transistor structure:  $L_{ap}=20\ \mu\text{m}$  and  $L_{go}=2.5\ \mu\text{m}$ .

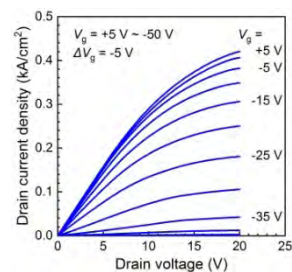


Figure 2. DC *I*–*V* characteristics of D-mode vertical Ga<sub>2</sub>O<sub>3</sub> transistor.

[1] M. H. Wong, M. Higashiwaki *et al.*, Appl. Phys. Lett. **113**, 102103 (2018).

[2] M. H. Wong, M. Higashiwaki *et al.*, IEEE Electron Device Lett. **40**, 431 (2019).

[3] M. H. Wong, M. Higashiwaki *et al.*, in Abstract of 77<sup>th</sup> Device Research Conference, 2019.

<sup>+</sup> Author for correspondence: mhigashi@nict.go.jp

## Studying the nucleation of GaP on v-grooved Si for III-V/Si device integration

E.L. Warren<sup>1</sup>,<sup>1</sup> T.E. Saenz,<sup>1,2</sup> A.G. Norman,<sup>1</sup> J.D. Zimmerman<sup>1,2</sup>

<sup>1</sup> NREL, Golden, CO 80401, USA

<sup>2</sup> Colorado School of Mines, Golden, CO 80401, USA

The direct heteroepitaxy of III-V materials on Si for high efficiency optoelectronic and photovoltaic applications has progressed greatly in recent years, but most studies have focused on polished wafers, that are compatible with microelectronics (e.g. CMOS) fabrication, but not photovoltaic technologies. There has been recent interest in growing III-Vs on “v-grooved” surfaces, where nanoscale patterning and facet selective etching is used to pattern nominally (001) Si surfaces with linear (111)-faceted v-groove structures. This v-grooved geometry suppresses antiphase boundaries (APBs), thereby enabling defect-free nucleation of polar III-V materials on nonpolar Si. However, for applications where cost is important, it also brings with it the challenge of creating the v-grooved pattern in a cost-effective way, without an expensive wafer-polishing step.

In this work, we show how v-groove structures can be prepared with cost-effective patterning approaches (nanoimprint lithography and interference lithography) on unpolished Si surfaces.<sup>1</sup> Unlike prior studies of growth of III-Vs on v-groove structures, which have focused on lattice mismatched heteroepitaxy of III-Vs (GaAs, InP, etc.), we have focused on GaP, which has a very small lattice mismatch with Si and enables us to understand the fundamentals of III-V nucleation on partially v-grooved surfaces, where multiple facets are exposed during growth. This is also an excellent platform to investigate the coalescence of selective area growth, a topic that is important for large-area applications such as photovoltaics.<sup>2</sup> We have systematically studied the nucleation conditions for GaP on v-groove Si and identified conditions that enable facet-selective nucleation without the formation of APBs, and lead to smooth, planar coalesced films.

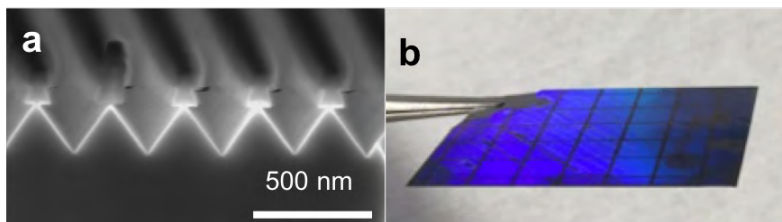


Figure 1 a) SEM of v-grooved Si with NIL resist still present; b) optical image of NIL-patterned unpolished Si

[1] E.L. Warren et al, Proc. IEEE PVSC, (2018).

[2] W.E. McMahon et al, APL Materials, (2018).

<sup>+</sup> Author for correspondence: emily.warren@nrel.gov

# Improving Heterointerfaces in Rapidly Grown III-V Electronic Devices using Dynamic Hydride Vapor Phase Epitaxy (D-HVPE)

**D. Roberts<sup>1</sup>, J. Simon,<sup>1</sup> K. Schulte,<sup>1</sup> A. Ptak<sup>1</sup>**

<sup>1</sup> *Materials Science Center, National Renewable Energy Laboratory, Golden CO 80401*

High growth rates and precursor utilization make hydride vapor phase epitaxy (HVPE) a powerful tool for the growth of homoepitaxial III-V materials, particularly GaN and GaAs [1,2]. However, most applications are limited to thick single layers rather than electronic devices that require multiple heterointerfaces. Single-chamber HVPE systems are hampered by the long residence times of vapor phase constituents, typically requiring a growth interrupt to create abrupt interfaces. The non-abrupt nature of interfaces created in single-growth-chamber systems limits the use of HVPE in heteroepitaxial devices. The recent development of dynamic HVPE (D-HVPE) addressed this issue by introducing a second, largely isolated growth chamber, allowing a sample to be shuttled between growth chambers with established steady-state reactions to produce high quality, chemically- and structurally-abrupt interfaces. D-HVPE-grown single- and dual-junction GaAs and GaAs/GaInP solar cell devices show efficiencies approaching that of materials grown by more conventional means such as MOVPE. [3]

Here we present an assessment of improved interface quality between isostructural samples grown by traditional HVPE and D-HVPE in a custom reactor. Time-resolved photoluminescence measurements reveal samples grown by D-HVPE have significantly higher lifetimes than samples grown by HVPE. Trap-assisted recombination is also present in samples grown by traditional HVPE, resulting in different calculated lifetimes at high- and low-level injection. We compare structure and morphological differences and discuss growth mechanisms of D-HVPE grown solar cells.

[1] E. Gil-Lafon, J. Cryst. Growth **222** 3 (2001) [2] K. Motoki, Jpn J. Appl. Phys. **40** (2001) [3] J. Simon, Crystals **9** 3 (2019)

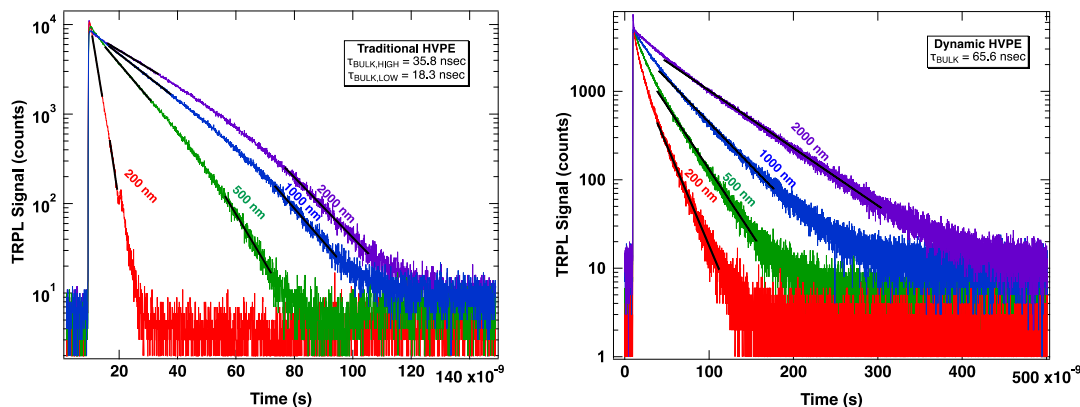


Figure 1 Photoluminescence decay for samples of different thickness for samples grown via conventional HVPE (left) and with D-HVPE (right). Extracted lifetime is shown in the inset.

<sup>+</sup> Author for correspondence: dennice.roberts@nrel.gov

# Real-Time Optical Monitoring of the Epitaxial Growth of Zincblende Semiconductors

**A. Lastras-Martínez,<sup>1</sup> L.E. Guevara-Macías,<sup>1</sup> J.G. Santiago-García<sup>1</sup>, and J. Ortega-Gallegos<sup>1</sup>**

<sup>1</sup> IICO, Universidad Autónoma de San Luis Potosí, S.L.P., México

Non-invasive optical probes such as reflectance anisotropy spectroscopy (RAS) are attractive for real-time monitoring of the epitaxial growth of cubic semiconductors given their high sensitivity and instrumental simplicity. RAS enhances the surface response against the bulk signal by taking advantage of the reduced symmetry of the near-surface region of cubic crystals. Nevertheless, although the surface specificity of RAS has been known for long time [1], its use for monitoring epitaxial growth had been hampered by the lack of both a rapid spectrometer to follow epitaxial growth and a full understanding of the physics underlining RAS line shapes.

In this talk we demonstrate the power of RAS to elucidate phenomena occurring during the very first stage of the MBE homoepitaxial growth of GaAs (first half monolayer (ML)). We present real-time RAS spectra acquired during growth, taking advantage of a recently developed rapid RAS spectrometer [2]. Typical time-dependent RAS spectra for growth under As-rich conditions (c(4x4) and (2x4) surface reconstructions) are shown in Fig. 1(a). A singular value decomposition (SVD) analysis of these spectra yields two physically independent components, termed B1 and B2 (Fig. 1(b)). Component B1 rises sharply upon starting growth and its amplitude changes sign as the surface reconstruction shifts from c(4x4) to (2x4) (Fig. 1(c)). All this takes place during the growth of the first half ML. Afterwards, the amplitude of B1 oscillates following layer-by-layer growth. In contrast, B2 shows relatively small changes along growth (Fig. 1(c)). Component B1 is associated with surface reconstruction that changes during growth, while the time evolution of B2 suggests that it is characteristic of As-terminated surfaces, regardless of their specific reconstruction.

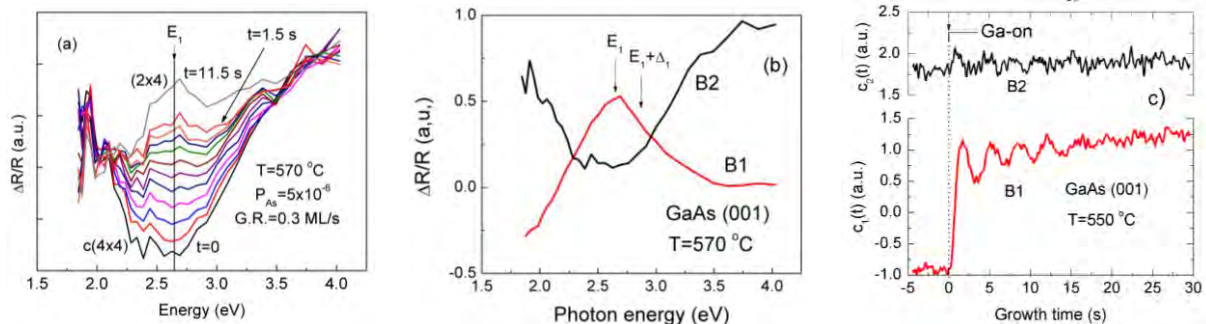


Figure. 1. (a) Time-resolved RAS spectra. (b) B1 and B2 basic spectral components. (c) Time-evolution during growth of the amplitude of B1 and B2 components. B1 amplitude rises sharply during the first half ML growth, while B2 amplitude remains relatively constant.

- [1] D.E. Aspnes, J.P. Harbison, A. Studna, and L.T. Florez, *J. Vac. Sci. Technol.* **A6**, 1327 (1988).  
 [2] D Ariza-Flores, J Ortega-Gallegos, O Núñez-Olvera, R E Balderas-Navarro, L F Lastras-Martínez and A Lastras-Martínez, *Meas. Sci. Technol.* **26**, 115901 (2015).

## Pulsed Laser Deposition of Epitaxial $\text{Sr}_3\text{Al}_2\text{O}_6$ as a Water-Soluble Sacrificial Layer for GaAs Deposition

**Imran S. Khan<sup>1+</sup>, Bill McMahon<sup>1</sup>, Andrew Norman<sup>1</sup>, Andriy Zakutayev<sup>1</sup>**

<sup>1</sup> National Renewable Energy Laboratory, Golden, CO, USA

Despite the record high efficiency for GaAs solar cells, its terrestrial application is limited due to both the particularly high costs related to the required single crystal substrates and the epitaxial growth. Significant substrate reuse is one strategy that has been heavily explored by the PV community, however, the usefulness of all the existing techniques is limited due to the need for toxic etchants, substrate re-polishing and/or expensive intermediate process steps. A water-soluble lift off layer could reduce costs by avoiding these potential downsides.

$\text{Sr}_3\text{Al}_2\text{O}_6$  (SAO) is a water soluble, cubic oxide (space group  $Pa-3$ ), with lattice constant  $15.84\text{\AA}$ . This is close to  $(2\sqrt{2})a_{\text{GaAs}} = 15.99\text{\AA}$ , giving a close lattice match between SAO  $\langle 100 \rangle$  and GaAs  $\langle 100 \rangle$  after  $45^\circ$  lattice rotation. We investigated the epitaxial growth of high structural quality SAO on single crystal  $\text{SrTiO}_3$  (STO) substrates by Pulsed Laser Deposition (PLD), and the feasibility of subsequently growing GaAs epitaxially on top of it. We identified that pulsed laser deposited SAO on STO is polycrystalline for substrate temperatures lower than  $650^\circ\text{C}$ , however the films could be epitaxially crystallized partially by high temperature annealing. Careful optimization of the growth parameters for obtaining epitaxial SAO on STO was explored, and we identified that the SAO film quality is strongly dependent on the growth temperature and  $\text{O}_2$  partial pressure. An STO capping layer was grown on the SAO to protect from moisture induced degradation, which was also epitaxial.

XRD spectra for the films with optimized deposition parameters showed SAO (400) and SAO (800) peaks that were epitaxially aligned to the STO (100) and STO (200) substrate peaks. TEM analysis revealed that the grown SAO films are epitaxially crystalline throughout the thickness. The epitaxial growth of the STO capping layer is a qualitative indication for the high quality of the SAO surface. Research activity is ongoing to experiment the practicability of growing GaAs on these sacrificial SAO films.

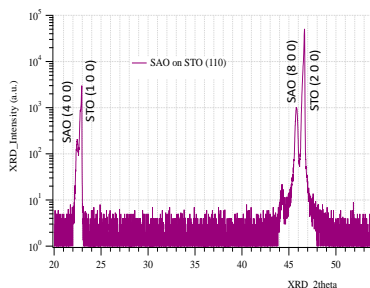


Figure: (left) XRD spectra, and (right) TEM image and FFT for the for SAO on STO (100) substrate.

<sup>+</sup> Author for correspondence: Imran.Khan@nrel.gov

# On the Theory of the Energetic Spectrum of Vicinal Superlattices: the Role of Crystal Potential

V. A. Petrov

*Institute of Radio Engineering and Electronics  
Russian Academy of Sciences, Moscow, Russia*

As is known, the existence of superlattice effects in 2D quantum wells (QWs) and inversion layers (ILs) in MOS structures on vicinal planes is due to the appearance in these systems of a new crystallographic period of translation in the plane of quantum wells  $A \gg a$  ( $a$  - lattice constant). The emergence in these vicinal superlattices (VSLs) of the periodic system of atomic steps allows to explain the appearance of minigaps (MGs) in the energetic spectrum of particles in QWs and ILs by the scattering of electrons on such steps. At the same time it is evident that the contribution to the MG formation should also be made by all crystallographic planes in the area of localization of the particle wave function.

This paper theoretically shows that the consideration of only crystal potential and of the potential locating the particle in VSL on vicinal planes results in the appearance of MGs even without taking into account of the step structure of the QW boundaries. A method has been developed that makes it possible to calculate the energetic spectrum of these systems for the arbitrary localizing potential by leaving the effective mass approximation in single-valley semiconductors of the GaAs type.

For the cases of a rectangular 2D quantum well and an inversion layer in the triangular quantum well approximation analytical expressions have been obtained for MGs magnitudes which depend on the parameters of the crystal and localizing potentials as well as on angles that define the orientation of the QW and IL planes in the crystal. It has been shown that for VSL of the GaAs type the magnitudes of MGs approximate several meV.

Keywords: superlattice, quantum well, crystal potential.



## Epitaxial relationship of Cu<sub>3</sub>N grown on YSZ(001) substrate by mist CVD method

**N. Wakabayashi,<sup>1</sup> R. Takigasaki,<sup>2</sup> T. Yamaguchi,<sup>1</sup> T. Onuma,<sup>1</sup> T. Honda<sup>1</sup>**

<sup>1</sup> Department of Applied Physics, School of Advanced Engineering, Graduate School of Engineering, Kogakuin University, Tokyo 192-0015, Japan.

<sup>2</sup> Department of Applied Physics, School of Advanced Engineering, Kogakuin University, Tokyo 192-0015, Japan.

Copper nitride (Cu<sub>3</sub>N) is Anti-ReO<sub>3</sub> type cubic structure. It is reported that the bandgap energy of single crystal Cu<sub>3</sub>N is about 1.4 eV and this can be applied as a solar energy conversion material [1]. Cu<sub>3</sub>N has typically grown by physical vapor deposition (PVD) using vacuum pressure [2]. Mist chemical vapor deposition (mist CVD) method is one of the cost-effective growth techniques and is possible to grow in atmospheric pressure [3]. Recently, we have succeeded in the epitaxial growth of Cu<sub>3</sub>N on *c*-plane sapphire by mist CVD method using NH<sub>3</sub> aqueous solution as a solvent. The epitaxial relationship in in-plane direction of this Cu<sub>3</sub>N film was Cu<sub>3</sub>N(100)// $\alpha$ -Al<sub>2</sub>O<sub>3</sub>(11-20). This indicates that the film had multi-domain structure, since  $\alpha$ -Al<sub>2</sub>O<sub>3</sub> has not cubic but corundum structure. [4]. In this study, Cu<sub>3</sub>N was grown on a YSZ(001) substrate by mist CVD method. The epitaxial relationship was evaluated.

Cu<sub>3</sub>N thin film was grown on a YSZ(100) substrate by vertical-type mist CVD method. Copper (II) acetylacetonate was used as a source material for the growth. The Cu (II) acetylacetonate was solved in NH<sub>3</sub> aqueous solution of 28%. The concentration of Cu was 0.1 mol/L. The mist, formed by the 2.4 MHz ultrasonic transducer, was transferred to the reaction area by nitrogen carrier gas. The Cu<sub>3</sub>N film was grown totally for 2 hours at the temperatures of 300°C.

The XRD  $\theta$ -2 $\theta$  pattern, shown in Fig. 1(a), indicates that the film has the epitaxial relationship of Cu<sub>3</sub>N(001)//YSZ(001) in the growth direction. The XRD  $\phi$  scan patterns, shown in Fig. 1(b), indicates that the film has the epitaxial relationship of Cu<sub>3</sub>N(100)//YSZ(100) in the in-plane direction. Thus, we have succeeded in the suppression of multi-domain structure, which is observed in the growth on  $\alpha$ -Al<sub>2</sub>O<sub>3</sub>, using the YSZ substrate with cubic structure.

In the presentation, different growth phenomena for Cu<sub>3</sub>N on  $\alpha$ -Al<sub>2</sub>O<sub>3</sub> and YSZ substrates are also discussed.

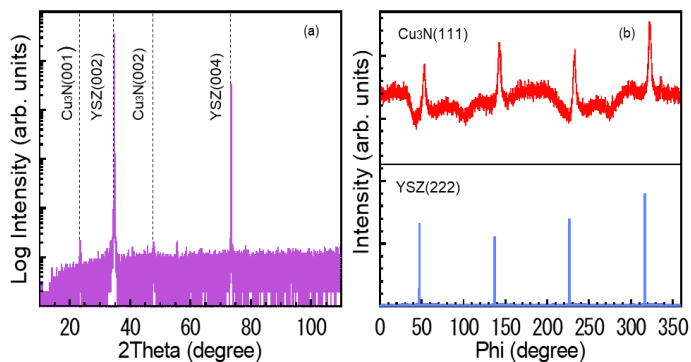


Figure 1. (a)  $\theta$ -2 $\theta$  pattern of Cu<sub>3</sub>N grown on YSZ (100), (b)  $\phi$  scan patterns of Cu<sub>3</sub>N (111) and YSZ (222).

[1] K. Matsuzaki *et al.*, Appl. Phys. Lett. **105**, 222102 (2014).

[2] Z.Q. Liu *et al.*, Thin Solid Films. **325**, 55 (1998).

[3] T. Kawaharamura *et al.*, J. Appl. Phys. Lett. **47**, 4669 (2008).

[4] T. Yamaguchi *et al.*, *in preparation*.

<sup>+</sup> Author for correspondence: cm19053@ns.kogakuin.ac.jp (N. Wakabayashi)  
: ct11761@ns.kogakuin.ac.jp (T. Honda)

## Halogen surface chemistries for atomically precise manufacturing on Si(100)

**K.J. Dwyer,<sup>1</sup> Michael Dreyer,<sup>1</sup> Karen Gaskell,<sup>2</sup> and R.E. Butera<sup>3, +</sup>**

<sup>1</sup> Department of Physics, University of Maryland, College Park, MD 20740, USA

<sup>2</sup> Department of Chemistry & Biochemistry, University of Maryland, College Park, MD 20740, USA

<sup>3</sup> Laboratory for Physical Sciences, 8050 Greenmead Drive, College Park, MD 20740, USA

Atomic-scale fabrication of electronic devices in silicon has been widely demonstrated using a scanning tunneling microscope (STM) and hydrogen-based surface chemistries to precisely place phosphorous donor atoms on the surface. Incorporation of PH<sub>3</sub> precursors into lithographic patterns formed from a hydrogen resist in a Si surface can produce metallic wires, quantum dots defined by electrostatic gates, and single donor atom qubits for quantum information (QI) research[1]. However, interest in acceptor dopants and hole-based devices necessitates the development of alternate precursor and/or resist chemistries for device fabrication. Halogen chemistry is potentially more favorable for acceptor incorporation than hydrogen[2], and to that end we explore halogen-based resists including Cl, Br, and I, along with metal-halide precursors to deposit acceptor dopants.

Here, we present results on the complete surface passivation of Si(100) using Cl, Br, and I, and demonstrate STM lithography at cryogenic and elevated temperatures [3]. We further study the stability of halogen-terminated Si(100) in ambient environments using x-ray photoelectron spectroscopy (XPS) to facilitate transport of samples outside of ultra-high vacuum environments. Finally, we present results of metal-halide adsorption on Si(100) as a viable path towards acceptor doping.

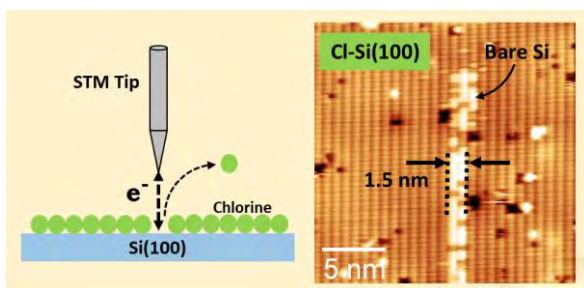


Figure 1. Schematic of STM lithography on Cl-Si(100). A 2-dimer wide lithographic line demonstrates atomic precision patterning.

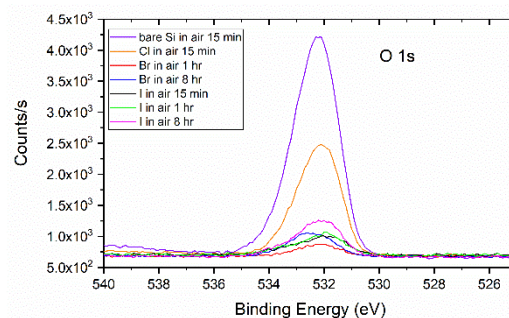


Figure 2. XPS spectra of O 1s peak as a function of halogen surface termination and exposure time in air.

[1] *Science*, **335**, 64 (2012)

[2] *Langmuir*, **27**, 6, 2613-2624 (2011)

[3] arXiv:1808.05690

+ Author for correspondence: rbutera@lps.umd.edu

# Novel Growth Mechanisms in van der Waals Epitaxy: 3D Morphologies of $\text{Bi}_2\text{Se}_3$

T. P. Ginley,<sup>1</sup> and S. Law<sup>1+</sup>

<sup>1</sup> University of Delaware, 201 DuPont Hall, Newark, DE, 19716

Van der Waals (vdW) materials, such as graphene, transition metal dichalcogenides, and bismuth chalcogenides, are an increasingly popular research topic due to their wide variety of applications. They are characterized by strongly bonded layers in the  $a$ - $b$  plane and weak vdW bonds between layers in the  $c$ -direction. Careful control of vdW materials could create designer stacks of 2D materials or unlock the unique physics of 3D topological insulators, resulting in improved optoelectronic, spintronic, and valleytronic technologies. Growth via Molecular Beam Epitaxy (MBE) is a promising avenue for improved material quality due to its' highly customizable growth conditions. Unlike traditional MBE, which relies on the strong interaction between the growth material and a lattice matched substrate, vdW epitaxy takes advantage of the weak vdW bonds to grow on substrates with vastly different crystal structures. Unfortunately, vdW epitaxy cannot be fully explained via the well-known mechanics of traditional MBE. Growth of atomically smooth layers remains challenging as vdW materials tend to grow in terraced “wedding cake” morphologies. Also, vdW materials favor the (001) orientation with the vdW gaps parallel to the growth surface. Other orientations have been reported via MBE but require extensive substrate pretreatment or pre patterning. Improved understanding of the growth mechanisms involved in vdW epitaxy could allow for improved material quality as well as exotic growth morphologies.

In this study, we use the topological insulator  $\text{Bi}_2\text{Se}_3$  as a prototypical vdW material for the exploration of growth mechanics. We chose to grow on GaAs(001) substrates as the interaction of adatoms with the post deoxidization reconstructed surface may provide greater insight than a less complex growth surface, such as previous work on sapphire substrates. It was found that growth at a substrate temperature of 425°C produced a significant amount of growth in the elusive (0015) orientation, with domains aligned along the GaAs[110] axis (Sample A). It is believed that bismuth aggregation due to thermal degradation as well as fast diffusion of bismuth along GaAs[110] combine to push growth into this orientation. A film grown on a 10nm  $(\text{Bi}_{0.5}\text{In}_{0.5})_2\text{Se}_3$  buffer layer results in the formation of  $\text{Bi}_2\text{Se}_3$  platelets with

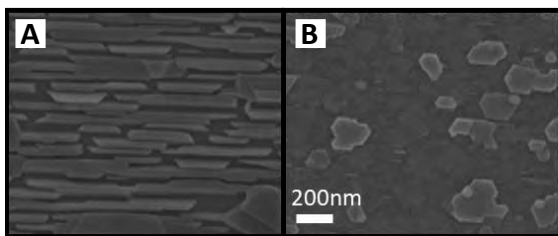


Figure 1: SEM images of  $\text{Bi}_2\text{Se}_3$  films grown on GaAs substrates with varying growth parameters.

sheer walls and flat tops (Sample B). Based on this research it is believed that vdW growth dynamics are dominated by the relative strength of film/adatom and substrate/adatom interactions. The morphologies reported here differ significantly from those reported on sapphire, implying that substrate interaction is key to understanding novel morphologies in vdW materials.

<sup>+</sup> Author for correspondence: slaw@udel.edu

# Electron Transport in Strain-Engineered Graphene

**Nadya Mason<sup>1+</sup>, Yingjie Zhang<sup>2</sup>, Stephen Gill<sup>1</sup>, Henry Hinnefeld<sup>1</sup>, Matthew Gilbert<sup>3</sup>,  
Narayan Aluru<sup>4</sup>**

<sup>1</sup> *Physics Department, University of Illinois, Urbana-Champaign USA*

<sup>2</sup> *Materials Science Department, University of Illinois, Urbana-Champaign, USA*

<sup>3</sup> *Electrical Engineering Department, University of Illinois, Urbana-Champaign, USA*

<sup>4</sup> *Mechanical Engineering Department, University of Illinois, Urbana-Champaign, USA*

There is wide interest in using strain-engineering to modify the physical properties of 2D materials, for both basic science and applications. Deformations of graphene, for example, can lead to the opening of band gaps, as well as the generation of pseudo-magnetic fields and novel electronic states. We demonstrate how controllable, device-compatible strain patterns in graphene can be engineered by depositing graphene on corrugated substrates. We discuss several techniques for creating corrugated substrates [1,2], focusing on periodic spherical curvature patterns in the form of closely packed nanospheres. We show how the smaller nanospheres induce larger tensile strain in graphene, and we explain the microscopic mechanism of this [3]. We also present experimental results demonstrating how a nearly periodic array of underlying nanospheres creates a strain superlattice in graphene, which exhibits mini-band conductance dips and magnetic field effects that depend on the magnitude of induced strain [4]. This control of the strain degree of freedom provides a novel platform both for fundamental studies of 2D electron behavior and for prospective applications in 2D electronic devices.

Figure 1. Left: simulation of graphene on nanospheres. Right: calculation of strain-induced superlattice dips.

*Supported by NSF under DMR-1720633 (MRSEC) and ENG-1434147, and the UIUC MRL.*

[1] S.T. Gill et al, *ACS Nano* **9**, 5799-5806 (2015).

[2] J. H. Hinnefeld et al, *Appl. Phys. Lett.* **112**, 173504 (2018).

[3] S.T. Gill et al, *Nano Letters* **18**, 6121 (2018).

[4] Y. Zhang et al, *njp:2D Materials and Applications* **2**, 31 (2018).

<sup>+</sup> Author for correspondence: nadya@illinois.edu

# Revealing exciton masses and dielectric properties of monolayer semiconductors with high magnetic fields

**M. Goryca,<sup>1+</sup> J. Li,<sup>1</sup> A.V. Stier,<sup>1</sup> T. Taniguchi,<sup>2</sup> K. Watanabe,<sup>2</sup> E. Courtade,<sup>3</sup> S. Shree,<sup>3</sup> C. Robert,<sup>3</sup> B. Urbaszek,<sup>3</sup> X. Marie,<sup>3</sup> and S. A. Crooker<sup>1</sup>**

<sup>1</sup> National High Magnetic Field Laboratory, Los Alamos, NM 87545, USA

<sup>2</sup> National Institute for Materials Science, Tsukuba, Ibaraki 305-0044, Japan

<sup>3</sup> Universite de Toulouse, INSA-CNRS-UPS, LPCNO, 31077 Toulouse, France

In semiconductor physics, many of the essential material parameters relevant for optoelectronics can be experimentally revealed via optical spectroscopy in sufficiently large magnetic fields. For the new class of monolayer transition-metal dichalcogenide (TMD) semiconductors, this field scale can be substantial – many tens of teslas or more – due to the relatively heavy carrier masses and the very large electron-hole (exciton) binding energies. For that reason many fundamental parameters of TMDs were – up to now – still assumed from density functional theory calculations [1-3] and have not been experimentally measured.

Here we report circularly-polarized absorption spectroscopy of the monolayer semiconductors MoS<sub>2</sub>, MoSe<sub>2</sub>, MoTe<sub>2</sub>, WS<sub>2</sub>, and WSe<sub>2</sub> in very high magnetic fields up to 91 T. By encapsulating exfoliated monolayers in hexagonal boron nitride (hBN), we achieve very high optical quality structures that allow to follow the diamagnetic shifts and valley Zeeman splittings of not only the 1s ground state of the neutral exciton but also its excited 2s, 3s, ..., ns Rydberg states (see Fig. 1). The energies and diamagnetic shifts provide a direct determination of the effective (reduced) exciton masses and the dielectric properties of these monolayer semiconductors [4-5]. Unexpectedly, the measured exciton masses are significantly heavier than predicted for Mo-based monolayers. Moreover, we also measure other important material properties, including exciton binding energies, exciton radii, and free-particle bandgaps. These results provide essential and quantitative parameters for the rational design of optoelectronic van der Waals heterostructures incorporating 2D semiconductor monolayers.

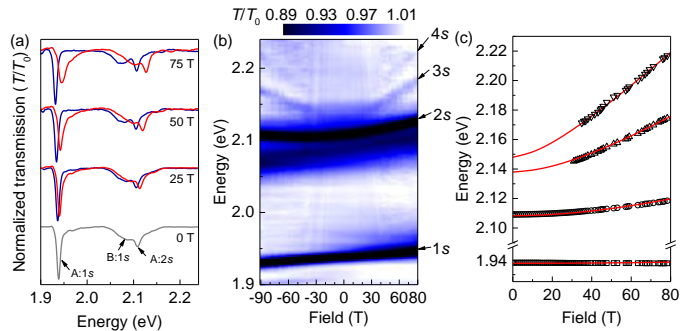


Figure 1. (a) Transmission spectra through monolayer MoS<sub>2</sub> encapsulated in hBN, in both circular polarizations. (b) Intensity map showing all spectra from -91 T to +80 T. The excited Rydberg states of the neutral exciton are visible. (c) The energies of each  $ns$  exciton state. Solid curves show model calculations.

- [1] A. Kormányos *et al.*, 2D Materials **2**, 049501 (2015).
- [2] T. C. Berkelbach *et al.*, Phys. Rev. B **88**, 045318 (2013).
- [3] D. Wickramaratne *et al.*, J. Chem. Phys. **140**, 124710 (2014).
- [4] A. V. Stier *et al.*, Phys. Rev. Lett. **120**, 057405 (2018).
- [5] M. Goryca *et al.*, Nat. Commun. **10**, 4172 (2019).

<sup>+</sup> Author for correspondence: mgoryca@lanl.gov

# Optical Determination of Ice-Induced Interfacial Strain on Single-Layer Graphene

**Subash Kattel<sup>1</sup>, Joseph R. Murphy<sup>1</sup>, Samuel Pasco<sup>1</sup>, John Ackerman<sup>2</sup>, Vladimir Alvarado<sup>2</sup>, and William D. Rice<sup>1</sup>**

<sup>1</sup>*Department of Physics, University of Wyoming, Laramie, WY, 82071*

<sup>2</sup>*Department of Chemical Engineering, University of Wyoming, Laramie, WY, 82071*

Ice formed on a material creates a strain that is indicative of its adhesive strength with another material. Previous determinations of ice adhesion strength, a critical parameter for understanding icing physics, have proven to be highly dependent on experiment-specific conditions, such as surface roughness, icing conditions, water purity, etc. In this work, we use Raman spectroscopy to contactlessly and non-destructively measure temperature-dependent ice-induced strain for the first time. To isolate the ice-material interface, we probe the vibrational modes of single layer graphene (SLG) from 20°C to -30°C with and without ice as shown in Figure 1(a). Along with the well-known temperature-dependent Raman shift of SLG, a clear,  $\sim 2 \text{ cm}^{-1}$  change in the 2D-frequency ( $2650 \text{ cm}^{-1}$ ) developed upon ice formation is shown in Figure 1(b). We found this change in the Raman shift occurred even between supercooled water and ice at the same temperature. This small, change in the Raman shift of SLG corresponds to a 0.013% strain, which we show through spatial Raman mapping has a rich variation over the ice-SLG interface, as depicted in Figure 2. This point-by-point spatial mapping of the ice-induced strain enables precise correlation with surface roughness evaluation methods and theoretical models. Our results demonstrate that vibrational spectroscopy of 2D monolayers can precisely and locally measure strain at ice-material interfaces.

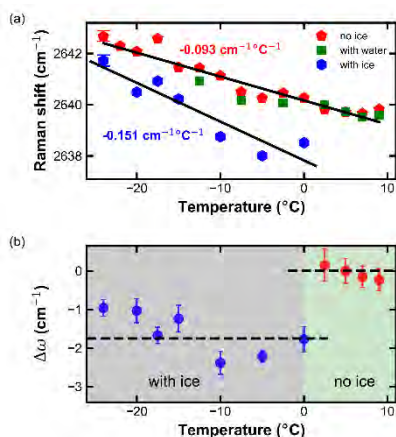


Figure 1 (a) Temperature-dependent Raman shift of the graphene 2D peak center position with no ice (red pentagons), with water (green squares) and ice (blue hexagons). (b) The difference in the 2D peak position of the graphene with and without ice, extracted from the temperature-dependent data shown in (a).

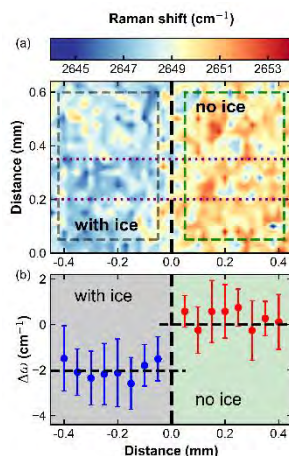


Figure 2 (a) Two-dimensional mapping of the SLG with and without ice. The figure shows the 2D peak position extracted from the fit in  $50 \mu\text{m}$  steps. (b) The difference in the 2D peak position of the SLG with and without ice extracted from the two dimensional mapping shown in (a). Both Fig.1 (b) and Fig.2 (b) shows an ice-induced Raman shift difference of  $\sim -2 \text{ cm}^{-1}$ .

Author for correspondence: wrice2@uwyo.edu

# Electron pairing by remote-phonon scattering in oxide-supported graphene

D. Shin,<sup>1</sup> M. V. Fischetti<sup>2</sup> and A. A. Demkov<sup>1</sup>

<sup>1</sup> Department of Physics, The University of Texas at Austin, Austin, TX 78712, USA

<sup>2</sup> Department of Materials Science and Engineering, The University of Texas at Dallas,

Richardson, TX 75080, USA

Using first principles calculations we have shown that placing graphene on a (111)-oriented perovskite SrTiO<sub>3</sub> (STO) surface provides a possible doping mechanism [1]. Further theoretical analysis presented here suggests that coupling of electrons in graphene to interfacial hybrid plasmon/optical modes via remote-phonon scattering may result in an effective attractive electron-electron interaction that, in turn, could lead to electron pairing and superconductivity [2]. Specifically, we consider top-gated graphene supported by STO as shown in Fig.1. Using the full dynamic polarizability within the random phase approximation (RPA) for the entire system (including the hybrid modes arising from the coupling of the graphene plasmons to the optical phonons of the STO substrate and gate insulator), we estimate the superconducting transition temperature in the strong-coupling limit. In Fig. 2, we show the estimated superconducting critical temperature as a function of carrier density for different oxide thicknesses. As the carrier density increases, the critical temperature increases. The critical temperature is higher in the system of thicker HfO<sub>2</sub> oxide since the electron-IPP interaction is stronger with thicker top-gate oxide.

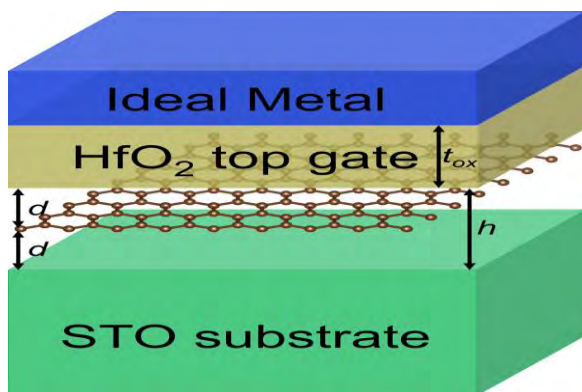


Figure 1. Schematic of a model used in our calculation. Here the STO substrate is assumed to be semi-infinite and the graphene layer is laterally infinite in the vacuum region between HfO<sub>2</sub> and STO.

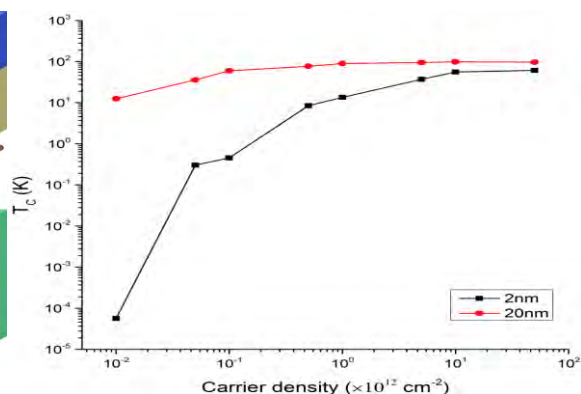


Figure 2. Estimated superconducting critical temperature as a function of carrier density and the two indicated values of the oxide thickness in the strong-coupling limit.

[1] D. Shin and A. A. Demkov, Phys. Rev. B **97**, 075423 (2018).

[2] D. Shin, M. V. Fischetti, and A. A. Demkov, Phys. Rev. B **100**, 125417 (2019).

+ Author for correspondence: demkov@physics.utexas.edu

## Modeling of Interfaces in All-Solid-State Li-ion Batteries

**Y. Qi<sup>†</sup>, M.W. Swift, and H.-K. Tian**

<sup>1</sup> *Department of Chemical Engineering and Materials Science, Michigan State University*

Paring solid electrolytes with Li metal anode and high voltage cathodes form promising all-solid-state Li-ion batteries with higher energy density and ultimately safety. With the rapid development of fast Li-ion conducting solid electrolytes, the major bottleneck for all-solid-state Li-ion batteries lies at the high interfacial resistance and Li dendrite growth. This talk will focus on new mechanism understanding obtained by atomistically-informed multi-scale modeling approaches.

The high interfacial resistance is due to two main factors: physical contact and chemical effect. The chemical effect was captured by a new density functional theory (DFT) based model, which predicts the potential map inside a solid-state battery and determines the potential drop, electrostatic dipole, and space-charge layer at the electrode/solid-electrolyte interface.[1] This new physics insight unified the seemingly contradictory experimental observations and led to new device design rules to promote interfacial ion transport in future solid-state batteries.[2] The physical contact was described by combining contact mechanics and 1D Newman battery model. The model suggested how much pressures should be applied to recover the capacity drop due to contact area loss.

To simulate Li dendrite growth inside polycrystalline solid electrolytes, we coupled DFT calculations with the phase-field method. This model successfully explained the experimentally observed dendrite intergranular growth and revealed that the trapped electrons at grain boundaries and surfaces may produce isolated Li-metal nucleation, leading to a sudden increase of Li-dendrite penetration depth. Based on the model, we developed new dendrite resistant criteria by comparing the basic material properties for a number of solid electrolytes including LLZO, Li<sub>3</sub>PS<sub>4</sub>, LATP, and LiPON. [3][4]

These modeling advancements will be integrated into a new framework to guide the development of all-solid-state Li-ion batteries.

[1] M.W. Swift and Y. Qi, Phys. Rev. Lett. 122, 167701 (2019)

[2] H.-K. Tian and Y. Qi, J. Electrochemical Society 164 (11), E3512-E3521

[3] H.-K. Tian, B. Xu, and Y. Qi Journal of Power Sources 392 (2018) 79–86

[4] H.-K. Tian, Z. Liu, Y. Ji, L.-Q. Chen, and Y. Qi, Chemistry of Materials 31 (2019) 7351-7359

<sup>†</sup> Author for correspondence: [yueqi@egr.msu.edu](mailto:yueqi@egr.msu.edu)



# Computational Predictions of Electronic Properties for Graphene Hybrids Interfaces using Density Functional Theory Relevant for Energy Storage and Generation

**S. Gupta<sup>1</sup> and N. Dimakis<sup>2</sup>**

<sup>1</sup> Department of Physics and Astronomy and Advanced Materials Institute, Western Kentucky University, 1906 College Heights Blvd. Bowling Green, KY 42101 (USA)

<sup>2</sup> Department of Physics and Astronomy, The University of Texas-Rio Grande Valley, TX 78539 (USA).

## Abstract

The interfacial interactions between transition metal oxides (vanadium oxide VO<sub>2</sub>, vanadium pentoxide V<sub>2</sub>O<sub>5</sub>, cobalt oxide CoO and Co<sub>3</sub>O<sub>4</sub>, manganese oxide MnO<sub>2</sub>) and water adsorbates on graphene supports as solvated interfaces and influence of defects in graphene are studied using periodic density functional theory (DFT) calculations in view of their significance for applied electrochemistry [1]. DFT complemented and synergized our experimental work. The optimized metal oxide adatom-graphene geometries identified the preferred adatom sites, whereas metal oxide-graphene strengths are correlated with the adatom distance from the graphene plane, the Metal-C overlap populations, and the adsorption energies. The presence of finite electronic density of states (DOS) near Fermi level and charge transfers between the adatom top layer and graphene supports reflect primarily covalent bonding nature. The presence of small orbital overlap integral of bonds between the s and p (and d) orbitals of the nearest carbon (graphene), carbon oxide (graphene oxide) and metal oxide atoms reveal localized orbital re-hybridization resulting in changes in DOS yielding high electrochemical activity. Moreover, for increased adatom coverage the extent of charge transfer reverses resulting in limited electroactivity. In fact, DFT calculations are corroborated with experimental findings, where graphene-based supports decorated with optimal mass loaded nanostructured Co<sub>3</sub>O<sub>4</sub> and MnO<sub>2</sub> (as well as V<sub>2</sub>O<sub>5</sub>) were capable of delivering maximum specific energy with storage capacity (C<sub>s</sub>) > 550 F.g<sup>-1</sup> in contrast to higher or lower loading [2]. The presence of defects in graphene materials results in new electronic states to endow unique functionalities that is not otherwise possible in the bulk and with adsorbed water molecules besides optimum C/O ratio in graphene oxide nanosheets that show redshift thus a decreasing bandgap and finite charge transfer from graphene to water molecules. The case examples studied in this work represent a first glimpse of what may become routine and integral step in materials design and discovery for alternative energy and sustainable environmental technologies [1].

[1] S. Gupta, N. Dimakis, Appl. Surf. Sci. 467-468, 760-772 (2019).

[2] S. Gupta, S. B. Carrizosa, B. McDonald, J. Jasinski, N. Dimakis, J. Mater. Res. 32, 301-322 (2017).

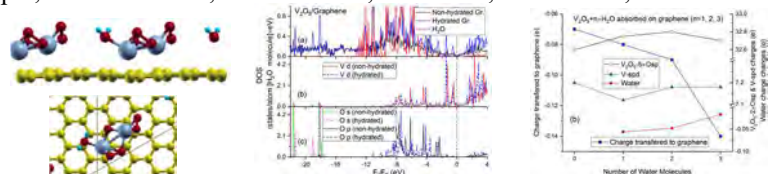


**Figure 1.** (left) Geometry optimization for V<sub>2</sub>O<sub>5</sub>/graphene, (middle) density of states, (right) charge transfer with varying number of adsorbed water molecules.

<sup>+</sup> Author for correspondence: sanju.gupta@wku.edu

# Properties of Two-Dimensional Titanium Carbide ( $\text{Ti}_3\text{C}_2\text{T}_x$ ) MXene for Energy Conversion: Effects of Interlayer Spacing, Flake Size and Electrochemical Environment

S. Gupta<sup>1</sup> W. Ringo<sup>1</sup>, M. Hu<sup>2</sup> and X. Wang<sup>2</sup>

<sup>1</sup> Department of Physics and Astronomy and Advanced Materials Institute, Western Kentucky University, 1906 College Heights Blvd. Bowling Green, KY 42101 (USA)

<sup>2</sup> Institute of Metal Research, Chinese Academy of Sciences, 72 Wenhua Road, Shenyang 110016 (China).

## Abstract

Two-dimensional (2D) layered materials are studied in efforts to discover new compounds and for their fascinating properties engineered by sheet-like structure and tunable surfaces. MXenes are an emergent class of layered transition metal carbides and carbonitrides synthesized that are useful at the grand challenges of *energy-water-sensing* nexus. This work reports systematic structural and electrochemical properties of titanium carbide ( $\text{Ti}_3\text{C}_2\text{T}_x$ ) MXenes phases of varying interlayer spacing, flake thickness and lateral size under different electrolytes. In addition to traditional electrode kinetics, we utilized surface sensitive scanning electrochemical microscopy (SECM) to gain complete understanding of rich surface chemistry and corresponding knowledge about the physicochemical processes (inherent electrochemistry and heterogeneous charge transfer characteristics) at the electrode/electrolyte (solid/liquid) interfaces. We employed electron microscopy, UV-Visible absorption spectroscopy, x-ray diffraction, and Raman spectroscopy to determine surface morphology, microscopic and electronic structure and lattice vibrational properties. It is shown that  $\text{Ti}_3\text{C}_2\text{T}_x$  or specifically, transition metal Ti undergoes irreversible oxidation and lithiated in a positive potential window, which strongly depends on the flake thickness and type (aqueous versus organic) of the electrolyte. Multi-layered and smaller  $\text{Ti}_3\text{C}_2\text{T}_x$  flakes exhibit faster electron transfer kinetics ( $k_{\text{ET}}=1.2 \text{ cm}\cdot\text{s}^{-1}$ ) with a  $[\text{Fe}(\text{CN})_6]^{4-/3-}$  redox probe compared to a few-layered  $\text{Ti}_3\text{C}_2\text{T}_x$  ( $k_{\text{ET}}=0.3 \text{ cm}\cdot\text{s}^{-1}$ ) in aqueous and organic electrolyte ( $k_{\text{ET}}=4.9 \text{ cm}\cdot\text{s}^{-1}$ ) with a  $[\text{Fe}(\text{CN})_6]^{4-/3-}$  redox probe compared to a few-layered  $\text{Ti}_3\text{C}_2\text{T}_x$  ( $k_{\text{ET}}=0.9 \text{ cm}\cdot\text{s}^{-1}$ ). In addition, the few-layered free standing  $\text{Ti}_3\text{C}_2\text{T}_x$  film electrode remains intact post-irreversible oxidation. These properties help to establish *structure-property-electroactivity* relationships among different types of  $\text{Ti}_3\text{C}_2\text{T}_x$  MXenes.

[1] S. Gupta, W. Ringo, M. Hu, X. Wang, *Nanomaterials* (*in press*, 2019).

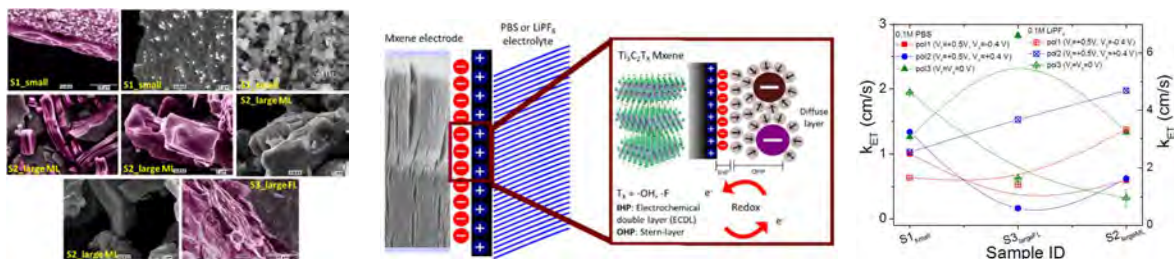


**Figure 1.** (left) SEM micrographs, (middle) cartoon for surface functionality and interfaces, (right) variation of electron transfer rate with flake size.

<sup>+</sup> Author for correspondence: sanju.gupta@wku.edu

## Bold page numbers indicate presenter

## — A —

Abi Jaoude, M.: PCSI-2MoM41, 41  
 Ackerman, J.: PCSI-1ThM13, 92  
 Ahmed, S.: PCSI-2WeM41, 72  
 Ahn, Y.H.: PCSI-1TuM9, 55  
 Alameri, D.: PCSI-2WeM42, 73  
 Alberi, K.: PCSI-2SuA29, 28  
 Alexander, A.: PCSI-2SuA30, 29  
 Alkhalid, T.: PCSI-2MoM41, 41  
 Alpha, C.: PCSI-2MoM41, 41  
 Altoe, V.: PCSI-2TuM39, 61  
 Alvarado, V.: PCSI-1ThM13, 92  
 Anderson, E.: PCSI-2MoA37, 49  
 Appelfeller, S.: PCSI-2MoM40, 40  
 Arey, B.: PCSI-2SuA30, 29  
 Argibay, N.: PCSI-1WeM11, 67  
 Aydil, E.: PCSI-1WeA9, 75

## — B —

Bannerjee, A.: PCSI-2TuM39, 61  
 Bardgett, D.: PCSI-2WeM39, 70  
 Barral, A.: PCSI-1TuM13, 56  
 Batteas, J.: PCSI-1WeM11, 67  
 Bauers, S.: PCSI-2WeM39, 70  
 Beaton, D.: PCSI-MoE9, 52  
 Beechem, T.: PCSI-2MoA37, 49  
 Benter, S.: PCSI-1MoA11, 46  
 Berry, J.: PCSI-TuE1, 62  
 Berthe, M.: PCSI-1MoA15, 47  
 Biacchi, A.: PCSI-2WeM40, 71  
 Bocheff, M.: PCSI-2SuA25, 27  
 Borgström, M.: PCSI-TuE9, 63  
 Brown-Heft, T.: PCSI-2SuA25, 27  
 Bruckmann, C.: PCSI-1MoM9, 34  
 Bussmann, E.: PCSI-2MoA37, 49  
 Butera, R.: PCSI-2WeA45, 88

## — C —

Cabrini, S.: PCSI-2TuM39, 61  
 Campbell, D.: PCSI-2MoA37, 49  
 Chandross, M.: PCSI-1WeM11, 67  
 Chang, Y.: PCSI-2SuA25, 27; PCSI-2SuA31, 30  
 Chatterjee, S.: PCSI-2SuA25, 27  
 Chen, C.-W.: PCSI-1WeA10, 76  
 Chin, S.-C.: PCSI-1WeA10, 76  
 Chiu, Y.-P.: PCSI-1WeA10, 76  
 Cossio, G.: PCSI-1WeM12, 68  
 Courtade, E.: PCSI-1ThM9, 91  
 Crooker, S.A.: PCSI-1ThM9, 91  
 Curry, J.: PCSI-1WeM11, 67

## — D —

Dähne, M.: PCSI-2MoM40, 40  
 Das, B.: PCSI-1WeA9, 75  
 De Palma, A.: PCSI-1WeM12, 68  
 Degen, J.: PCSI-1TuM1, 54  
 Dehankar, A.: PCSI-1TuM19, 59  
 Demkov, A.: PCSI-1ThM14, 93; PCSI-1WeA15, 78  
 Dimakis, N.: PCSI-2ThM39, 95  
 Divan, R.: PCSI-2WeM42, 73  
 Dong, R.: PCSI-2WeM42, 73  
 Dreyer, M.: PCSI-2WeA45, 88  
 Du, L.: PCSI-1MoM10, 35  
 Dunin-Borkowski, R.: PCSI-1MoA15, 47; PCSI-1WeA10, 76  
 Dwyer, K.: PCSI-2WeA45, 88

## — E —

Ebert, P.: PCSI-1MoA15, 47; PCSI-1WeA10, 76  
 Eddy, Jr., C.R.: PCSI-2SuA31, 30  
 Eisele, H.: PCSI-1MoA15, 47; PCSI-1MoM9, 34; PCSI-2MoM40, 40  
 Erickson, T.: PCSI-1TuM13, 56

## — F —

Faeth, B.: PCSI-MoE1, 51  
 Fagan, J.: PCSI-2WeM40, 71

Fedorov, A.: PCSI-2SuA25, 27  
 Ferrari, V.: PCSI-1TuM13, 56  
 Fischetti, M.: PCSI-1ThM14, 93  
 Flatté, M.: PCSI-1TuM14, 57; PCSI-SuE1, 31  
 Franz, M.: PCSI-2MoM40, 40

## — G —

Galazka, Z.: PCSI-1MoM9, 34  
 Galbiati, M.: PCSI-1SuA18, 26  
 Gamache, P.: PCSI-2MoA37, 49  
 Gaskell, K.: PCSI-2WeA45, 88  
 Gater, D.: PCSI-2MoM41, 41  
 Ginley, T.: PCSI-2WeA49, 89  
 Ginting, E.: PCSI-1MoM10, 35  
 Gorman, B.: PCSI-2WeM39, 70  
 Goryca, M.: PCSI-1ThM9, 91  
 Goto, K.: PCSI-2WeA31, 81  
 Grandidier, B.: PCSI-1MoA15, 47  
 Griffin, S.: PCSI-2TuM39, 61  
 Grine, A.: PCSI-2MoA37, 49  
 Gunter, M.: PCSI-2MoA37, 49  
 Guo, T.: PCSI-2SuA25, 27  
 Guo, Y.: PCSI-1WeA1, 74  
 Gupta, G.: PCSI-1MoA9, 44  
 Gupta, S.: PCSI-2ThM39, 95; PCSI-2ThM40, 96

## — H —

Harmon, N.: PCSI-1TuM14, 57; PCSI-SuE1, 31  
 Hasegawa, Y.: PCSI-MoE10, 53  
 Higashiwaki, M.: PCSI-2WeA31, 81  
 Hight Walker, A.: PCSI-2WeM40, 71  
 Hofmann, J.: PCSI-1MoM9, 34  
 Hong, S.S.: PCSI-1MoM11, 36  
 Hsing, C.-R.: PCSI-1WeA10, 76  
 Hsu, H.-C.: PCSI-1WeA10, 76  
 Hsu, H.Y.: PCSI-1WeA14, 77; PCSI-1WeA16, 79; PCSI-1WeA17, 80; PCSI-1WeM10, 66  
 Hu, M.: PCSI-2ThM40, 96  
 Huang, B.-C.: PCSI-1WeA10, 76  
 Hunt, D.: PCSI-1TuM13, 56

## — I —

Inbar, H.: PCSI-2SuA25, 27  
 Isakovic, A.: PCSI-2MoM41, 41

## — J —

Jo, W.: PCSI-2MoM42, 42  
 Johnston-Halperin, E.: PCSI-1TuM19, 59  
 Jones, K.: PCSI-1WeM12, 68

## — K —

Karbach, D.: PCSI-2WeM42, 73  
 Kattel, S.: PCSI-1ThM13, 92  
 Katzenmeyer, A.: PCSI-2MoA37, 49  
 Kawakami, R.: PCSI-1TuM19, 59  
 Khan, I.: PCSI-2WeA42, 85  
 Kim, K.H.: PCSI-1TuM9, 55  
 Knutsson, J.: PCSI-1MoA11, 46  
 Kriekebaum, J.M.: PCSI-2TuM39, 61  
 Krishnamoorthy, S.: PCSI-1MoM19, 37  
 Ku, H.S.: PCSI-2TuM31, 60  
 Kubicki, M.: PCSI-2MoM40, 40  
 Kuehl, V.: PCSI-2WeM40, 71  
 Kuljanishvili, I.: PCSI-2WeM42, 73  
 Kumagai, Y.: PCSI-2WeA31, 81

## — L —

Lake, R.: PCSI-2TuM31, 60  
 Lastras-Martinez, A.: PCSI-2WeA41, 84  
 Law, S.: PCSI-2WeA49, 89  
 Lee, H.: PCSI-1WeM9, 65  
 Lee, H.W.: PCSI-1TuM9, 55  
 Lee, J.: PCSI-1TuM9, 55  
 Lee, J.S.: PCSI-2SuA31, 30  
 Lefebvre, I.: PCSI-1MoA15, 47  
 Lehmann, S.: PCSI-1MoA11, 46  
 Leighton, C.: PCSI-1WeA9, 75  
 Leung, T.C.: PCSI-1WeA14, 77; PCSI-1WeA16, 79; PCSI-1WeA17, 80; PCSI-1WeM10, 66

Li, J.: PCSI-1ThM9, 91  
 Li, W.: PCSI-1WeA15, 78  
 Li, X.E.: PCSI-1SuA2, 24; PCSI-1WeM12, 68  
 Lin, M.C.: PCSI-1WeA14, 77; PCSI-1WeA16, 79; PCSI-1WeA17, 80; PCSI-1WeM10, 66  
 Lindner, S.: PCSI-2MoM40, 40  
 Liu, W.C.: PCSI-1WeM10, 66  
 Liu, X.: PCSI-2TuM39, 61  
 Liu, Y.: PCSI-1MoA11, 46; PCSI-2WeM42, 73  
 Liu, Z.: PCSI-1WeM11, 67  
 Long, J.: PCSI-2TuM31, 60  
 Lu, P.: PCSI-2MoA37, 49  
 Lu, T.-M.: PCSI-2MoA37, 49  
 Lucero, J.: PCSI-2MoA37, 49  
 Luk, T.: PCSI-2MoA37, 49  
 Luo, Y.: PCSI-1TuM19, 59  
 Lynn, K.G.: PCSI-1MoM19, 37

## — M —

Ma, Y.: PCSI-1TuM13, 56  
 Maiti, M.: PCSI-1WeA9, 75  
 Manno, M.: PCSI-1WeA9, 75  
 Marie, X.: PCSI-1ThM9, 91  
 Masegi, H.: PCSI-1MoA10, 45  
 Mason, N.: PCSI-1ThM1, 90  
 McCluskey, M.: PCSI-2WeM41, 72  
 McFadden, A.: PCSI-2SuA31, 30  
 McMahan, B.: PCSI-2WeA42, 85  
 McMillan, S.: PCSI-1TuM14, 57  
 Meng, K.Y.: PCSI-1TuM13, 56  
 Mikkelsen, A.: PCSI-1MoA11, 46  
 Minor, A.: PCSI-2TuM39, 61  
 Mishra, M.: PCSI-1MoA9, 44  
 Misra, S.: PCSI-2MoA37, 49  
 Moore, L.: PCSI-2WeM42, 73  
 Moore, Q.: PCSI-1WeM11, 67  
 Moore, W.: PCSI-1WeA9, 75  
 Murakami, H.: PCSI-2WeA31, 81  
 Murphy, J.: PCSI-1ThM13, 92

## — N —

Nam, S.: PCSI-SuE9, 32  
 Nguyen, D.-L.: PCSI-1WeA10, 76  
 Nie, W.: PCSI-2MoM31, 38; PCSI-2MoM39, 39  
 Norman, A.: PCSI-2WeA39, 82; PCSI-2WeA42, 85  
 Nys, J.-P.: PCSI-1MoA15, 47

## — O —

Ogletree, D.F.: PCSI-2TuM39, 61  
 Olszta, M.: PCSI-2SuA30, 29  
 Ooi, Y.K.: PCSI-1MoM19, 37

## — P —

Palmstrom, C.J.: PCSI-1MoA11, 46; PCSI-2SuA25, 27; PCSI-2SuA31, 30  
 Pappas, D.: PCSI-2TuM31, 60  
 Pasco, S.: PCSI-1ThM13, 92  
 Pendharkar, M.: PCSI-2SuA25, 27  
 Pennachio, D.J.: PCSI-2SuA31, 30  
 Perez-Hoyos, E.: PCSI-1TuM19, 59  
 Perkins, J.: PCSI-2WeM39, 70  
 Petrov, V.: PCSI-2WeA43, 86  
 Pharis, D.: PCSI-1TuM19, 59  
 Plissard, S.: PCSI-1MoA15, 47  
 Posadas, A.: PCSI-1WeA15, 78  
 Ptak, A.: PCSI-2WeA40, 83  
 Pulzara Mora, A.O.: PCSI-1TuM18, 58  
 Pulzara Mora, C.A.: PCSI-1TuM18, 58

## — Q —

Qi, Y.: PCSI-2ThM31, 94  
 Quan, J.: PCSI-1WeM12, 68

## — R —

Ranga, P.: PCSI-1MoM19, 37  
 Read, D.: PCSI-2SuA25, 27  
 Rice, A.: PCSI-2SuA29, 28

## Supplemental Document Author Index

- Rice, W.: PCSI-2WeM40, 71  
Rice, W.D.: PCSI-1ThM13, 92  
Richardson, C.: PCSI-2SuA30, **29**  
Ringo, W.: PCSI-2ThM40, 96  
Ritter, J.: PCSI-2WeM41, 72  
Robert, C.: PCSI-1ThM9, 91  
Roberts, D.: PCSI-2WeA40, **83**; PCSI-2WeM39, **70**  
Robertson, J.: PCSI-1WeA1, **74**  
Robinson, J.: PCSI-1WeM1, **64**  
Rogge, S.: PCSI-2MoA29, **48**  
Rosenberg, S.G.: PCSI-2SuA31, 30  
— S —  
Saenz, T.: PCSI-2WeA39, 82  
Saleh, M.: PCSI-1MoM19, 37  
Sankar, R.: PCSI-1WeA10, 76  
Scarpulla, M.A.: PCSI-1MoM19, **37**  
Schlom, D.: PCSI-MoE1, 51  
Schmucker, S.: PCSI-2MoA37, **49**  
Schnedler, M.: PCSI-1MoA15, **47**; PCSI-1WeA10, 76  
Schulte, K.: PCSI-2WeA40, 83  
Schulze, C.: PCSI-1MoM9, 34  
Searles, T.: PCSI-2WeM40, 71  
Sharp, I.: PCSI-1MoA1, **43**  
Shen, K.: PCSI-MoE1, **51**  
Shin, D.: PCSI-1ThM14, 93  
Shree, S.: PCSI-1ThM9, 91  
Siddiqi, I.: PCSI-2TuM39, 61  
Simon, J.: PCSI-2WeA40, 83  
Smith, A.R.: PCSI-1TuM13, **56**  
Son, J.: PCSI-1TuM9, **55**  
Song, J.: PCSI-1SuA10, **25**  
Stier, A.V.: PCSI-1ThM9, 91  
Sun, R.: PCSI-1MoM19, 37  
— T —  
Talin, A.: PCSI-2WeM31, **69**  
Taniguchi, T.: PCSI-1ThM9, 91  
Thomas, A.: PCSI-2SuA30, 29  
Timm, R.: PCSI-1MoA11, **46**  
Tracy, L.: PCSI-2MoA37, 49  
Tsai, H.: PCSI-2MoM39, **39**  
— U —  
Urbaszek, B.: PCSI-1ThM9, 91  
— V —  
Voigt, B.: PCSI-1WeA9, **75**  
— W —  
Wakabayashi, N.: PCSI-2WeA44, **87**  
Walker, J.: PCSI-2WeM40, **71**  
Walter, J.: PCSI-1WeA9, 75  
Wang, X.: PCSI-2ThM40, 96  
Wang, Y.: PCSI-1WeA17, 80  
Ward, D.: PCSI-2MoA37, 49  
Warren, E.: PCSI-2WeA39, **82**  
Watanabe, K.: PCSI-1ThM9, 91  
Weddle, C.: PCSI-2SuA30, 29  
Wei, C.-M.: PCSI-1WeA10, 76  
Wells, J.: PCSI-2MoA41, **50**  
Wilson, N.: PCSI-1MoA11, 46  
Winter, J.: PCSI-1TuM19, 59  
Wong, M.H.: PCSI-2WeA31, 81  
Wu, F.: PCSI-1WeM11, **67**  
Wu, X.: PCSI-2TuM31, 60  
— X —  
Xu, J.: PCSI-1TuM19, 59  
Xu, L.L.: PCSI-1WeA14, 77; PCSI-1WeA16, **79**;  
PCSI-1WeA17, 80; PCSI-1WeM10, 66  
Xu, T.: PCSI-1MoA15, 47  
— Y —  
Yang, F.-Y.: PCSI-1TuM13, 56  
Yang, S.: PCSI-MoE1, 51  
Young, E.: PCSI-1MoA11, 46  
Yu, E.: PCSI-1WeM12, 68  
— Z —  
Zakutayev, A.: PCSI-2WeA42, 85; PCSI-2WeM39, 70  
Zhang, Z.: PCSI-1WeA1, 74  
Zhao, H.: PCSI-1MoM1, **33**  
Zhao, N.: PCSI-1WeA14, **77**; PCSI-1WeA16, 79  
Zhou, J.: PCSI-1MoM10, **35**  
Zielinski, R.: PCSI-1MoM9, 34  
Zimmerman, J.: PCSI-2WeA39, 82